Aus dem Institut für Pathologie der Universität Heidelberg
Abteilung für Neuropathologie
und
Klinische Kooperationseinheit Neuropathologie
Deutsches Krebsforschungszentrum
(Direktor: Prof. Dr. med. Andreas von Deimling)

In vitro and *in vivo* modeling of gliomagenesis based on the Idh1^{R132H} mutation

Inauguraldissertation
zur Erlangung des Doctor scientiarum humanarum (Dr.sc.hum.)
an der
Medizinischen Fakultät Heidelberg
der
Ruprecht-Karls-Universität

vorgelegt von

Viktoria Fischer

aus
Bochum

2018

Dekan: Prof. Dr. med. Wolfgang Herzog

Doktorvater: Prof. Dr. med. Andreas von Deimling

Meiner Familie

List of Abbreviations

2-HG	2-hydroxyglutarate
4-OHT	4-hydroxytamoxifen
5hmC	5-hydroxymethylcytosine
5mC	5-methylcytosine
ALT	alternative lengthening of telomeres phenotype
AML	acute myeloid leukemia
AT	annealing temperature
ATP	adenosine triphosphate
ATRX	alpha-thalassemia/mental retardation syndrome X-linked
BCA	bicinchoninic acid
CIC	capicua transcriptional repressor, human
Cic	capicua transcriptional repressor, murine
clC	cleaved caspase
clPARP	cleaved Poly (ADP) Ribose Polymerase
CreERT2	cyclization recombination fused to hormone binding domain of a modified estrogen receptor
CT	computed tomography
CTB	Cell Titer Blue Cell Viability Assay
CTG3D	Cell Titer-Glo3D Cell Viability Assay
ES	embryonic stem cell
ET	elongation time
FMZ	^{18}F-flumazenil
FDG	^{18}F-fluorodeoxyglucose
FFPE	formalin fixed paraffin embedded tissue
Flp	flippase, recombinase
Foxn1	forkhead box protein N1, murine
FRT	flippase recognition target cassette
FUBP1	far upstream element binding protein 1
G-CIMP	CpG island methylator phenotype
GBM	glioblastoma
GFP	green fluorescent protein
HE	haematoxilin eosin staining
HGDH	D- and L-2-HG dehydrogenase
HRP	horseradish peroxidase
IDH1	isocitrate dehydrogenase, human
Idh1	isocitrate dehydrogenase, murine
iEEG	intracranial elektroencephalogram
JmjC	Jumonji C domain
Ki-67	antigen Ki-67
LOH	loss of heterozygosity
MALDI-TOF	Matrix Assisted Laser Desorption Ionization - Time of Flight
MEG	magnetoencephalography

MES	2-(*N*-morpholino)ethansulfonsäure
MHC	major histocompatibility complex
MOPS	3-(*N*-morpholino)propansulfonsäure
MRI	magnetic resonance imaging
NAD	nicotinamide adenine dinucleotide
NADH	nicotinamide adenine dinucleotide, reduced
NADP	nicotinamide adenine dinucleotide phosphate
NADPH	nicotinamide adenine dinucleotide phosphate, reduced
NCH	Neurochirurgie Heidelberg
NMDA	*N*-methyl-D-aspartate receptor
NP40	nonidet-P40
NSC	neural stem cell
p53	protein 53
PBS	phosphate buffered saline
PCA	perchloric acid
PDD	papain dispase DNase
PET	positron emission tomography
pHH3	phospho histone H3
pTERT	promoter TERT mutation
ROS	reactive oxygen species
rpm	revolutions per minute
SDS	sodium dodecyl sulfate
SDS-PAGE	sodium dodecyl sulfate polyacrylamide gel electrophoresis
SLC7AI	cysteine-glutamate antiporter xCT
SUV	PET CT standard uptake value
TBS-T	tris-buffered saline (with Tween)
TERT	telomerase reverse transcriptase
TET	ten-eleven translocation methylcytosine dioxygenase
TP53	tumor protein 53, gene
α-KG	alpha-ketoglutarate
γH2AX	phosphorylated histone 2AX

Table of contents

Table of contents 9

1 Introduction 11
- **1.1 Diffuse gliomas** 11
- **1.2 Grading of tumors of the central nervous system** 11
- **1.3 Molecular markers** 12
- **1.4 Isocitrate dehydrogenases (IDHs)** 13
  - **1.4.1 The "oncometabolite" 2-HG** 15
  - **1.4.2 Clinical features of *IDH*-mutant glioma** 17
  - **1.4.3 Mutant IDH1 as therapeutic target** 20
- **1.5 *IDH1* and secondary alterations in gliomagenesis** 21
  - **1.5.1 Association of *IDH* mutations with *TP53* and *ATRX* mutations in astrocytoma** 23
  - **1.5.2 Association of *IDH* mutations with 1p/19q co-deletions in oligodendroglioma** 23
- **1.6 Aims of the study** 24

2 Materials & Methods 26
- **2.1 Matings of mice with different conditional alleles** 26
- **2.2 Generation of Cic flox mice** 26
- **2.3 Chemicals** 27
- **2.4 Genotyping** 27
- **2.5 Preparation of neural stem cells** 28
- **2.6 Passaging and induction of genetic alterations** 29
- **2.7 Proliferation assay** 30
- **2.8 SDS-Page and Western blot** 30
- **2.9 Reverse transcription PCR** 33
- **2.10 Soft agar assay** 34
- **2.11 2-HG assay** 35
- **2.12 Dotblot** 37
- **2.13 Histology of neurospheres** 37
- **2.14 Immunohistochemistry** 38
- **2.15 Intracranial injections of neural stem cells** 39
- **2.16 Imaging and analysis** 41

3 Results 44
- **3.1 Generation of Cic flox mice** 44
- **3.2 Generation of neural stem cells with different genetic alterations** 44
  - **3.2.1 Induction of genetic alterations and validation of established cell lines** 45
- **3.3 Functional characterization of Idh1^{R132H} p53$^{-/-}$ NSCs: short-term effects** 47
  - **3.3.1 Cell viability** 47
  - **3.3.2 Colony formation in soft agar** 49
  - **3.3.3 Analysis of apoptotic proteins** 50
  - **3.3.4 Production of 2-HG** 51
- **3.4 In vivo allograft model** 51
  - **3.4.1 Intracranial injections** 52
  - **3.4.2 General problems with immunodeficient mice during the time of the experiment** 52
- **3.5 Functional characterization of Idh1^{R132H} p53$^{-/-}$ NSCs: long-term effects** 53
  - **3.5.1 Cell viability** 53
  - **3.5.2 Colony formation in soft agar** 54
  - **3.5.3 Analysis of apoptotic proteins** 55
  - **3.5.4 Analysis of cell cycle markers in long-term cells** 56
  - **3.5.5 Analysis of epigenetic effects of Idh1^{R132H}** 57
  - **3.5.6 Production of 2-HG** 58
- **3.6 Loss of Idh1^{R132H} in long-term cell lines** 59
  - **3.6.1 Loss of Idh1^{R132H} *in vivo*?** 61
- **3.7 MRI monitoring of BALB/c nude mice after intracranial injections** 62

3.7.1 9.4 T scans ... 64
3.8 Immunohistochemistry ... **65**
3.9 *In vitro* analysis of a *Cic* knock-out alone and in an Idh1^{R132H} background ... **68**
3.9.1 Cell viability ... 68
3.9.2 Colony formation in soft agar ... 70
3.9.3 Effects on epigenetics ... 70
3.9.4 Production of 2-HG ... 71
3.10 PET imaging: IDH1^{R132H} and its relation to epileptogenesis ... **72**

4 Discussion ... **76**
4.1 Effects of Idh1^{R132H} ... **77**
4.2 The difference between short- and long-term inductions ... **80**
4.3 Loss of Idh1^{R132H} *in vitro* ... **84**
4.4 Migration of induced NSCs *in vivo* ... **85**
4.5 Cell type ... **86**
4.6 Additional mutation ... **87**
4.7 Genetic background of mice ... **87**
4.8 Detection of implanted cells ... **88**
4.9 Implementation of Cic$^{-/-}$ in an Idh1^{R132H} background ... **89**
4.10 Functional neuroimaging of glioma xenografts with IDH1^{R132H} mutation ... **91**

5 Summary ... **93**

6 Zusammenfassung ... **94**

7 References ... **96**

8 Supplement ... **110**

9 Acknowledgements ... **115**

Publications ... **119**

Eidesstattliche Versicherung ... **121**

1 Introduction

Brain tumors, especially gliomas, are a disease that cannot be cured with the current methods, although different treatment strategies are available. This could be a consequence of missing glioma models. To understand how these tumors arise and how they can be tackled, it is of utmost importance to develop a defined model mimicking the genetic features of human glioma.

1.1 Diffuse gliomas

Gliomas are the most frequent intrinsic tumor of the central nervous system. They can be divided into diffuse and non-diffuse gliomas that show a more circumscribed growth pattern. The diverse gliomas are classified according to their microscopic similarities with putative cells of origin along glial precursor cell lineages (Wesseling and Capper, 2017). This work focusses on diffuse gliomas, which are characterized by an extensive infiltrative growth into the surrounding CNS parenchyma.

1.2 Grading of tumors of the central nervous system

The classification of brain tumors has been based on the idea that tumors can be distinguished by histological differences in combination with potential cells of origin and their levels of differentiation for nearly one century. The pioneering work by Bailey and Cushing in 1926 first described the association between histology and prognosis (Bailey and Cushing, 1926). The WHO classifications of 2000 and 2007 started to combine the histological features with genetic differences between different tumor entities. During the last years and especially since the last update, the WHO classification of 2016, well-established molecular parameters are incorporated into the classification of diffuse gliomas (Louis *et al.*, 2016b).

Histological grading of diffuse gliomas and the respective malignancy grade (WHO grade II, III or IV) is based on the presence or absence of mitotic activity, nuclear pleomorphism, cellularity, necrosis and florid microvascular proliferation. The histological grading combined with genetic alterations, clinical findings (e.g. patient age, tumor location, etc), radiological features (e.g. contrast enhancement), surgical resection and proliferation index values, gives an indication on the response to therapy and outcome. The genetic profile has become increasingly important, as some genetic alterations have important prognostic implications. One example is the presence of an isocitrate dehydrogenase 1 (*IDH1*) mutation in diffuse gliomas that contributes to the overall estimate of prognosis. In previous classifications, all

astrocytic tumors were grouped together. Nowadays all diffusely infiltrating gliomas (whether astrocytic or oligodendroglial) are classified based on their growth pattern, their behavior and their *IDH1* mutational status. According to the new classification, diffuse gliomas include WHO grade II and III astrocytic tumors, the grade II and III oligodendrogliomas, the grade IV glioblastomas (GBMs) and the related and partly unspecified gliomas, as for example those of childhood (Figure 1) (Louis *et al.*, 2016a; Louis *et al.*, 2016b; Wesseling and Capper, 2017).

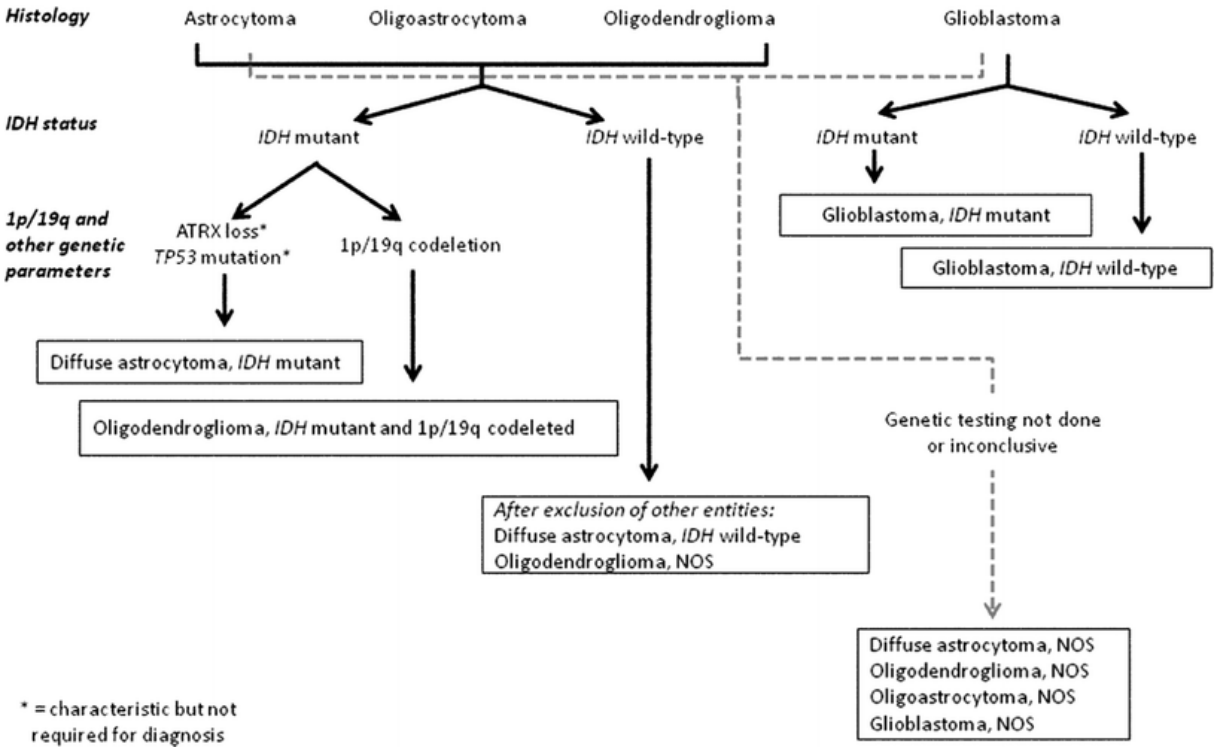

Figure 1. Summary of the WHO classification of brain tumors 2016. Diagram showing a simplified algorithm for classification of diffuse gliomas based on a combination of histological and genetic features, according to the WHO CNS classification 2016. The diagnosis does not necessarily proceed from histology first to molecular genetic features afterwards, because molecular signatures sometimes outweigh histological characteristics (Louis *et al.*, 2016b). (NOS = not otherwise specified).

1.3 Molecular markers

Extensive research provided methods to unravel the status of the whole cancer genome. These methods include whole genome sequencing, whole exome sequencing, mRNA sequencing and expression profiling. Application of these methods provided a large landscape of genomic alterations in diffuse gliomas. As an example, whole exome sequencing revealed on average 16 somatic mutations in astrocytomas, 36 in anaplastic astrocytomas and 46-50 in GBMs (Killela *et al.*, 2014). However, only a few of these genetic alterations are practically useful in classifying diffuse gliomas. These genetic alterations have to be detected at significant frequencies, have to draw clear lines to divide subgroups and these subgroups should be

associated with clinically significant features. The few genetic alterations fulfilling these criteria are hypothesized to be those that are involved in gliomagenesis. These alterations are mainly observed in lower grade gliomas, in contrast to those that play important roles during progression (Otani *et al.*, 2017). Among the key genetic alterations that are important for the molecular classification of diffuse gliomas are *IDH1/2* mutations. These are often accompanied by different other alterations, which will be explained in the following.

1.4 Isocitrate dehydrogenases (IDHs)

Mutations in the isocitrate dehydrogenases type 1 and 2 (*IDH1/2*) were first described in large subsets of gliomas in 2008 (Balss *et al.*, 2008; Parsons *et al.*, 2008). Before that, only one study in 2006 had reported on a single $IDH1^{R132C}$ mutation in a cohort of eleven colorectal cancer samples (Sjoblom *et al.*, 2006). After 2008, the number of publications on *IDH* mutations and cancer has strongly increased. In the initiating study, 22 human GBM samples were screened for about 20,000 protein coding genes, from which five patients carried the highly specific point mutation $IDH1^{R132H}$ (Parsons *et al.*, 2008). Further studies showed that more than 70% of diffuse grade II and III gliomas and secondary GBMs display mutations in the *IDH1* gene (Balss *et al.*, 2008; Watanabe *et al.*, 2009; Yan *et al.*, 2009).

IDH1/2 mutations occur in different seemingly unrelated neoplasms such as gliomas, acute myeloid leukemia (AML), chondrosarcomas and cholangiocarcinomas (Amary *et al.*, 2011a; Mardis *et al.*, 2009; Wang *et al.*, 2013). In gliomas, *IDH1/2* mutations generally occur in younger adults (20-60 years) and are more common in grade II and III astrocytomas and oligodendrogliomas compared to GBMs (Bleeker *et al.*, 2009; Parsons *et al.*, 2008; Yan *et al.*, 2009). GBMs that arose from lower grade gliomas are called secondary glioblastomas. About 60-80% of these secondary GBMs exhibit a mutation. In contrast, de novo primary GBMs mostly do not have this mutation (Toedt *et al.*, 2011; Watanabe *et al.*, 2009; Yan *et al.*, 2009). More than 90% of the mutations involve *IDH1* and about 90% of these mutations are transitions of CGT to CAT in codon 132, resulting in a replacement of the arginine residue with a histidine ($IDH1^{R132H}$). There are also other point mutations at codon 132, resulting in different amino acid substitutions. In *IDH2* mutations homologous to those in *IDH1* occur in R172 (Ward *et al.*, 2010). *IDH1/2* mutations occur always heterozygously, by which the tumor always retains one wild type copy of the gene.

IDH1 occurs in the cytosol and peroxisomes and is encoded by the *IDH1* gene on chromosome 2q. It catalyzes the reversible oxidative decarboxylation of isocitrate to α-ketoglutarate (α-KG) thereby reducing $NADP^+$ to NADPH. The same reaction is catalyzed in mitochondria by IDH2, encoded by the *IDH2* gene on chromosome 15q (Stoddard *et al.*, 1993). Both enzymes function as homodimers and are important for cellular defense against oxidative damage and in the regulation of α-KG dependent dioxygenases (Hausinger, 2004; Jo *et al.*, 2002; Lee *et al.*, 2004; Lee *et al.*, 2002). In contrast, IDH3, functions as a heterotetramer in the tricarboxylic acid cycle. It catalyzes the irreversible conversion of isocitrate to α-KG producing of NADH (Figure 2) (Ramachandran and Colman, 1980). There appear to be no glioma specific mutations in the subunits of IDH3 (Krell *et al.*, 2011).

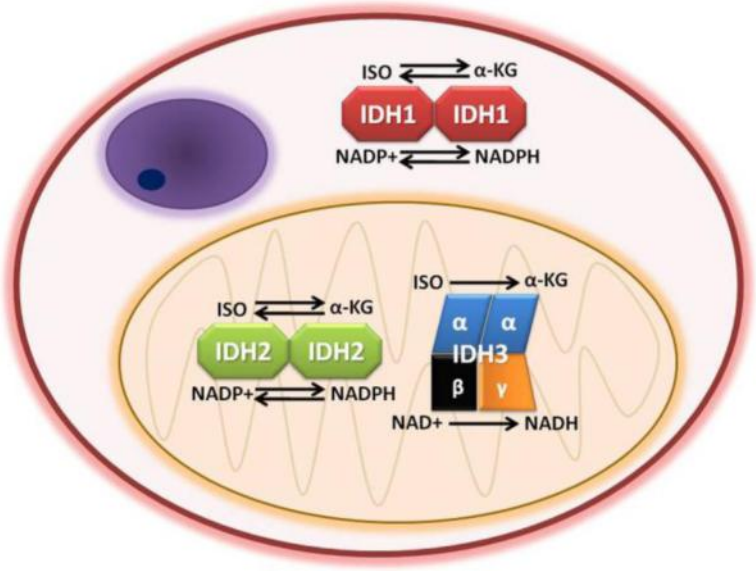

Figure 2. Overview about the cellular locations and function of IDH1, IDH2 and IDH3. IDH1 and IDH2 are homodimers whereas IDH3 appears as a heterotetramer, consisting of different subunits. All of the three enzymes oxidize isocitrate to α-KG. IDH1 and IDH2 use $NADP^+$ as a cofactor and generate NADPH. In contrast, IDH3 utilizes NAD^+ and produces NADH. IDH1 is located in the cytosol and also peroxisomes, whereas IDH2 and IDH3 appear in mitochondria. In general, IDH1 and IDH2 can convert α-KG back to isocitrate, but IDH3 works unidirectional only (Horbinski, 2013). (IDH = isocitrate dehydrogenase; ISO = isocitrate; α-KG = α-ketoglutarate)

IDH1/2 mutations always occur in the catalytic domain, targeting codons of essential argenins. This implies a mechanism of dominant inhibition or gain-of-function. Actually, both scenarios are reality. It could be shown that the R132H point mutation results in both, a loss of function and in a gain of a neoenzymatic activity of IDH1 (Dang *et al.*, 2010). Mutant IDH1 enzyme prefers to bind and reduce α-KG to D-2-hydroxyglutarate (2-HG), consuming

NADPH. It does not longer bind isocitrate and decarboxylates it to α-KG. Subsequently, it was shown that mutant gliomas have multi-fold elevated levels of 2-HG compared to their wildtype counterparts, with tissue concentrations of 10-30 mM. 2-HG production was also measured in other cancer types with different *IDH1* and *IDH2* mutations (Amary *et al.*, 2011b; Borger *et al.*, 2012; Gross *et al.*, 2010; Sellner *et al.*, 2010; Ward *et al.*, 2012; Ward *et al.*, 2010). Although all *IDH1/2*-mutant tumors produce 2-HG, the production varies dependent on the type of the mutation. The R132H type of IDH1 and R172 of IDH2 are the weakest 2-HG producers (Jin *et al.*, 2011). There appears to be an inverse correlation of the type of $IDH1^{R132}$ mutation with the amount of 2-HG produced (Pusch *et al.*, 2014). Thus, different types of *IDH1/2* mutations appear in different types of tumors with the respective production of 2-HG. As an example, there is a strong $IDH1^{R132H}$ preponderance in gliomas, whereas AMLs more likely harbor an *IDH2* mutation (Abbas *et al.*, 2010). In gliomas, when the R132C variant of *IDH1* could be detected, it tends to be found in astrocytoma, whereas mutations of *IDH2* appear more often in grade III oligodendroglioma (Hartmann *et al.*, 2009). These findings support the assumption that the amount of 2-HG produced depends on the tumor site, but might also somehow affect which kind of tumor is formed. In contrast to *IDH1/2* mutations, up until today no cancer-associated mutations of *IDH3* were described, probably because it might be difficult to gain a neoenzymatic function in a heterotetrameric complex via a single point mutation (Krell *et al.*, 2011).

1.4.1 The "oncometabolite" 2-HG

The dicarboxylic acid 2-HG has a chiral center and therefore two different enantiomers, (R)-2-HG and (S)-2-HG exist, which are also termed D- and L-2-HG (Figure 3). Both are unwanted byproducts of mitochondrial metabolism, with intracellular levels below 0.1 μM (Kranendijk *et al.*, 2012). D- and L-2-HG dehydrogenase (HGDH), catalyze the reaction of 2-HG to α-KG and are thus responsible to keep the concentration of 2-HG on this low level.

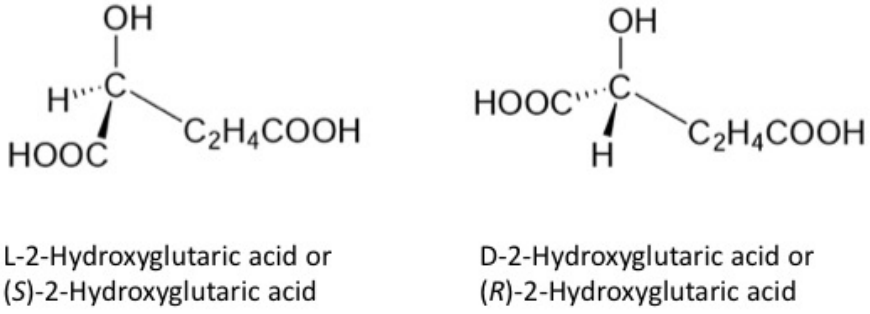

Figure 3. The two stereoisomers of 2-HG. Depiction of the two stereoisomeric forms of 2-HG, called S- and R-enantiomers, also denoted L and D isomer.

Prior to the studies on 2-HG, studies mostly focused on the metabolic disease 2-hydroxyglutaric aciduria. The disease is either caused by a deficiency in one of the two HGDH enzymes, resulting in an accumulation of the respective 2-HG, or by an *IDH* mutation. The later was detected in some cases with elevated 2-HG levels, but without a mutation in the HGDH genes, after the *IDH* mutations were described in tumors. In contrast, HGDH mutations do not occur in glioma (Brehmer *et al.*, 2011; Krell *et al.*, 2011). Patients suffering from D-2-HG aciduria suffer from encephalopathy with cardiomyopathy and dysmorphisms as well as developmental delay and hypotonia (Struys, 2006). L-2-HG aciduria patients were found to develop brain tumors, seizures and leukoencephalopathy (Steenweg *et al.*, 2010). IDH mutated tumors only produce the D-2-HG type isomer (Choi *et al.*, 2012; Dang *et al.*, 2010). It was shown that mutant cells secrete 2-HG into the extracellular space *in vitro* and *in vivo*, which might suggest that 2-HG also affects surrounding non-neoplastic cells (Dang *et al.*, 2010; Fathi *et al.*, 2012). Amongst others, the diverse effects of 2-HG are the generation of elevated ROS levels, inhibition of cytochrome c oxidase and ATP synthase and a lower rate of aerobic glycolysis (Latini *et al.*, 2005; Latini *et al.*, 2003). 2-HG blocks prolyl-hydroxylation of collagen that influences collagen maturation and finally leads to basement membrane aberrations (Sasaki *et al.*, 2012). However, various studies conducted during the last years implicate the epigenome as a critical target of 2-HG in cancer.

Histone methylation is a process of epigenetic control, whereby methyl groups are added to specific amino acid residues of histone proteins. This process regulates the chromatin state. These modifications affect e.g. genomic imprinting, DNA repair and gene expression (Tian and Fang, 2007). The metabolite 2-HG was found to inhibit α-KG-dependent Jumonji C (JmjC) domain-containing histone demethylases, such as JHDM1A, JMJD2A and JMJD2C, by competing with α-KG (Chowdhury *et al.*, 2011; Lu *et al.*, 2012; Xu *et al.*, 2011). In line with the inhibition of these demethylases, methylation of H3K9, H3K27 and H3K36 is increased when *IDH1/2* mutations are present (Lu *et al.*, 2012). In addition to blocking histone demethylases, 2-HG is also able to inhibit TET1/2 methylcytosine hydroxylases, which is important for DNA demethylation (Chowdhury *et al.*, 2011; Figueroa *et al.*, 2010; Xu *et al.*, 2011). Inhibition of DNA demethylation promotes global hypermethylation, influencing global gene expression (Figure 4). This phenomenon is commonly seen in neoplasms with *IDH1/2* mutations (Turcan *et al.*, 2012; Xu *et al.*, 2011). The glioma CpG island methylator phenotype (G-CIMP) describes this phenomenon in glioma (Noushmehr *et al.*, 2010). 2-HG alters global histone and DNA methylation promoting epigenetic rewiring,

which might promote tumorigenesis. Although 2-HG is often called oncometabolite, it is believed that the presence of 2-HG alone is not sufficient to induce gliomagenesis. Given the fact that 2-HG can inhibit cellular differentiation, mutant IDH1/2 might not be sufficient to induce an infiltrating, tumorigenic phenotype (Lu *et al.*, 2012). It rather creates an environment extending the opportunity for further tumor promoting mutations to occur in undifferentiated cells.

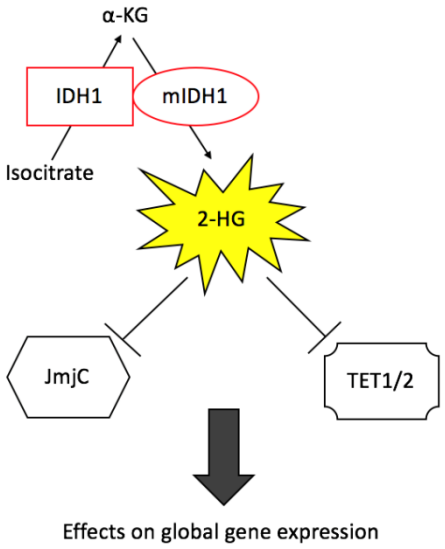

Figure 4. Production of 2-HG by mutant IDH1 alters gene expression. 2-HG produced from mutant IDH1 inhibits Jumonji C (JmjC) domain histone demethylases and methylcytosine hydroxylases (TET1/2). This leads to an increase of histone methylation and DNA hypermethylation. These alterations induced by IDH1 are proposed to increase proliferation accompanied by a decrease of cellular differentiation, which might be important during tumorigenesis.

1.4.2 Clinical features of *IDH*-mutant glioma

Tumors harboring an *IDH* mutation are preferentially located in the frontal lobes compared to *IDH* wild-type glioma. During imaging, *IDH*-mutant tumors do take up less contrast enhancing agent, except for the case that they are recurrent or of higher grade (Beiko *et al.*, 2014). This might be explained by the fact that the blood-brain barrier is more intact compared to patients with an *IDH* wild-type tumor.

IDH1^{R132H} and epilepsy

One of the initial symptoms in patients suffering from low-grade glioma is the occurrence of epileptic seizures (Chang *et al.*, 2008; van Breemen *et al.*, 2007). The frequency of seizures depends on histology as well as tumor grading and location. It was shown that patients with low-grade temporal, insular or frontal tumors have a predisposition to develop seizures

(Chang *et al.*, 2008; Stockhammer *et al.*, 2012). Seizure burden of glioma patients constitutes a major problem as it impacts cognitive function and decreases their quality of life (Klein *et al.*, 2003). Accordingly, there is a definite need to better understand epileptogenesis in a glioma background. Furthermore, there is an increasing number of studies describing the relation of seizure occurrence and a concomitant $IDH1^{R132H}$ mutation (Chen *et al.*, 2017b; Feyissa *et al.*, 2018; Kerkhof *et al.*, 2015; Li *et al.*, 2018; Neal *et al.*, 2018; Toledo *et al.*, 2017). Interestingly, seizures are not only a symptom of *IDH* mutant glioma but also occur in the metabolic disease L-2-HG aciduria, suggesting that 2-HG might impact epileptogenesis (Steenweg *et al.*, 2010; Stockhammer *et al.*, 2012). As 2-HG is secreted into the culture medium *in vitro* and the extracellular space *in vivo*, it might influence the surrounding non-neoplastic cells (Dang *et al.*, 2010; Fathi *et al.*, 2012). Additionally, 2-HG has a structural similarity with glutamate, which means that it might also bind to NMDA receptors. NR1/NR2A NMDA receptors are activated by 2-HG, examined in neuronal cultures (Kolker *et al.*, 2002). In line with this, it was found that there is an increased expression of NMDA receptors in the tumor area, consisting of NR1, NR2A and NR2B subunits, which is also the area of seizure initiation (Kohling *et al.*, 2006; Shamji *et al.*, 2009).These findings suggest that seizures in patients with an *IDH*-mutant glioma are not initiated due to tumor infiltration or mass effects, but rather points towards a direct effect of the extracellular 2-HG on the surrounding cells. However, little is known about this relation in patients yet, which might be examined by use of for example specific radio tracers that can be applied during imaging. Functional neuroimaging with positron emission tomography (PET) is commonly used as a tool for presurgical investigation of epileptic foci (von Oertzen, 2017). One of the well-known radiotracers is ^{18}F-fluorodeoxyglucose (FDG) to image glucose metabolism. It was shown that metabolic activity for glucose might be decreased in regions extending beyond the seizure onset zone until the contralateral hemisphere. Further, the severity of the seizure was correlated with a larger extent of hypometabolism (Hashiguchi *et al.*, 2007; Vinton *et al.*, 2007; Wong *et al.*, 2010). Propagation of interictal epileptic activity recorded by magnetoencephalography (MEG) determined with voxel by voxel analysis, corresponds to a reduced hypometabolism area detected in FDG-PET (Shibata *et al.*, 2017).

Detection

Although the understanding of *IDH1/2* mutations is incomplete, there is an urgent need in screening for their presence in the context of glioma classification according to the last WHO update described above. In addition, several glioma-mimicking diseases were shown not to be

associated with an *IDH* mutation, rendering this marker even more useful (Capper *et al.*, 2011). Due to the high frequency and discriminative power of the $IDH1^{R132H}$ mutation, extensive research was done to develop a mutation-specific monoclonal antibody for reliable detection on immunohistochemical samples (Capper *et al.*, 2010; Capper *et al.*, 2009). Even in biopsies with only a low number of glioma cells next to non-neoplastic tissue, the antibody reliably detects mutated cells (Sahm *et al.*, 2012a). Although this antibody is an excellent tool for the detection of $IDH1^{R132H}$ in samples, it cannot screen for rare IDH1 as well as IDH2 mutations. Thus, follow-up testing of immunonegative cases with methods such as PCR and Sanger sequencing is necessary. It was also shown that the high levels of 2-HG released by the tumor can serve as a biomarker detectable with an enzymatic assay from brain tumor biopsies or serum of AML patients (Balss *et al.*, 2012). Compared to standard detection methods such as mass spectrometry or magnetic resonance spectroscopy, this assay seems to be more sensitive and has cost and time advantages (Choi *et al.*, 2012; Sahm *et al.*, 2012b).

Prognosis

Tumors with an *IDH* mutation are less aggressive compared to their WHO grade-matched wild-type counterparts (Nobusawa *et al.*, 2009; Parsons *et al.*, 2008; Sanson *et al.*, 2009; Yan *et al.*, 2009). This is due to a large proportion of *IDH* wild-type astrocytomas representing underdiagnosed glioblastomas (Hasselblatt *et al.*, 2018). In contrast to grade III-IV *IDH* mutated tumors, grade III tumors lacking the mutations behave in the same aggressive way as wild-type grade IV tumors (Yan *et al.*, 2009). Moreover, patients harboring an *IDH* mutation are in general younger and have a better prognosis for survival (Hartmann *et al.*, 2010; Olar *et al.*, 2015). As an example, in the study of Olar et al. 558 grade II and III gliomas were analyzed and it was reported that the median survival of patients with an *IDH* mutation is 12.41 years (grade II) and 13.35 years (grade III), whereas it was only 4.82 years (grade II) and 1.97 years (grade III) for wild-type tumors (Olar *et al.*, 2015). Overall survival in patients with GBM harboring an *IDH* mutation (three years) versus non-mutated tumor (one year) is even worse (Hartmann *et al.*, 2010). Given the fact that 2-HG is believed to be an oncometabolite, it contradicts the survival benefit of patients harboring an *IDH* mutation. This could be explained by the lower median age of patients with the mutation and the concomitant metabolic changes leading to an enhanced chemo- and radiosensitive environment supporting effective treatment against these tumors (Houillier *et al.*, 2010). Meanwhile the classification of glioma underwent major changes and *IDH* mutations are now an essential diagnostic marker by which the tumors are distinguished (Louis *et al.*, 2016b). Based on this work,

tumors with and without *IDH* mutations are not compared to each other anymore because they are different entities.

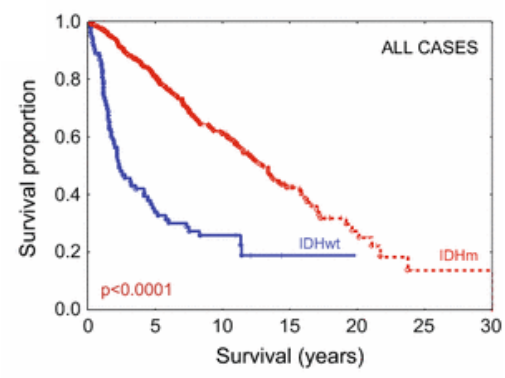

Figure 5. Kaplan-Meier estimate from a study of 558 pooled grade II and III diffuse gliomas. Discriminating between *IDH* wild-type and *IDH* mutated tumors shows a better overall survival in case of tumors with *IDH* mutation (Olar *et al.*, 2015).

1.4.3 Mutant IDH1 as therapeutic target

The high frequency and the fact that the *IDH* mutations appear in multiple tumor entities, provide a likely approach for targeted cancer therapy. Suppression of mutant IDH1 with a concomitant decrease in 2-HG led to inhibition of proliferation and a decrease of the clonogenic potential (Jin *et al.*, 2012). These data suggest that mutant IDH1 might be a valid therapeutic target.

Indeed, intensive research about IDH1 led to the development of inhibitors as for example BAY 1436032. This inhibitor was recently described as a pan-inhibitor that reduces 2-HG levels in cells carrying different *IDH1* codon 132 mutations. Orally administered BAY 1436032 significantly prolongs survival in a mouse model with transplanted human astrocytoma xenografts harboring the $IDH1^{R132H}$ mutation (Pusch *et al.*, 2017). Since 2016 this inhibitor is tested in clinical phase I/II trials.

Another approach to affect mutant IDH1 is the induction of antitumor immunity through a peptide-based vaccine targeting $IDH1^{R132H}$. It could be shown that $IDH1^{R132H}$ contains an immunogenic epitope that can be used for mutation-specific vaccination. Peptide vaccination of mice harboring human MHC class I and II presenting $IDH1^{R132H}$ peptide aminoacid 123-142, evokes a mutation specific antitumour immune response. As this *IDH* mutation exists in all tumor cells of the glioma, this mutation-specific anti-$IDH1^{R132H}$ vaccine seems to be a viable therapeutic strategy to treat these tumors (Schumacher *et al.*, 2014).

1.5 *IDH1* and secondary alterations in gliomagenesis

Mutations of *IDH1* appear during early stages of gliomagenesis, which is followed by additional genetic alterations. The below explained alterations commonly describe different tumor entities, namely oligodendroglioma and astrocytoma, which are the focus of this project.

TP53

TP53, is the gene encoding protein 53 (p53) and is involved in many different types of cancer. The p53 protein is an important cell-cycle checkpoint regulator between G_1/S and G_2/M transition. If cell cycle arrest and DNA repair was not successful, it triggers the apoptotic cell death pathway (Brown and Wouters, 1999). In further consequence, a knock-out of *TP53* would lead to missing DNA repair, allowing DNA damage to occur unimpeded and to a decrease in apoptosis. This scenario is well known for human cancers. Additionally, enhanced proliferation and accumulation of further mutations takes place. Most of the mutations are missense mutations, inducing an impaired function of p53 and are located on several spots in exons 4-10. As known for the two-hit theory of tumor suppressor genes, the allele on chromosome 17p next to the mutant allele is also mutated. Examining expression of p53 with immunohistochemistry is often used in diagnostics (Otani *et al.*, 2017; Takami *et al.*, 2015). *TP53* mutations are found in 25-30% of GBMs, >50% of astrocytomas and anaplastic astrocytomas (Ohgaki and Kleihues, 2011).

ATRX

Alpha-thalassemia/mental retardation syndrome X-linked (*ATRX*) is a gene located on the X chromosome q13 and encodes for the ATRX protein. ATRX plays an important role in chromatin remodeling and functions at the telomeres. Given the fact that *ATRX* is located on the X chromosome, a single inactivating mutation is sufficient for a complete loss of ATRX function. This loss of ATRX induces telomere destabilization, alternative lengthening of telomeres (ALT phenotype) and probably leads to genetic instability. Mutations of *ATRX* were detected in 33% of grade II and 46% of grade III gliomas, as well as in 80% of secondary and 7% of primary GBMs. This alteration overlaps with *IDH1/2* and *TP53* mutations across tumors of different WHO grades (Liu *et al.*, 2012). The mutation type of *ATRX* is either truncating mutations or missense mutations. Mutations can be detected with a negative staining in immunohistochemistry, serving as a surrogate marker in clinical practice (Liu *et al.*, 2012; Reuss *et al.*, 2015).

1p/19q Loss of heterozygosity (LOH)

A 1p/19q loss of heterozygosity belongs to the molecular signature of oligodendroglioma and appears in all of the cases (Louis *et al.*, 2016b). This particular location of the chromosomal arms originates due to an unbalanced translocation with a break point in the area of the centromeres. In a cohort of 764 gliomas, genome-wide characterization revealed that all tumors with a complete 1p/19q co-deletion are mutated on either *IDH1* or *IDH2* (Labussiere *et al.*, 2010). Whole exome sequencing studies analyzed the genes that are affected by the translocation. It was found that inactivating mutations of the tumor suppressor genes *FUBP1*, located on chromosome 1p, and *CIC*, located on chromosome 19q, appear subsidiary to the co-deletion (Bettegowda *et al.*, 2011; Sahm *et al.*, 2012c). Mostly, gliomas harboring a 1p/19q co-deletion present morphological features of oligodendroglioma and are associated with sensitivity to chemo- and radiation therapy in addition to a better prognosis (Cairncross *et al.*, 2013).

CIC

The Drosophila Capicua (cic) HMG-box repressor is a key sensor of receptor tyrosine kinase (RTK) signaling in both *Drosophila* and mammals. Recent evidence suggests that CIC affects RTK-dependent responses, which are linked to cell proliferation and cancer (Tseng *et al.*, 2007). The repressive function of CIC to the downstream targets of the RAS/MAPK pathways points towards a role as a tumor suppressor gene in carcinogenesis. *CIC* is altered in the majority of oligodendrogliomas by somatic mutations and insertions/deletions (Bettegowda *et al.*, 2011; Yip *et al.*, 2012). About 70% of oligodendrogliomas harbor a *CIC* mutation whereas it is only very rarely found in astrocytomas (Sahm *et al.*, 2012c; Yip *et al.*, 2012). It is believed that *CIC* mutations in association with *IDH1* mutations cooperatively regulate tumorigenesis (Jiao *et al.*, 2012; Sahm *et al.*, 2012c). In line with this, a cooperative increase of intracellular 2-HG level was reported. This led to a reduction of clonogenicity and slower proliferation in the cell lines. However, it remains unclear how this regulates or fosters tumorigenesis *in vivo* (Chittaranjan *et al.*, 2014).

pTERT

Telomerase reverse transcriptase (TERT) is the catalytic site of the telomerase complex and upregulation of TERT increases telomerase activity. This ability is an essential criterion for cancer cells, as it allows indefinite extension of the telomeres and by this, immortalization. Mutations located in the promoter region of *TERT* (*pTERT*) were first described in melanoma

and were later discovered in glioma as well. *pTERT* mutations do occur almost always at one of two hot spots as C to T transitions and the frequency of mutations depends on the type of glioma. Mutations are often found in primary GBM and oligodendroglioma but rarely in diffuse and anaplastic astrocytoma. Both telomerase activity affecting mutations, *ATRX* and *pTERT*, occur mutually exclusive in glioma (Arita *et al.*, 2013; Horn *et al.*, 2013).

1.5.1 Association of *IDH* mutations with *TP53* and *ATRX* mutations in astrocytoma

IDH1 mutations are believed to occur before *TP53* or 1p/19q co-deletions and they are strongly associated with both alterations. A high percentage of grade II and III diffuse astrocytomas and secondary GBMs harbor mutations of the *TP53* gene. The percentage for *IDH* mutated infiltrating astrocytomas with this secondary alteration is even higher. In diffuse astrocytomas (WHO grade II), 63% contain an alteration of *TP53* and an *IDH1* mutation (Watanabe *et al.*, 2009). Furthermore, in a series of 939 tumors, 80% of anaplastic astrocytomas WHO grade III) harboring an *IDH* mutation also have a *TP53* mutation.

The combination of *IDH1* and *TP53* mutation is associated with inactivating mutations of *ATRX*. 363 brain tumors with different histology were analyzed for *ATRX* mutations. They occurred most frequently in grade II and III astrocytomas (67%) and secondary GBMs (57%). In contrast, the alterations did only occur in low percentages in primary GBMs (4%), oligodendroglial tumors (14%) and pediatric GBMs (20%). Except from one tumor, all infiltrating gliomas harboring an *ATRX* alteration additionally had an *IDH1* mutation. Of those tumors, 94% exhibited an alteration in *TP53*. An ALT phenotype could be associated with 98% of the tumors with an *ATRX* mutation and a concomitant *IDH1* mutation. Thus, *IDH1* mutant astrocytomas show a common molecular signature with *TP53* and *ATRX* mutations and are often associated with ALT (Figure 6) (Jiao *et al.*, 2012).

1.5.2 Association of *IDH* mutations with 1p/19q co-deletions in oligodendroglioma

1p/19q co-deletions and *IDH* mutations are defining oligodendroglioma and are mutually exclusive with the molecular signature of astrocytoma, which is *IDH*, *TP53* and *ATRX* mutations. Patients with oligodendroglial tumors bearing the 1p/19q co-deletion and *pTERT* mutations usually have a better prognosis compared to astrocytomas. In a study with heterogeneously treated patients, median overall survival was eight years (Jiao *et al.*, 2012). In summary, the molecular signature describing oligodendroglioma consists of *IDH* as well as *pTERT* mutations and the co-deletion of the chromosomal arms 1p/19q (Figure 6).

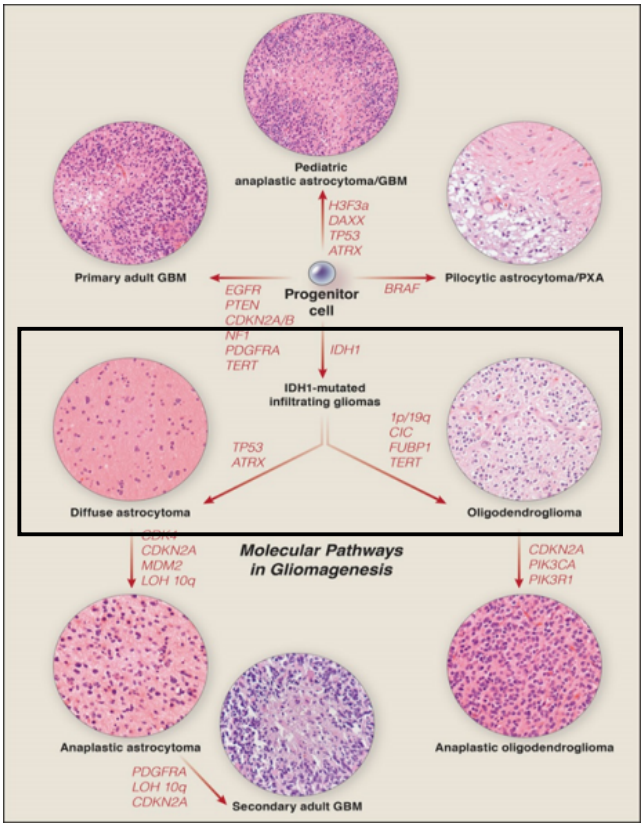

Figure 6. Overview of the altered genes that define different subgroups of gliomas. The black box indicates the molecular alterations important for this project having major implications for the development of astrocytoma and oligodendroglioma. AA = anaplastic astrocytoma, GBM = glioblastoma, PXA = pleomorphic xanthoastrocytoma. Modified from (Appin and Brat, 2015).

The knowledge on molecular alterations defining astrocytoma and oligodendroglioma was essential in defining the aims of the study as described below.

1.6 Aims of the study

The overall aim of this project was to develop a mouse glioma model based on neural stem cells (NSCs) that derive from conditional Idh1^{R132H} knock-in mice. Regarding the different molecular landscapes of glioma subtypes, stem cells were prepared that harbor specific secondary mutations. Subsequently, the *in vitro* behavior of those cells was compared to the single mutants. Next, intracranial injections were performed with the murine neural stem cells into immunodeficient mice. Objectives of this project were as follows:

1. NSCs will be established harboring the conditional knock-in Idh1^{R132H} mutation and/or additional p53$^{-/-}$ mutations. Validation of the respective cell lines will be performed and effects of the mutations examined on functional level.

2. A conditional Cic knock-out mouse model will be established and NSCs produced from these mice. After validation, the knock-out of Cic will be investigated alone and in the presence of $Idh1^{R132H}$ on functional level.
3. Next, intracranial injections will be performed with the established NSCs having the glioma lineage-defining mutations.
4. The maximal observation duration of tumor growth monitored by regular MRI investigations will be one year post NSC injection. Afterwards, all tumor samples will be characterized on histological level and compared to the hallmarks of human glioma subtypes.
5. Due to its close correlation in patients, the co-occurrence of $Idh1^{R132H}$ and epileptic seizures will be investigated with functional imaging.

2 Materials & Methods

2.1 Matings of mice with different conditional alleles

For the generation of NSCs, mice with different genotypes were crossed to yield littermates with the desired combination of conditional alleles. First, Idh1PM/flex (B6-Idh1tm1(R132H)Avd/N) mice with a Bl6/N background, carrying the homozygous conditional Idh1^{R132H} allele, were mated with mice harboring the heterozygous Rosa CreERT2 transgene (B6;129-Gt(ROSA)26Sortm1(cre/ERT2)Tyj). Consequently, littermates carried the heterozygous Idh1^{R132H} mutation with the heterozygous Rosa CreERT2 transgene or were non-inducible controls. To yield the genetic alterations that were described in astrocytoma, the heterozygous Idh1PM/flex and Rosa CreERT mice were crossed with mice carrying the homozygous *Tp53* floxed alleles (Trp53tm1Brd). Prior to NSC generation, matings were scheduled where mice carrying the heterozygous Idh1^{R132H} allele, the heterozygous Rosa CreERT2 transgene and the homozygous *Tp53* floxed allele were crossed with mice harboring the homozygous *Tp53* floxed allele only. As a result, littermates always carried the homozygous *Tp53* floxed alleles either with or without the Idh1^{R132H} allele and were either inducible or not, serving as negative controls.

2.2 Generation of Cic flox mice

Attempts to mate homozygous Cic flox mice (JM8-Cictm1a(KOMP)Wtsi) resulted in small litters and genotyping has shown that no homozygous littermates were born at all. After searching for possible reasons, it was found that the original ES constructs were incorrectly annotated. Obviously, the flippase recognition target (FRT) cassette containing e.g. the resistance gene was still present in the cells and homozygous expression is lethal in mice. To get rid of the resistance cassette, homozygous *Cic* mice were crossed with flippase (Flp) mice, expressing the recombinase flippase, which mediated the recombination of the FRT sites. Prior to the next matings, littermates were genotyped to check for successful recombination and in a next step, mice were crossed in order to eliminate Flp again to finally yield the correct *Cic* construct.

Subsequently, for the generation of neural stem cells with the common genetic alterations of oligodendroglioma, matings were started with mice carrying the heterozygous Idh1^{R132H} allele, the heterozygous Rosa CreERT2 transgene and the homozygous *Cic* floxed alleles and mice carrying the homozygous *Cic* floxed alleles only. Also in these matings, littermates carried single as well as double mutants and the respective controls.

2.3 Chemicals

If not otherwise mentioned, all standard chemical products were purchased from Sigma Aldrich.

2.4 Genotyping

Tail DNA isolation was performed with the SampIN™ Direct PCR Kit (highQu, DPK0105) according to manufacturer's protocol. After adding 50 µl of the lysis buffer and protease buffer mastermix, tails were first lysed for 5 min at 75 °C. Subsequently, tubes were vigorously vortexed once and further incubated for 10 min at 95 °C. Addition of 450 µl PCR H_2O and a 1 min centrifugation step at max rpm (Eppendorf, 5415R) was carried out before supernatant could be applied for genotyping PCRs. Exact concentration of extracted DNA was measured with NanoDrop (PeqLab) and approximately 100 ng were applied for PCR. If genotyping of cell lines was performed, DNA was extracted with the NucleoSpin Tissue Kit (Macherey-Nagel), according the manufacturer's protocol. PCRs were conducted with the Allin TM HS Red Taq polymerase, which is also part of the highQu kit. The PCR approach was adjusted dependent on the gene of interest and the combination of primers needed (Table 1), as well as the annealing temperature (AT) and the elongation time (ET) of the PCR program (Table 2). Thermocycling was carried out with a T-personal 48 PCR machine (Biometra).

Table 1. PCR approach for genotyping. Calculation was adjusted according to the combination of primers.

2x Allin TM HS Red Taq	10 µl
Primer I-IV	each 1 µl
DNA	1 µl
H_2O	ad 20 µl

Table 2. Thermocycling conditions for genotyping. Annealing temperature and elongation time were adapted according to the respective primers. Black arrow indicated number of cycles.

95 °C	2 min
95 °C	15 s
Annealing temperature (adjusted)	15 s
72 °C	Elongation time (adjusted)
20 °C	∞

35x

Subsequently to PCR, the whole sample (20 µl) was loaded onto a 2% agarose gel (AXYGEN Bioscience) with ethidiumbromide (Roth). Low range DNA ladder was used (Fast Ruler, Thermo Scientific) as size marker.

Table 3. Overview of all genotyping PCRs and specificities. Respective primers are listed in supplement table 2.

Genotype	Primer	AT (°C)	ET (s)	Cycles	Gel (min)	Wild-type (bp)	Mutant (bp)
$Idh1^{R132H}$	P259/262	58	9	35x	90	529	600 (targeted allele)
p53 flox	P307/308	66	5	35x	65	270	350 (targeted allele)
Rosa	P268/269 /270	55	5	35x	40	603 (P268/269)	800 (P268/270, P270 is located in Cre)
Cic	P636/638	58	9	35x	60	551	769 (targeted allele)
Flp I	P643/644	58	9	35x	60	-	725 (P643/644 both bind to Flp)
Flp II	P645/646	58	9	35x	60	324	-
FRT control I	P636/637	56	5	35x	60	-	383 (only if NeoR is removed)
FRT control II	P636/404	58	9	35x	60	-	401 (only if NeoR is removed and recombination ensued)

2.5 Preparation of neural stem cells

Newborn mice were sacrificed on day P1 with decapitation. In the following, heads were collected in falcon tubes with 5 ml ice-cold phosphate buffered saline, PBS (Gibco) and the respective tails were kept in tubes for genotyping purposes. Under sterile conditions, the whole brain was removed, the cerebellum was discarded and the cerebrum was chopped into fine pieces with a scalpel. For subsequent enzymatic dissociation, material was collected in a falcon tube containing 5 ml sterile filtered Papain Dispase DNase (PDD) solution. Enzymatic dissociation was performed for 30 min at room temperature on a rolling incubator.

Table 4. Recipe for preparation of the PDD solution. After solving of the supplements, solution was sterile filtered and stored at -20 °C.

Supplement	Concentration / Volume added	Company
Hank's balanced salt solution (HBSS), without Mg^{2+} and Ca^{2+}	100 ml	Gibco
$MgSO_4$	12.4 mM / 149 mg	AppliChem
Papain	0.01% / 370 µl	Sigma-Aldrich P-3125
Dispase 2	0.1% / 100 mg	Roche 165859
DNase	0.01% / 1 ml	Roche 1284932

After incubation, suspension was centrifuged for 5 min at 800 rpm. Supernatant was removed and the remaining pellet was washed and resuspended in 1 ml PBS. This was performed twice. Thereafter 1 ml of Neurobasal medium (Gibco) with supplements was added to the pellet and it was dissociated by pipetting up and down with a 1 ml tip. Finally, dissociated cells were transferred into T25 ultra-low attachment flasks (Corning, 3815), containing 5 ml Neurobasal medium (Table 5). Cells were kept under standard cell culture conditions (Neurobasal medium, 37 °C, 5% CO_2).

Table 5. Recipe for Neurobasal medium for NSC cultivation. The listed supplements were added to 500 ml of Neurobasal medium.

Supplement	Concentration	Company
B27 Supplement	5%	Gibco
GlutaMAX	1%	Gibco
Murine EGF	20 ng/ml	Peprotech, 315-09
Murine basic-FGF	20 ng/ml	Peprotech, 450-33
Penicillin/Streptomycin	1%	Gibco

2.6 Passaging and induction of genetic alterations

All newly prepared NSCs were cultured under standard cell culture conditions as described above. After preparation, cells were incubated until neurospheres were clearly visible. For passaging, cell suspension was transferred into a falcon tube and neurospheres were allowed to descend until a pellet was visible. The supernatant, containing single cells and dead cells, was discarded leaving behind 1 ml. Using a 1 ml pipette, neurospheres were mechanically dissociated by pipetting up and down. For standard passaging, the 1 ml single cell suspension was filled back into the culture flask, containing about 5 ml fresh Neurobasal medium.

For the induction of the genetic alterations via the Cre recombinase system, 1 µM 4-Hydroxytamoxifen (4-OHT, Sigma-Aldrich) was directly added to the cell culture medium after passaging of the cells. To make sure that the time of treatment was sufficient, 4-OHT remained in the culture medium for one week. An exception for this was the induction of the knock-out of *Cic*. Given the fact that the genomic region that has to be recombined is fairly large, treatment with 4-OHT was carried out twice. This strategy led to successful induction of the knock-out. Before the start of the experiments, all induced cell lines were checked for induction with Western blot, PCR as well as immunohistochemistry.

For preparation of the cells for the respective assays, cells were counted with a Spector 2.0 Handheld Automated Cell Counter (Merck Millipore).

2.7 Proliferation assay

The CellTiter-Glo 3D Cell Viability Assay (Promega, G9683) was used to analyze the proliferative capacity of the cells. This assay is designed to analyze cell viability in spheroids growing in 3D cultures. The reagent of this assay permeates large spheroids. The CellTiter-Glo 3D reagent allows the luminescent measurement of the ATP levels, which serve as an indicator for cell viability. ATP is released by cell lysis and is used by Luciferase to generate a luminescent signal that correlates with the number of viable cells in the respective culture or microtissue. The CellTiter-Glo 3D Cell Viability Assay was performed in 96-well plate (Corning, 353296) format with 5000 cells per well, containing 100 µl of medium in total (unless otherwise described). Cells were seeded in eight replicas and induced cell lines were always compared to non-inducible controls. Cell viability measurements were carried out after indicated incubation times, which was mainly on day 0, 3 and 5. On the respective day of the experiment, 100 µl of the CellTiter-Glo 3D reagent was pipetted into each well and the 96-well plate was mixed while shaking at room temperature for 6 min. In the following, the luminescent signal was detected with a FLUOstar Omega plate reader (BMG Labtech).

2.8 SDS-Page and Western blot

For Western blot experiments, unless otherwise described, 300 µl cell suspension from induced cells and their respective controls were transferred into Eppendorf tubes. After centrifugation at 1000 rpm for 3 min, cell pellet was washed with 500 µl PBS and centrifugation was repeated at 3000 rpm. Next, supernatant was discarded and pellets were resuspended in 60 µl NP40 lysis buffer (150 mM NaCl, 50 mM Tris-HCl, 0.1% Nonidet-P40

(biomol), pH 8.0) + protease inhibitor cOmplete mini, EDTA-free (Roche)). Lysis was carried out by three freeze-and-thaw cycles. Centrifugation at 11000 rpm for 10 min was used to remove the residual debris. The supernatant containing the isolated proteins was collected in a new tube. For exact measurement of the protein concentration, a bicinchoninic acid (BCA) assay was performed. This assay was carried out using the Piece Protein Assay Reagent (Thermo Scientific) according to manufacturer's protocol. The fluorescent signal was detected after 30 min incubation at 37 °C with a FLUOstar Omega plate reader (BMG Labtech). Samples were prepared in PCR tubes (Biozym), containing 5 µl of 4x LDS sample buffer (NuPAGE Novex system, Thermo Scientific), 2 µl of 10x Sample reducing agent (NuPAGE Novex system, Thermo Scientific), 30 µg protein and water ad 20 µl. Samples were quickly spun down and incubated at 96 °C for 5 min. Afterwards, tubes were quickly put on ice before the whole sample was loaded on ready-to-use 4-10% Bis-Tris protein gels (Invitrogen). SDS-PAGE chamber (X Cell Sure Lock, Invitrogen) was filled with MOPS buffer (NuPAGE Novex system, Thermo Scientific) and gel was running for 60 min at 200 V. However, if proteins of interest were smaller than 20 kDa, MES (NuPAGE Novex system, Thermo Scientific) instead of MOPS buffer was used. Afterwards, the gel was transferred onto a 0.45 µm nitrocellulose membrane (for proteins smaller than 20 kDa, 0.22 µm, Invitrogen), with a semidry-blotting device (FastBlot B44, Biometra) for 60 min and 100 mA per gel. To check for the transmission of the protein, a Ponceau S (AppliChem) staining was performed for 2 min, before membrane was blocked. Blocking was performed with 5% milk powder (AppliChem) dissolved in Tris-buffered saline-Tween, TBS-T (TBS, AppliChem; 0.05% Tween, Fisher Scientific) at room temperature for 60 min while shaking. This step was followed by overnight incubation with primary antibodies at 4 °C (Table 7). Primary as well as secondary antibodies were diluted in 5% milk/TBS-T. After overnight incubation, secondary antibodies were incubated for 60 min at room temperature. Washing in between the different steps was always done three consecutive times for 10 min with TBS-T. If proteins of interest were very large (>140 kDa), protein was loaded onto 3-8 % Tris-Acetate gels (Invitrogen) and Tris-Acetate buffer (NuPAGE Novex system, Thermo Scientific) was used during gel electrophoresis. Subsequently, wet-blotting was performed instead of semidry blotting. To do so, protein gel and a 0.45 µm nitrocellulose membrane was embedded into a wet blot chamber (X Cell II Blot Module, Invitrogen) in between eight sponges and filled with transfer buffer (Table 6). After blotting for 60 min at 220 mA, the protocol was further carried out the same way as described above for smaller proteins.

Table 6. Recipe for preparation of transfer buffer. For Western blot analysis of proteins smaller than 140 kDa, 5 ml 10% SDS was also added.

Supplement	Volume added	Company
20x Transfer buffer	50 ml	NuPAGE Novex system, Thermo Scientific
Methanol	100 ml	Sigma-Aldrich
Antioxidant	1 ml	NuPAGE Novex system, Thermo Scientific
	Ad 1 l	

Table 7. Primary antibodies used for Western blot experiments. Antibodies were diluted in 5% milk/TBS-T and incubated at 4 °C overnight while rolling.

Antibody	2nd Antibody	Dilution for WB	Clonality	Size (kDa)	Company
β-Actin	rabbit	1:1000	monoclonal	42	Cell Signaling
$IDH1^{R132H}$	mouse	1:300	monoclonal	47	Dianova
p53	mouse	1:300	monoclonal	53	Cell Signaling
CIC	rabbit	1:1000	polyclonal	164	Abcam
Cleaved Caspase 3	rabbit	1:300	polyclonal	17, 19	Cell Signaling
Cleaved Caspase 7	rabbit	1:300	polyclonal	20	Cell Signaling
Cleaved PARP	rabbit	1:300	polyclonal	89, 116	Cell Signaling
P-Histone H2AX	rabbit	1:500	monoclonal	15	Cell Signaling
H2A	mouse	1:500	monoclonal	14	Cell Signaling

Table 8. Secondary antibodies used for Western blot experiments. Antibodies were diluted in 5% milk/TBS-T and incubated at room temperature for 60 min while rolling. By use of fluorescent antibodies, incubation was carried out in the dark.

Antibody	Species reactivity	Dilution for WB	Company
Goat anti-mouse IRDye 680RD, 700 nm	mouse	1:10000	LI-COR Biosciences
Goat anti-rabbit IRDye 680RD, 700 nm	rabbit	1:10000	LI-COR Biosciences
Goat anti-mouse IRDye 800CW, 800 nm	mouse	1:10000	LI-COR Biosciences
Goat anti-rabbit IRDye 800CW, 800 nm	rabbit	1:10000	LI-COR Biosciences
Anti-rabbit IgG HRP-linked Antibody	rabbit	1:4000	Cell Signaling
Anti-mouse IgG HRP-linked Antibody	mouse	1:4000	Cell Signaling

Western blot analysis was performed after incubation with either HRP-linked antibodies or fluorescent antibodies with a LI-COR Odyssey Fc imaging system (LI-COR Biotechnology). Prior to development of the blot, HRP substrate LumiGLO Reserve chemiluminescent substrate (KPL) was added to the membrane, incubating for 2 min, when HRP-linked antibodies were used. Afterwards, exposure time of the imaging system was 10 min for these

antibodies and 2 min for fluorescent antibodies respectively. The used secondary antibodies are listed in table 8.

2.9 Reverse transcription PCR

Reverse transcription PCRs were performed to analyze the knock-out of *Cic* on RNA level. Before cDNA was synthetized, RNA was extracted from 300 µl cell suspension following the manufacturers protocol, with the NucleoSpin RNA Kit (Macherey-Nagel). RNA concentration of the samples was measured with Nano Drop and 1 µg was used for subsequent cDNA synthesis. Protocol for cDNA synthesis was carried out following manufacturers protocol belonging to the Revert Aid H Minus First Strand cDNA Synthesis Kit (Fermentas), with some adjustments. In a first step, 1 µg RNA was added to 0.2 µg random hexamer primer and nuclease-free water ad 11.5 µl. After incubation for 5 min at 65 °C, samples were placed on ice. The following steps were carried out as per protocol, adapted to random hexamer primers. Subsequently, PCR for detection of *Cic* was carried out with GoTaq G2 DNA polymerase (Promega) as listed in table 9.

Table 9. Reaction setup for GoTaq G2 polymerase-mediated PCR amplification.

Component	25 µl reaction
GoTaq DNA polymerase	12.5 µl
10 µM forward primer (P714 or 716)	1.25 µl
10 µM reversed primer (P715 or 717)	1.25 µl
template cDNA	1 µl
nuclease-free water	9 µl

The reaction components were gently mixed and quickly spun down before tubes were transferred to a PCR machine. Thermocycling was adapted due to annealing curves analysis and elongation times suitable for the primers chosen, before the final protocol was carried out as listed in table 10.

Table 10. Thermocycling conditions for GoTaq polymerase-mediated PCR amplification. * was adapted due to the *Cic* primers chosen. Black arrow indicates number of cycles.

98 °C	30 s
98 °C	5 s
52 °C*	10 s
72 °C	30 s*
72 °C	2 min
10 °C	∞

30x

2.10 Soft agar assay

The CellTiter-Blue Cell Viability Assay (Promega, G9683) was used to measure the colony formation rate in an anchorage-independent manner. This assay is a single treatment assay, measuring cell viability using a redox indicator dye resazurin, which allows examining colony formation rate using fluorescence. Viable cells are able to carry out the reduction of resazurin to the fluorescent product resorufin, which dead cells do not, due to membrane damage. After this reaction has taken place, resorufin leads to a strong increase in fluorescence, which is directly proportional to the number of viable cells. Fluorescence measurements after conversion to resorufin were carried out at the excitation and emission peaks 579 nm and 584 nm respectively. Before cells could be seeded, the following 2x and 4x media were prepared in 50 ml Neurobasal medium (for information about the respective supplements, see table 5).

Table 11. Preparation of 2x and 4x medium for soft agar layers. The respective supplements were diluted in 50 ml Neurobasal medium in total.

Supplement	2x Medium	4x Medium
B27 Supplement	2 ml	4 ml
GlutaMAX	1 ml	2 ml
Murine EGF	20 µl	40 µl
Murine bFGF	20 µl	40 µl
Penicillin/Streptomycin	1 ml	2 ml

In addition, 4x agar was prepared and for this purpose, 2.8 g low-gelling agarose (Sigma-Aldrich) was slowly diluted during boiling up in a microwave and stirring in between. Before cells could be seeded, the freshly prepared 4x agar was diluted 1:1 with 2x medium (both at 44 °C) and 50 µl was pipetted into each well of the 96-well plate (Greiner, 655976). Plates were left at 4 °C overnight before preparation of the cell dilutions. For preparation of the next agar layer, bottom layer agar was prepared at 44 °C as explained above and cell suspensions,

finally containing 2000 cells/well, were prepared in 37 °C pre-warmed 2x medium. Immediately before seeding, cell suspension was mixed with bottom layer agar 1:1 and gently mixed with a pipette. In the following, cells were seeded in eight replicas and induced cell lines were always compared to non-inducible controls. Wells in which air bubbles were clearly visible, or in which any of the agar layers was accidentally touched with a pipette tip, were excluded from experiments. After seeding, plates were allowed to cool down for 30 min at room temperature before 50 µl of 4x medium was added per well. Subsequently, plates were incubated for 24 h at 37 °C before a final layer containing 50 µl normal Neurobasal medium was also added (Figure 7).

Cell viability measurements were carried out after seven days of incubation at 37 °C. On the respective day of the experiment, 40 µl of the CellTiter Blue reagent was added to each well and the 96-well plate was further incubated at 37 °C for eight hours. In the following, the fluorescent signal was detected with a FLUOstar Omega plate reader (BMG Labtech).

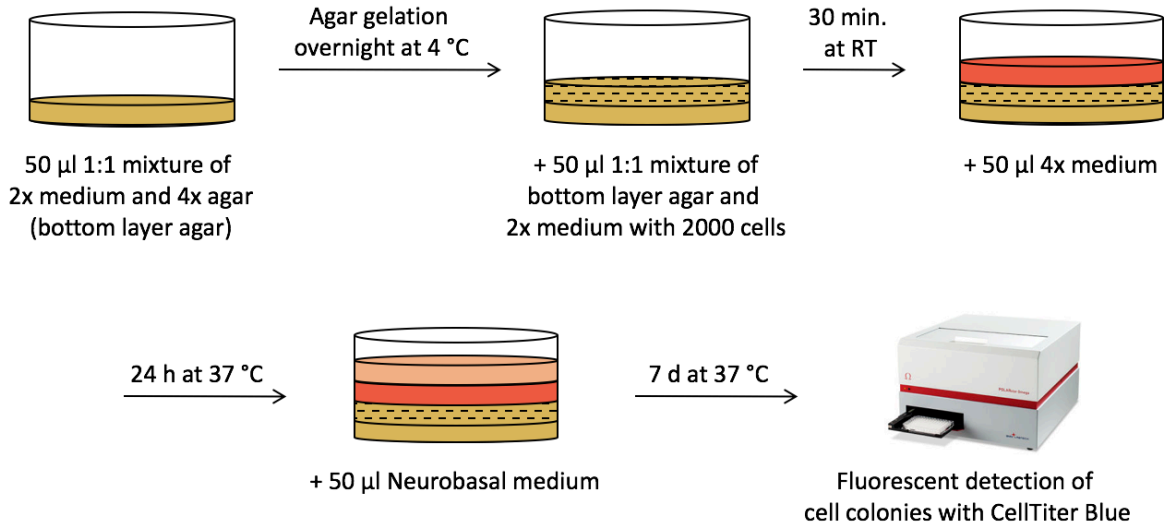

Figure 7. Schematic representation of the soft agar assay. Details and quantities are given per well. RT = room temperature.

2.11 2-HG assay

The concentration of 2-HG present in either supernatant or cell lysates was measured by an enzymatic quantification assay, which was developed in the Department of Neuropathology at Heidelberg University (Balss *et al.*, 2012).

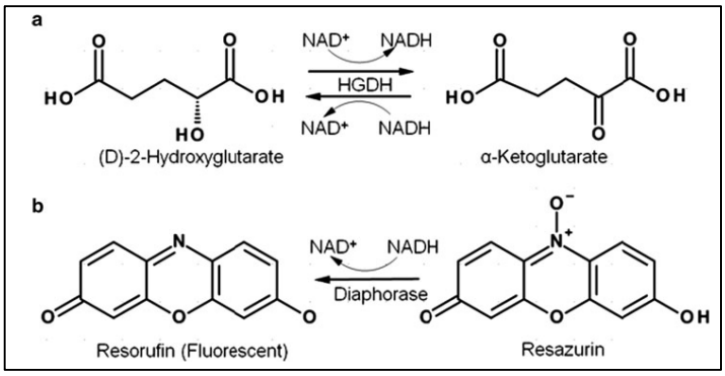

Figure 8. Schematic of the 2-HG quantification assay. a) 2-Hydroxyglutarat dehydrogenase (HGDH) catalyzes the conversion of 2-HG to α-KG and the reduction of NAD^+ to NADH. b) The level of NADH is detected by the conversion of resazurin to resorufin, catalyzed by diaphorase. Resorufin as a fluorescent product is excited at 540 nm and subsequently detected at 610 nm (Balss *et al.*, 2012).

The enzyme HGDH catalyzes the oxidation of 2-HG to α-KG and the simultaneous reduction of NAD^+ to NADH (Figure 8). NADH is used by the enzyme diaphorase to convert resazurin to the fluorescent resofurin. By this the amount of 2-HG in the probe linearly correlates with the resofurin signal measured.

To quantify 2-HG in the supernatant, 500,000 cells were seeded per well in 6-well ultra-low attachment culture plates (Corning) and grown for four days before harvesting. The content of each well was transferred into Eppendorf tubes and centrifuged for 5 min at 1000 rpm. To detect intracellular 2-HG levels, cell pellets were washed with PBS and subsequently lysed in 125 µl of NP40 buffer, as described in chapter 2.8. Before the measurement, 25 µl perchloric acid (PCA) was added to 100 µl of the sample and 5 min incubated on ice to precipitate proteins and metabolites that would otherwise disturb the assay. Next, the samples were centrifuged at 14,000 rpm for 7 min. Subsequently, 100 µl of the supernatant were transferred to new tubes, already containing 5 µl of neutralization solution (BioVision, Deproteinizing Sample Preparation Kit, K808-200). Incubation on ice and centrifugation was repeated once and supernatants were transferred to new tubes. A serial dilution from 0 to 500 µM 2-HG diluted in standard Neurobasal medium served as a standard. The assay was carried out in 96-well plates (BRANDplates, 781608) and technical triplicates. 75 µl of the prepared master mix was used per well. The master mix contained 100 mM HEPES pH 8 (AppliChem), 100 µM NAD^+ (AppliChem), 0.01 µg/µl HGDH (produced by Jessica Eisel, as described in (Balss *et al.*, 2012)), 0.01 U/ml diaphorase (MP Biomedical) and 125 µM resazurin (AppliChem), diluted in H_2O. 25 µl of the respective samples was added per well. The reaction was

incubated in the dark for 15 - 60 min at room temperature. Afterwards, fluorescence was measured with the FLUOstar Omega reader at 540 nm and 610 nm excitation and emission respectively.

2.12 Dotblot

The dotblot method was chosen to investigate whether the different alterations induce differences in DNA methylation. For this purpose, DNA was blotted onto a membrane and levels of 5-methylcytosine (5mC) and 5-hydroxymethylcytosine (5hmC) were analyzed with the respective antibodies. DNA concentrations for dotblot experiments were measured precisely with the QUBIT dsDNA BR assay (Thermo Scientific) after 10 min of sonification. This assay was applied, because it detects DNA and not RNA by specific intercalation into double-stranded DNA. Analysis was performed in duplicates and a standard row of 0, 1, 5, 10 and 20 ng/µl control DNA was used. Samples were measured with the FLUOstar Omega plate reader at 485 nm and 530 nm. For further sample preparation, DNA was denatured (2mM NaOH, 50 mM EDTA) for 10 min at 95 °C and afterwards neutralized (2M Ammoniumsulfate, pH 7) for 10 min on ice. Serial dilutions in TE-buffer were prepared on ice from 1000 ng to 31.25 ng. Subsequently, 50 µl of all samples in duplicates were loaded onto a nylon membrane (GE Healthcare, positive charged transfer membrane, RPN 203B), which already had been fixed in the dotblot apparatus (BioRad). After application of vacuum inducing the blotting process, membranes were washed, baked at 80 °C for 2 h (Jouan) and air dried overnight. Before incubation with antibodies, membrane loading was assessed with methylene blue. Blocking of the membrane was done as explained in section 2.8. Incubation with primary (Table 12) as well as secondary antibodies (Table 8) were both done for 1 h. The antibodies were diluted in 5% milk/TBS-T. Blots were developed with HRP substrate at the LI-COR imaging system as explained in paragraph 2.8.

Table 12. Primary antibodies used for dotblot experiments. Respective antibodies were diluted in 5% milk/TBS-T.

Antibody	Concentration	Company
Hydroxymethylcytosine (5hmC)	1:1000	Active Motif #39791
Methylcytosine (5mC)	1:1000	Active Motif #39649

2.13 Histology of neurospheres

For histology, neurospheres were spun down for 5 min at 500 rpm. The supernatant was removed and the pellet was carefully resuspended in 4% buffered formalin (54 mM NaH_2PO_4,

28 mM Na_2HPO_4) and fixed overnight at 4 °C. On the next day, the fixed spheres were pipetted in recesses of a 1.5% low-gelling agarose (Sigma-Aldrich) block that was produced with a hand-crafted form. The embedding in paraffin as well as the preparation of the slices and the respective control haematoxylin & eosin (HE) stainings were performed by technicians of the Clinical Cooperation Unit Neuropathology, Heidelberg. Subsequent immunohistochemistry was performed manually as described in 2.14.

2.14 Immunohistochemistry

1 µm slices were cut from paraffin embedded (FFPE) blocks with a Microm HM 355 S microtome (Thermo Fisher). Slices were dried at 80 °C for 15 min and stained manually with the respective antibodies. Slices were rehydrated by washing twice in xylene, following washing twice in 100% ethanol, once 90% ethanol, once 70% ethanol and finally in water, each for 2 min. Then slices were pretreated with Cell Conditioner 1 (pH 8; Ventana Medical Systems, 950-124) for 30 min at 100 °C. Subsequently, slices were incubated in 3% H_2O_2 (ChemSolute) diluted in TBS for 15 min at room temperature, following blocking with 5% FCS/TBS for 60 min. Primary antibodies (Table 13) were diluted in 5% FCS/TBS and incubated at 4 °C overnight. Slices were then incubated for 60 min with an immune peroxidase polymer anti-rabbit (Histofine Simple Stain MAX PO, Nichirei, 414141F). Afterwards, development of the stainings was performed with an 1:50 dilution of DAB for standard signal amplification (DAB-2V, Nichirei, 4253121F). Each slice was developed separately and staining was monitored with a standard microscope to yield the optimal signal. Counterstaining for detection of the cell nuclei and re-paraffinization with increasing concentrations of ethanol and xylene was performed in the routine laboratory of the Clinical Cooperation Unit Neuropathology. In case of mouse primary antibodies, the Histofine Mousestain Kit (Histofine, Nichirei, 414322F) was used in addition to the general staining protocol, following the manufacturers' protocol.

Table 13. List of the primary antibodies used for immunohistochemistry experiments. Dilutions and pretreatment were established on mouse brain slices.

Antibody	2nd Antibody	Dilution for IHC	Pretreatment	Clonality	Company
$IDH1^{R132H}$	mouse	1:50	C1	monoclonal	Dianova
p53	mouse	1:100	C1	monoclonal	Cell Signaling
CIC	rabbit	1:50	C1	polyclonal	Sigma-Aldrich
Cre-recombinase	rabbit	1:250	C1	polyclonal	Sigma-Aldrich
Foxn1	rabbit	1:100	C1	polyclonal	Antibody-online
SOX2	rabbit	1:1000	C1	polyclonal	Abcam
Ki-67	rabbit	1:500	C1	polyclonal	Abcam
pHH3	mouse	1:500	C1	polyclonal	Cell Signaling

2.15 Intracranial injections of neural stem cells

The *in vivo* study for the allograft model was approved by the governmental authorities (Regierungspräsidium Karlsruhe, Germany). Additional supervision was done by institutional animal protection officials in accordance with the US National Institutes of Health guidelines Guide for the Care and Use of Laboratory Animals (License number G-38/15 and G-155/12). Genetically altered NSCs and their respective controls were stereotactically implanted into the brains of 64 7-9-week-old female BALB/c nude mice (CAnN.Cg-Foxn1nu/Crl; Charles River Laboratories, USA). For PET experiments, six BALB/c nude mice with the same age were implanted with NCH551b cells and two with NCH644 cells. NCH551b is a primary patient-derived secondary glioblastoma cell line that has an endogenous $IDH1^{R132H}$ mutation. NCH644 derives from a human primary glioblastoma, but lacks the $IDH1^{R132H}$ mutation. Both human cell lines were cultivated by and obtained from Dr. Stefan Pusch.

Prior to surgeries, cells were mechanically dissociated and counted as described in 2.6. Subsequently, the needed amount of cells was spun down for 5 min at 300 rpm or if a pellet was not clearly visible, at 800 rpm. The supernatant was very carefully removed. The cell pellet was carefully resuspended in PBS to obtain a cell suspension with 100,000 cells/µl. Thereafter, cells were kept on ice until transplantation.

Before surgery, mice were anaesthetized with an intraperitoneally injected Ketamin/Xylazin narcosis according to table 14, in a volume of 90 µl/10 g bodyweight. After injection, a remarkable number of mice died due to respiratory problems. To avoid these problems, later surgeries were performed with Isofluran (Baxter), starting with 3% at the beginning of narcosis, which was decreased to 2.5 % during the intracranial injection.

Table 14. Composition of injection anesthesia. Narcosis was freshly prepared every day and supplements were carefully measured with a syringe.

Substitution	Concentration	Added volume	Company
Ketamin (Ketavet)	100 mg/ml	1.5 ml	Pfizer
Xylazin (Rompun)	20 mg/ml	0.5 ml	Bayer
NaCl		8 ml	

After a small cut with a scalpel (No. 21, Feather), the skin of the head was carefully put aside to view the location of the bregma. The intracranial injection was carried out 2 mm right of the sagittal suture, 3 mm rostral of the occipital suture and 3.5 mm deep. The exact location of implantation in the frontal cortex is depicted in figure 9.

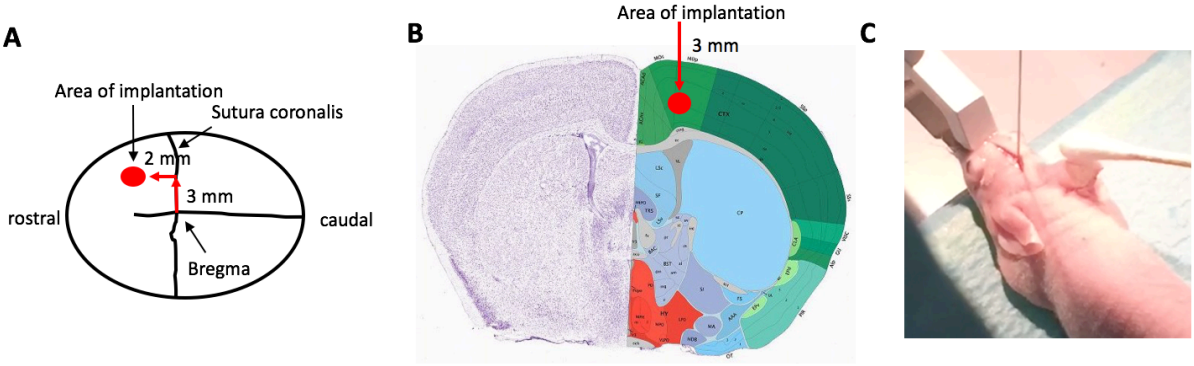

Figure 9. Scheme of the area of implantation. A NSCs were intracranially injected into the right frontal cortex, 2 mm right of the sagittal suture and 3 mm rostral of the occipital suture. **B** Depth of implantation above the ventricle indicated from coronal perspective (picture B was modified from the mouse brain atlas, C57BL/6J section 8). **C** Picture of a mouse during intracranial injection.

Prepared cell solutions in PBS were implanted at a concentration of 100,000 cells/µl with a stereotactic device (51600, Stoelting) and injector device (Quintessential Stereotaxic Injector, 53311, Stoelting) for exact application of the cells. Before cells were injected at a flow rate of 1 µl/min, the injection needle (Hamilton, Syr 10 µl, 701N) was pulled back 0.5 mm. After injection of 200,000 cells, cells were allowed to settle for two more min before the syringe was removed. Cell suspension for application was renewed after every second implantation to avoid that cells coagulate. After removing the syringe, wounds were sewed with two surgical knots (Ethilon, Polyamide 6, black, 45 cm) and a dose of 100 µl Carprofen/PBS (50 mg/ml, Zoetis) was subcutaneously injected in the neck.

The health condition of each mouse was monitored daily for abortion criteria, which are loss of 20% body weight, ataxia, apathy or paralysis. Mice showing any of these symptoms were euthanized directly.

2.16 Imaging and analysis

During the experiment, mice were monitored with 1.5 T MRI scans to analyze possible space-consuming lesions or tumor formation before the occurrence of any other symptoms. MRI scans were performed in cooperation with Dr. Manfred Jugold and Dr. Viktoria Eichwald at the imaging department for animals at the DKFZ Heidelberg. Measuring was performed according to the Bruker-RARE-sequence with the parameters listed in table 15. T1 measurements were only performed in case of a detected lesion during T2 scans. If T1 weighted recordings were performed, 70 µl of 0.5 mmol contrast enhancing agent (magnevist, Bayer) was injected per mouse 10 min prior imaging.

Table 15. Imaging parameters set for T2 and T1 weighted scans during 1.5 T examinations.

	T2 weighted image	T1 weighted image
Method	Bruker-RARE	Bruker-RARE
No. of slices	20	20
Image size	128	128
Scan-time	2.17 min	2.4 min
Slice thickness	1 mm	1 mm
Echotime (TE)	85 ms	12 ms
Pulse-repeating time (TR)	4301.8 ms	647.392 ms

PET-CT imaging

Imaging was performed using an Inveon™ dedicated PET linked to a multimodality CT (Siemens Medical Solutions). For PET analysis, 4 h prior to tracer injection mice were fasted with free access to drinking water. Before imaging, mice were anaesthetized with 3.5% sevoflurane in air and 6-8 MBq of [18F] FDG were injected via the lateral tail vein in a total volume of 100 µl. During uptake of the radiotracer, mice were kept anaesthetized and kept warm with a heating pad. After an uptake time of 45 min, ten-minute static PET scans were

acquired. Afterwards, reconstruction was performed using filtered back projection (FBP) and OSEM2D.

In addition to PET scans, anatomical CT scans were used for fusion imaging. The exposure time was 300 ms and scanning parameters were an X-ray voltage of 50 kV with an anode current of 500 µA. 180 rotation steps were done with a total rotation of 360°. The binning factor was 2 and the field of view was adjusted to 90.56 mm × 53.09 mm. For the reconstruction of images, a downsample factor of 2 was set. Afterwards, analysis of the reconstructed images was performed with the vendor software package Inveon™ Research Workplace (IRW) 2.2.

9.4 T MRI

During the last week of the mouse study, mice were also screened with a 9.4 T MRI to get a more precise image with a better spatial resolution. These experiments were carried out with the help of Dr. Ulf Neuberger and Manuel Fischer at the University of Heidelberg. Measurements were performed with a Biospec 94/20 9.4 T MRI and analysis was performed with the Paravision 6.0.1. software. If T1 weighted images had to be acquired, 0.5 mmol/ml contrast enhancing agent (Dotarem) was injected 10 min prior to imaging (Table 16).

Table 16. Scanning settings for T2 and T1 weighted images during 9.4 T examinations.

	T2 weighted image	T1 weighted image
Method	TuroboRARE	RARE
No. of slices	15	15
Image size	256 x 256	200 x 200
Scan-time	2.40 min	5.0 min
Slice thickness	0.7 mm	0.5 mm
Echotime (TE)	33 ms	6 ms
Pulse-repeating time (TR)	2500 ms	1000 ms

Brain preparation

The brains of the euthanized mice were carefully extracted and fixated at 4 °C overnight in 4% buffered formalin solution (54 mM NaH_2PO_4, 28 mM Na_2HPO_4). Before slice preparation, fixated brains were embedded in paraffin with a HistoStar Embedding

Workstation (Thermo Fisher). As shown in figure 10, the caudal parts of the brains were cryopreserved immediately after preparation by placing the specimens in liquid nitrogen and immediate storage at -80 °C.

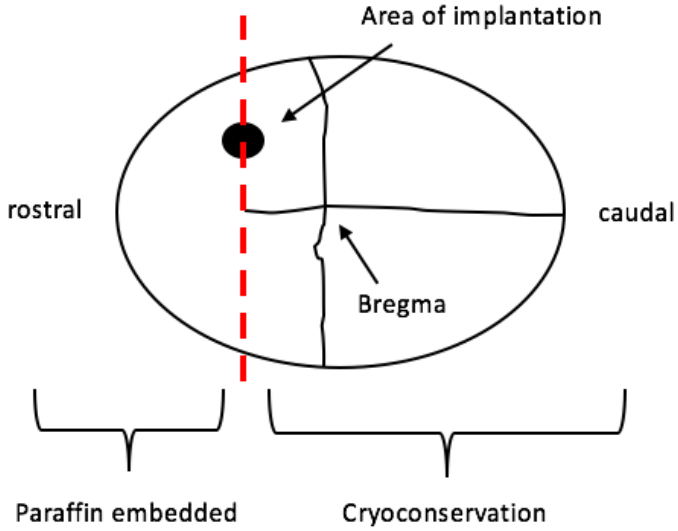

Figure 10. Schematic of the preparation of mice brains. The brain was cut in sagittal position through the area of implantation, which was still observable as a small dot in most of the cases. Rostral parts were fixed in formalin for preparation of paraffin slices, whereas caudal parts were cryoconserved for 2-HG measurements.

Statistics

All statistics was performed with Graph Pad Prism 7. Unless otherwise described, statistical significance was analyzed with two-sided unpaired t-tests of mean values and a p-value <0.05 was assessed as significant. Details are given in the legend of the respective figures.

3 Results

3.1 Generation of Cic flox mice

Targeted Agouti ES-cells were obtained from Prof. Günther Schutz, DKFZ Heidelberg and implanted into Bl6/N blastocysts, which was performed by the transgenic mice core facility of the DKFZ. The resulting chimeras were checked for successful germline transmission.

Attempts to generate homozygous Cic flox mice resulted in small litters and genotyping showed that no homozygous littermates were born at all. It was found that the original ES constructs were incorrectly annotated. The flippase recognition (FRT) cassette containing the Neomycin resistance gene was still present in the cells and homozygous expression is lethal in mice. To get rid of the resistance cassette, heterozygous *Cic* mice were crossed with flippase (Flp) mice. Prior to the next mating, littermates were genotyped to check for successful recombination and in a next step, mice were crossed with Bl6/N in order to eliminate Flp again to finally yield the correct *Cic* construct.

3.2 Generation of neural stem cells with different genetic alterations

Being able to investigate the role of the $Idh1^{R132H}$ mutation during the process of gliomagenesis and its effect in combination with other genetic alterations *in vitro* and *in vivo*, neural stem cells (NSCs) were prepared. These cells derive from conditional knock-in $Idh1^{R132H}$ mutated mice that are inducible via the Cre-recombinase system. Several combinations of stem cells were prepared, which includes different genotypes and the respective controls. The Cre-recombinase system was chosen in order to prevent embryonic lethality of $Idh1^{R132H}$ mice (Sasaki *et al.*, 2012). For cells harboring an additional astrocytoma-lineage defining mutation, NSCs were prepared carrying the conditional $Idh1^{R132H}$ mutation, the Rosa CreERT2 transgene and a conditional *Tp53* knock-out, in different combinations (Table 17). For cells mimicking the genetic features of oligodendroglioma, the conditional $Idh1^{R132H}$ mice were crossed with Cic floxed mice with the inducible Cre-recombinase system. All NSCs were prepared on day P1 and cultured under standard NSC conditions.

Table 17. Established main neural stem cell cultures and their inherent genotypes. C = conditional allele, T = transgenic allele.

Idh1^{R132H} genotype	ROSA-CreERT2 genotype	p53 genotype	Cic genotype
C/+	T/+	-	-
C/+	+/+	-	-
+/+	T/+	C/C	-
+/+	+/+	C/C	-
C/+	T/+	C/C	-
C/+	+/+	C/C	-
+/+	T/+	-	C/C
+/+	+/+	-	C/C
C/+	T/+	-	C/C
C/+	+/+	-	C/C

3.2.1 Induction of genetic alterations and validation of established cell lines

For induction of genetic alterations, 1 µM 4-Hydroxytamoxifen (4-OHT) was added to the culture medium 24 hours after passaging to induce Cre-recombination. 4-OHT treatment leads to heterozygous expression of mutant Idh1^{R132H} alone or concomitant the knock-out of *Tp53* or Cic. To make sure that the time for recombination is sufficient, 4-OHT was left in the culture medium for one week. In case of *Cic* knock-out cells, treatment with 4-OHT was repeated once after the first week, because of incomplete recombination after single treatment. Being able to compare effects of the induced genetic alterations, non-inducible control cells carrying the same floxed alleles but lacking Cre-recombinase, were included for all experiments. Finally, genotypes were validated with SDS-PAGE and Western Blot to ensure successful and complete induction. Western blot analysis using the Idh1^{R132H}-mutant specific antibody reveals that inducible cells express the conditional knock-in mutation Idh1^{R132H}, whereas controls lack the inducible expression. *Tp53* knock-outs are confirmed with the respective antibody (Figure 11 A). To further validate the successful induction of both genetic alterations, immunohistochemistry was performed with the same antibodies (Figure 11 B). Application of these specific antibodies clearly shows that induction by 4-OHT was successful.

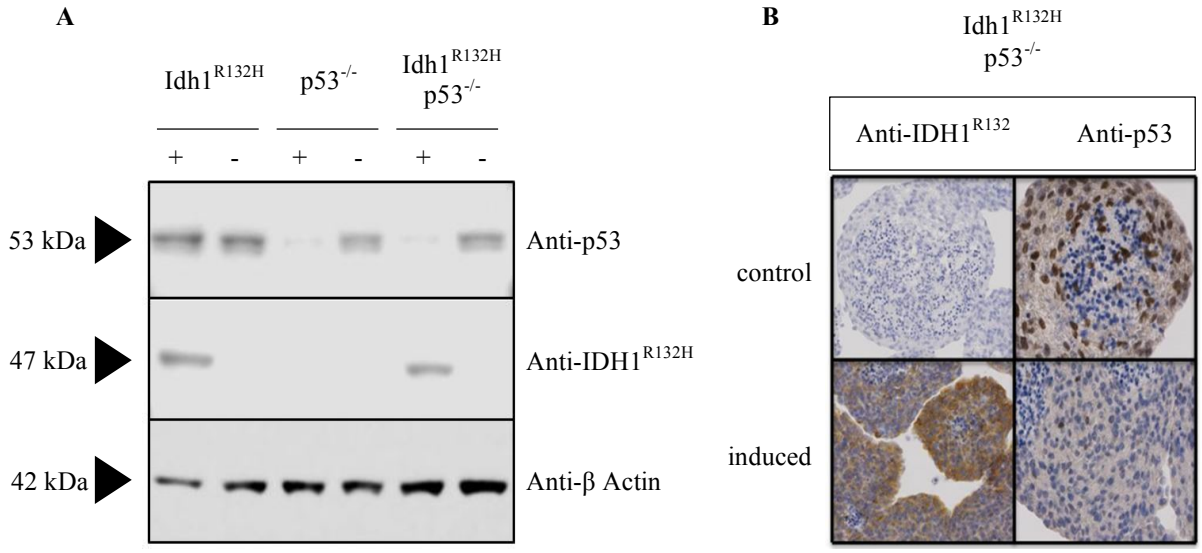

Figure 11. Validation of Idh1^{R132H} p53$^{-/-}$ cells. A Western Blot results confirming the presence of Idh1^{R132H} mutated protein and *Tp53* knock-out of the respective cell lines and controls after 4-OHT treatment. **B** Immunohistochemical staining against the Idh1^{R132H} mutation reveals a cytoplasmic signal of the induced spheres only, indicating that recombination was successful. Staining against p53 shows a strong nuclear signal in control cells, whereas it is barely seen after induction of the knock-out.

Reliable expression signals of Cic protein could not be achieved with all antibodies tested. The combination of the wet-blot method, the optimal primary antibody concentration and development with a chemiluminescent secondary antibody, leads to reliable detection of Cic at 164 kDa (Figure 12 A).

Immunohistochemistry with the same antibodies further supports the successful knock-out of *Cic* in combination with or without the Idh1^{R132H} mutation (Figure 12 B). Cic protein shows strong cytoplasmic staining, which almost completely vanishes in Cic$^{-/-}$ cells. *Cic* knock-out is also detectable on RNA level. *Cic* coding cDNA is not detectable in Cic$^{-/-}$ cells in comparison to controls (Figure 12 C).

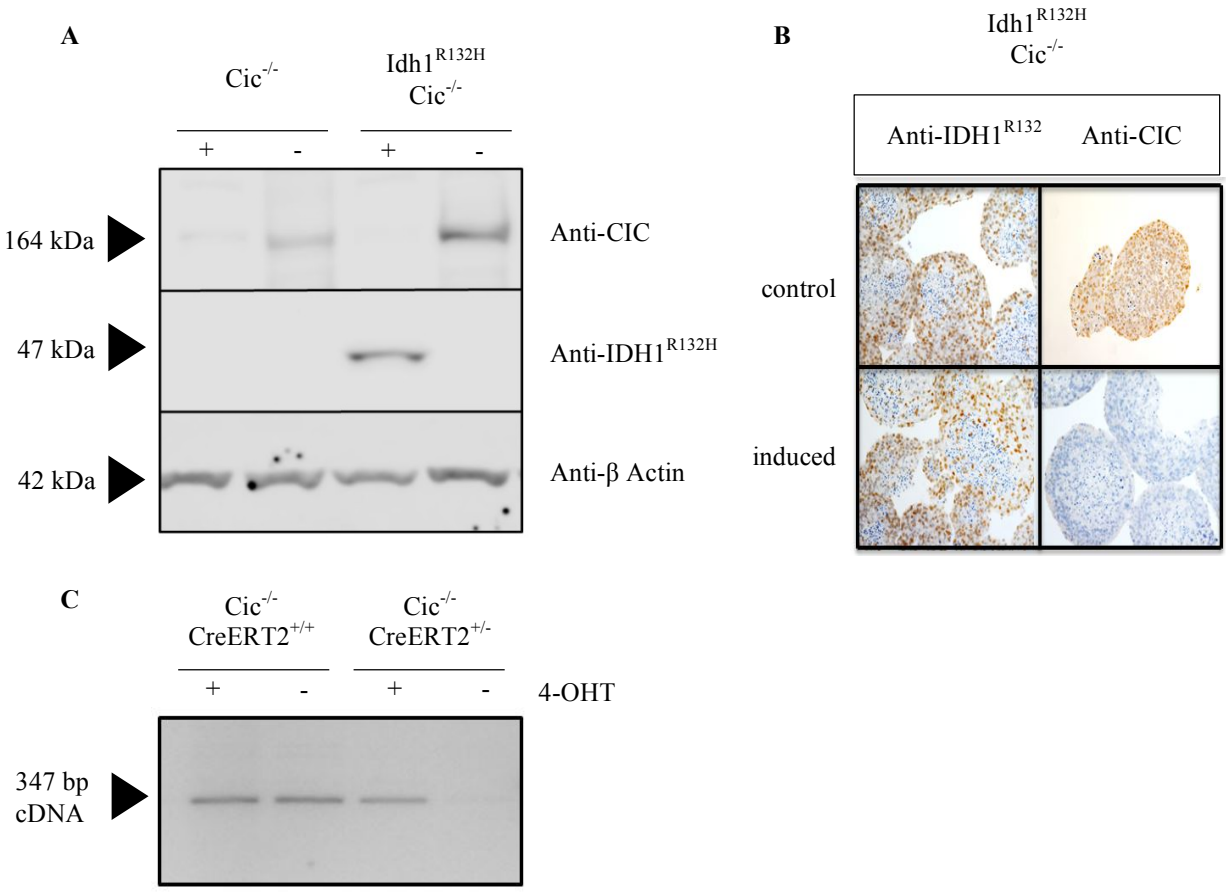

Figure 12. Validation of Idh1^{R132H} Cic$^{-/-}$ cells. A Western Blot results confirming the presence of Idh1^{R132H} mutated protein and *Cic* knock-out in the respective cell lines and controls after two treatments with 4-OHT. Mutation-specific antibodies were used for detection after wet-blotting on a nitrocellulose membrane. **B** Immunohistochemistry shows that the cytoplasmic signal of Cic is not detectable anymore in knock-out cells. **C** Results of a reverse transcription PCR with primers spanning Exon 10 and 11, indicating the knock-out of *Cic* on RNA level.

3.3 Functional characterization of Idh1^{R132H} p53$^{-/-}$ NSCs: short-term effects

The following chapter summarizes the results of the functional characterization of newly established cell lines harboring an Idh1^{R132H} mutation with or without a knock-out of *Tp53*. The findings are related to cell lines with alterations induced and validated two weeks before the start of the experiments, which will be referred to as short-term.

3.3.1 Cell viability

An increase of cell viability of induced cells could not be observed. Experiments show that the induction of the Idh1^{R132H} mutation in inducible cell lines and subsequent production of 2-HG decreases cell viability up to 44.3 ± 20.2%, compared to respective controls (Figure 13 A). In line with this, measurements of cell viability across 5 days show a decreased slope of the growth curve of Idh1^{R132H} mutated cells compared to controls. Normalized to control on

day 5, Idh1^{R132H} mutated cells grow on average 7.8% per day. In contrast, control cells have a growth increase of 18.7% daily (Figure 13 B). The cell number after induction of both alterations is slightly increased compared to Idh1^{R132H} alone, 70.3 ± 9.8% vs. 44.3 ± 20.2%. This is however still a significant decrease compared to controls. The proliferation of p53$^{-/-}$ cells is 58.6 ± 23.8% compared to control cells (Figure 13 A). The slope of the growth curve of p53$^{-/-}$ cells is slightly decreased (11.6%) compared to respective controls (19.4%). Same observations can be made for double mutant cells that also have a decreased growth behavior compared to controls (12.8% vs. 19.2% daily).

A

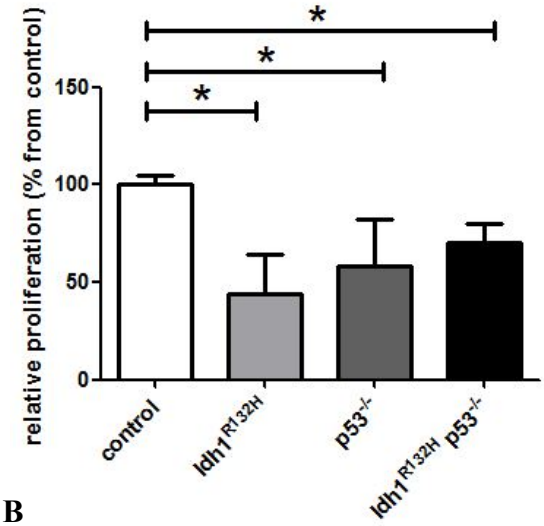

B

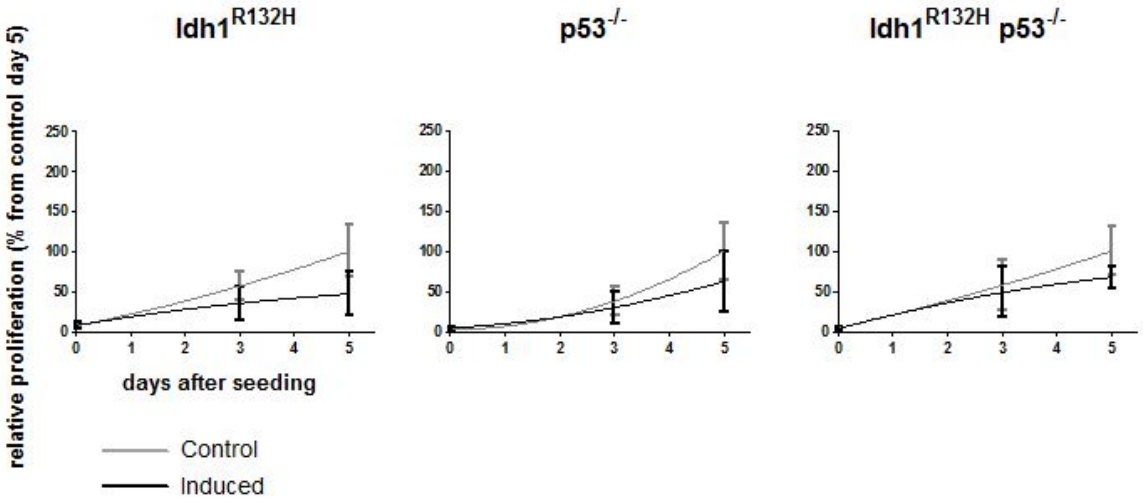

Figure 13. Induction of Idh1^{R132H} and subsequent production of 2-HG significantly decreases cell viability. A After induction and validation of the genotypes, 5000 cells were seeded per well in 96-well plate format and measurements using the CellTiter-Glo 3D Cell Viability Assay were performed five days after seeding. Idh1^{R132H} leads to a significant decrease of cell viability. A significantly reduced cell number is also observed when a knock-out of *Tp53* was induced alone or in the presence of Idh1^{R132H}, which is however weakened compared to Idh1^{R132H} alone. Bar plot of CellTiter-Glo3D assay data, normalized to average

control. **B** Time series of the CellTiter-Glo 3D Cell Viability Assay reveals that cells harboring the Idh1^{R132H} mutation show a distinctive growth disadvantage compared to a single knock-out of *Tp53* or double mutants. Measurements were performed after 0, 3 and 5 days of incubation. Diagram of the CellTiter-Glo 3D Cell Viability Assay, normalized to average control on day 5. (Indicated significances: two-sided unpaired students t-test, * = $p<0.05$, n = 3).

3.3.2 Colony formation in soft agar

Anchorage-independent growth is described as a hallmark of carcinogenesis, as transformed cells have the ability to grow independently of a solid surface. The soft agar assay is a well described method to check for this potential *in vitro* and is reported to be one of the most important tests to examine malignant transformation in cells (Borowicz *et al.*, 2014). To check for this ability, cells were embedded in soft agar layers and were allowed to grow for 7 days in 96-well plates before quantification using the resazurin-based CellTiter-Blue Cell Viability assay. Experiments indicate that cells harboring an Idh1^{R132H} mutation only, show a significantly reduced colony number compared to controls (88.9 ± 3.9%). In contrast, if cells harbor a *Tp53* knock-out only or in combination with the Idh1^{R132H} mutation, sphere formation is slightly increased (107.7 ± 6.3% and 107.1 ± 7.3% respectively) compared to controls, and significantly increased to Idh1^{R132H} alone (Figure 14).

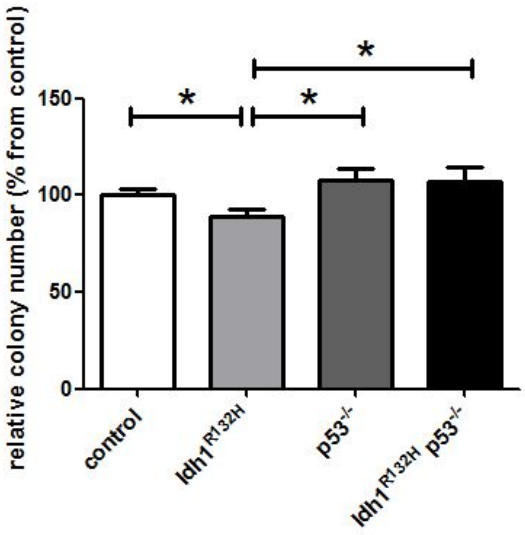

Figure 14. Induction of Idh1^{R132H} significantly decreases colony formation rate in soft agar. Previously induced and validated cell lines were used to seed 2000 cells per well embedded in a soft agar matrix in 96-well plates. After 7 days of incubation, measurements were performed using the CellTiter-Blue Assay. Idh1^{R132H} alone leads to a significant decrease of colony formation. In contrast, if cells harbor a single knock-out of *Tp53* or a combination of both alterations, there is a tendency towards an increase of colony formation rate. Bar plot of the soft agar assay data, normalized to average control after one week of incubation. (Indicated significances: two-sided unpaired students t-test, * = $p<0.05$, n = 3).

3.3.3 Analysis of apoptotic proteins

Differences in the phenotype of single and double mutants can be detected with cell viability and colony formation analysis. As a next step, it was aimed to understand these differences. It is of interest whether Idh1^{R132H} cells with a decreased proliferative capacity have a higher rate of apoptosis. To analyze the level of apoptosis, proteins were analyzed that are described to play an important role during later steps of apoptosis. The apoptotic marker proteins cleaved Caspase 3 (clC3), cleaved Caspase 7 (clC7) and cleaved Poly (ADP) ribose Polymerase (clPARP) were analyzed in Western blot. Results show that apoptosis is slightly increased in cells harboring the Idh1^{R132H} mutation compared to controls. Expression of the apoptotic proteins clC3, clC7 and clPARP is on average 127.9 ± 138.7%, 320.2 ± 250.4% and 95.1 ± 51.7%, respectively. In contrast, a knock-out of *Tp53* shows a tendency towards a decrease of the level of apoptosis. The level of clC3 is 77.5 ± 24.9%, clC7 44.7 ± 6.3% and clPARP 59.5 ± 58.6%. A reduction of apoptosis could also be observed in double mutant cells, which is comparable to the *Tp53* knock-out cells. Abundance of clC3 protein is reduced to 66.2 ± 82.6% compared to controls, as well as 65.2 ± 61.1% and 75.7 ± 60.0% for clC7 and clPARP respectively (Figure 15).

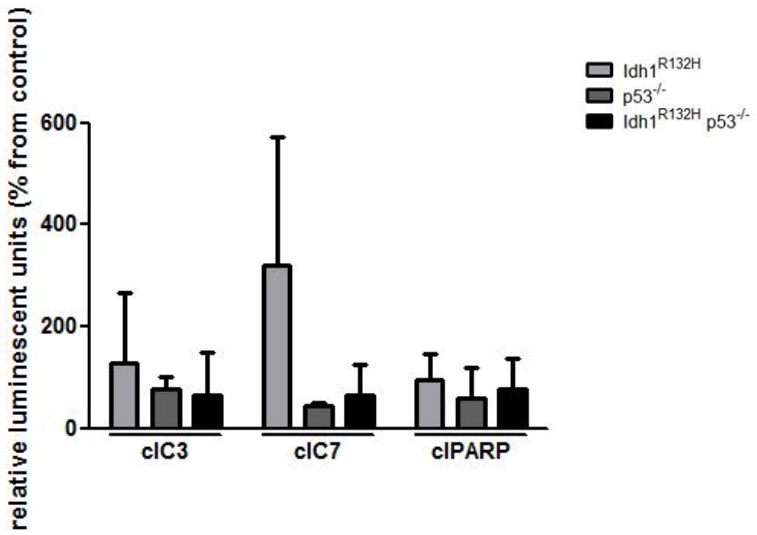

Figure 15. Induction of Idh1^{R132H} slightly enhances levels of apoptosis. Whole cell lysates were prepared from 300 µl cell suspension taken from previously induced and validated cell lines. After BCA, lysate was subjected to Western blot analysis with antibodies to the apoptotic proteins clC3, clC7 and clPARP. Expression of Idh1^{R132H} shows a tendency towards an increase of apoptosis. The presence of a knock-out of *Tp53*, either alone or in combination with the Idh1^{R132H} mutation results in a decreased level of apoptosis, observed in all proteins tested. Bar plot of the expression of apoptotic proteins, normalized to average control. (Indicated significances: two-sided unpaired students t-test, n = 3 and n = 2 for clC3).

3.3.4 Production of 2-HG

The intracellular level of 2-HG produced after induction of the Idh1^{R132H} mutation was detected by an enzymatic 2-HG quantification assay. Cells harboring an Idh1^{R132H} mutation produce high amounts of 2-HG, which are not altered when Idh1^{R132H} is accompanied by a knock-out of *Tp53* (Figure 16). Mean intracellular 2-HG concentrations across three replicas are 2.7 ± 0.7 mM for single Idh1^{R132H} mutated cells and equally 2.7 ± 0.7 mM for cells harboring both alterations. In contrast, p53$^{-/-}$ cells do not produce 2-HG (0.4 ± 0.1 mM), which is below the quantification limit of the assay.

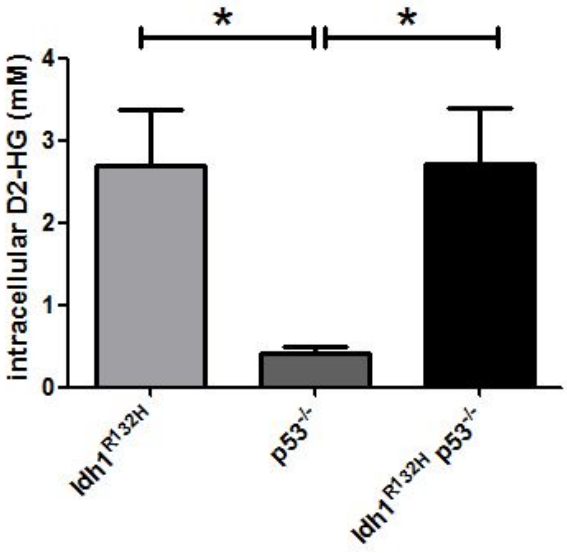

Figure 16. Cells harboring an Idh1^{R132H} mutation produce 2-HG, which is not altered by a concomitant knock-out of *Tp53*. 300 µl of previously induced and validated cells was taken for lysate production and protein concentration was determined with BCA. 2-HG concentration produced after induction of the alteration was determined with a 2-HG quantification assay. The presence of Idh1^{R132H} alone leads to a significant production of 2-HG, whereas this is absent in single *Tp53* knock-out cells. A combination of both alterations induces a similar production of 2-HG, compared to cells with Idh1^{R132H} only. Bar plot of the 2-HG assay carried out in triplicates, normalized to average control. (Indicated significances: two-sided unpaired students t-test, * = $p<0.05$, n = 3).

3.4 In vivo allograft model

To test, whether the *in vitro* results translate into the *in vivo* situation, the induced NSCs were intracranially injected into BALB/c nude mice. BALB/c mice were chosen for these experiments as previous research from brain tumor xenograft implantations has shown that tumors develop best in these mice (Pusch, 2016).

3.4.1 Intracranial injections

Intracranial injections of NSCs were performed with the main genotypes listed in table 1. Mice were anaesthetized with a well-established anesthesia consisting of Ketamin and Xylazin. However, this protocol did not lead to the expected success, as almost 50% of mice died due to respiratory problems during awakening phase from anesthesia. The anesthesia protocol was adjusted as for example not injecting the whole amount the same time, or changing the proportion of Ketamin and Xylazin. Given that this did not improve the situation, later surgeries were carried out under Isofluran narcosis.

3.4.2 General problems with immunodeficient mice during the time of the experiment

During the time of the experiment several problems concerning the animals arose. These problems did not influence the result of the *in vivo* study in general, but led to the loss of mice and decreased the final number of animals that were alive until termination of the experiment (Table 18). The loss was mainly due to health issues caused by inbreed problems, the observation period of one year and different types of infections, such as an abscess of the eye.

Table 18. Overview about the different groups of mice implanted with the respective genetically altered NSCs. The first number is related to the mice that were initially implanted, whereas the number in brackets is related to mice that took part in all MRI screens.

Genotype injected NSCs	Number of mice (alive until termination of the experiment)
Idh^{R132H}	6 (4)
Idh^{R132H} control	6 (0)
$p53^{-/-}$	6 (3)
$p53^{-/-}$ control	6 (2)
Idh^{R132H} $p53^{-/-}$	10 (5)
Idh^{R132H} $p53^{-/-}$ control	6 (1)
$Cic^{-/-}$	6 (6)
$Cic^{-/-}$ control	6 (3)
Idh^{R132H} $Cic^{-/-}$	6 (6)
Idh^{R132H} $Cic^{-/-}$ control	6 (1)

3.5 Functional characterization of Idh1^{R132H} p53$^{-/-}$ NSCs: long-term effects

After intracranial injections of the induced NSCs into immunodeficient mice, cells were further cultivated for six months. This should show whether the Idh1^{R132H} mutation has an effect across a long-term, as this mutation is known to influence epigenetic processes that might take more time until effects are measurable. To be able to better compare the effects of long-term cells to cells shortly after initial induction, each figure additionally shows a transparent figure of the short-term result in the following paragraph.

3.5.1 Cell viability

After a cultivation period of sixth months, it was first checked whether long-term induction of the alterations changes the proliferative potential of the cells by using the ATP-based Cell Titer-Glo 3D Cell Viability assay, as described above. The growth disadvantage observed in newly induced Idh1^{R132H} cells alone, is almost abrogated after cultivation for several months (44.3 ± 20.2% vs. 70.4 ± 34.0% after long-term cultivation). A knock-out of *Tp53* shows comparable results to Idh1^{R132H} mutated cells, as the relative proliferation is 72.2 ± 35.7% compared to controls. Surprisingly, Idh1^{R132H} mutation with a concomitant knock-out of *Tp53* leads to a significantly enhanced proliferation compared to Idh1^{R132H} alone (133.9 ± 26.0% vs. 70.4 ± 34.0%; Figure 17 A). A significant difference could also be observed between the knock-out of *Tp53* and double mutants (72.2 ± 35.7% vs. 133.9 ± 26.0%). Analysis of the growth behavior of these cells shows that there is a tendency towards a decrease of the relative proliferation of Idh1^{R132H} cells across time. Compared to controls (18.6%), mutated *Idh1* cells have a growth behavior of 11.3% daily. The induction of a *Tp53* knock-out across a long term does not significantly alter the slope of the growth curve compared to their respective controls (14.3% vs. 19.5%). In contrast, cells harboring both genetic alterations exhibit a tendency towards a steeper growth curve with a slope of 25.3% per day, compared to respective controls (19%). The course of the growth curve is in line with the cell number measured on day 5 of the experiment, as double mutants have an enhanced proliferation rate (Figure 17 B).

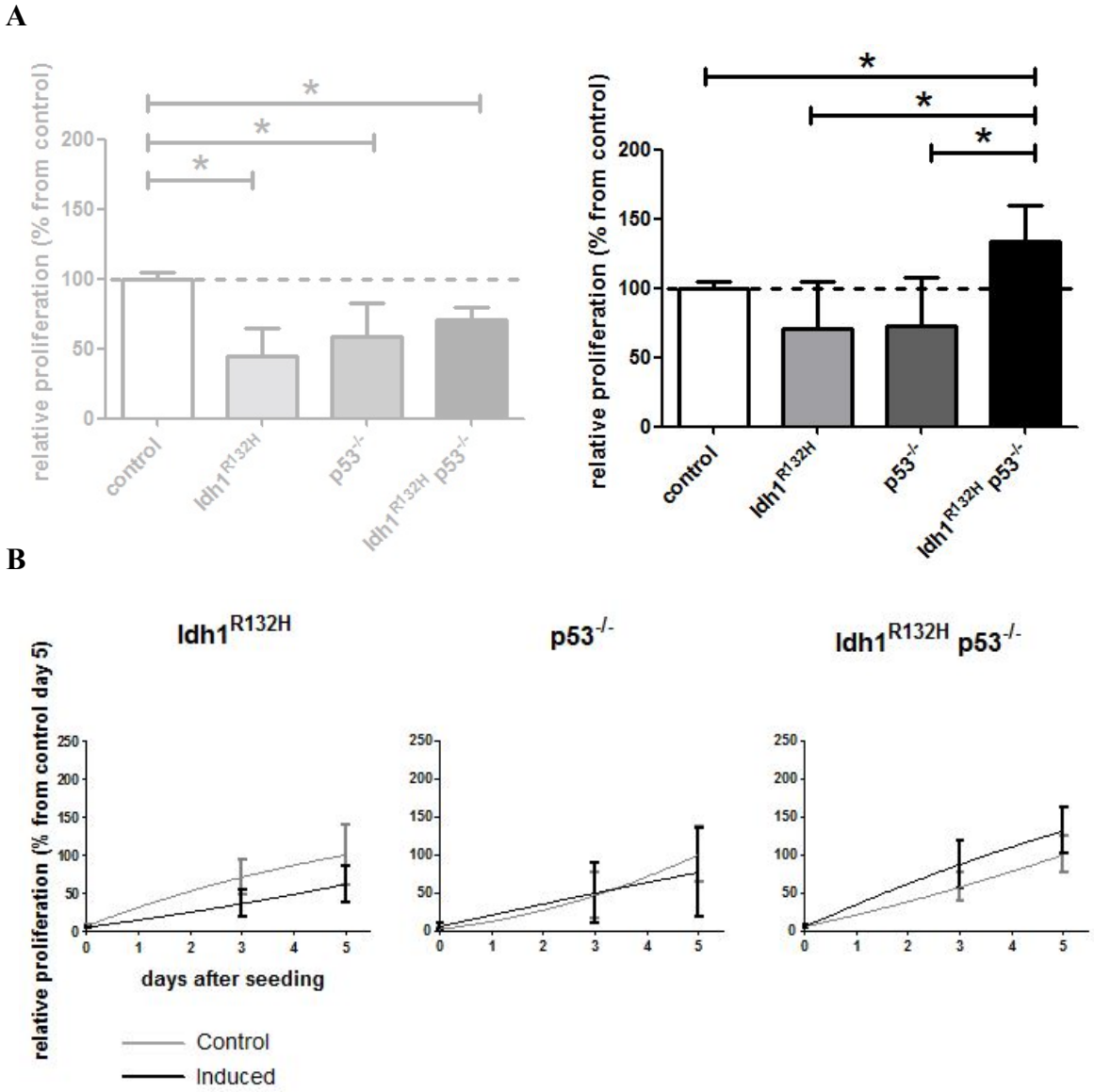

Figure 17. Idh1^{R132H} cells with a concomitant knock-out of *Tp53* develop an increased proliferative potential after six months of induction. A Six months after initial induction, 5000 cells were seeded per well in 96-well plates and measurements using the CellTiter-Glo 3D Cell Viability Assay were performed after five days of incubation. One single alteration either Idh1^{R132H} or p53$^{-/-}$ does not alter cell viability, if cells were cultivated for 6 months. Double mutants have an enhanced proliferation, which is not observed after initial induction of the alterations. Bar plot of CellTiter-Glo3D assay normalized to average control. **B** Consecutive measurements of the CellTiter-Glo 3D Cell Viability Assay on day 0, 3 and 5 reveal that cells harboring the Idh1^{R132H} mutation show a flattened growth curve compared to controls. A single knock-out of *Tp53* does not alter growth curve, whereas double mutants grow faster compared to controls. Diagram of the CellTiter-Glo 3D Cell Viability Assay shows proliferation normalized to average control on day 5. (Indicated significances: two-sided unpaired students t-test, * = $p<0.05$, n = 3).

3.5.2 Colony formation in soft agar

Long-term cells were also embedded in soft agar as described above and colony formation was analyzed after 7 days. Cells harboring the Idh1^{R132H} mutation show a significantly reduced colony number compared to controls (36.3 ± 32.1%). p53$^{-/-}$ cells do not exhibit an

altered growth capacity in soft agar matrix compared to controls (85.9 ± 11.7%). In contrast, if the knock-out of *Tp53* is combined with Idh1^{R132H}, cells show an enhanced ability to form colonies in soft agar (Figure 18). The relative colony number of double mutants is 326.3 ± 183.7% compared to the respective control cells. Cells harboring both alterations across a period of 6 months, show a more tumorigenic phenotype with an increased proliferative potential, compared to newly induced cells.

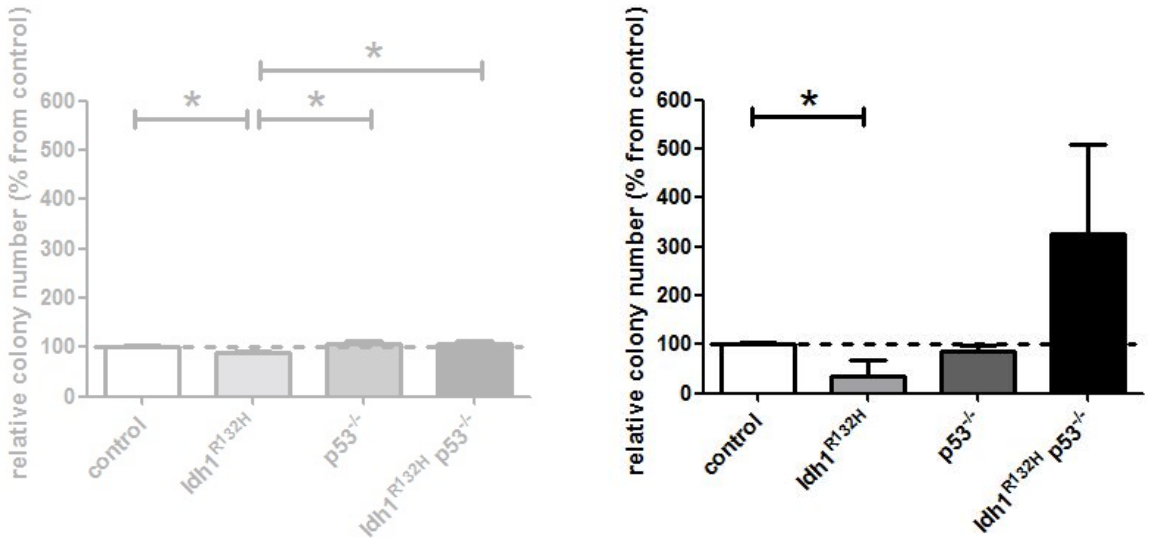

Figure 18. Idh1^{R132H} p53$^{-/-}$ cells show an enhanced colony formation rate six months after initial induction. Long-term cell lines were embedded in soft agar matrices in a density of 2000 cells per well. CellTiter-Blue Assay was performed seven days after seeding of the cells. Idh1^{R132H} alone leads to a significant decrease of colony formation compared to controls. If cells harbor a single knock-out of *Tp53* colony formation rate is not altered. In contrast, a combination of both alterations leads to an enhanced formation of colonies in soft agar. Bar plot of the soft agar assay shows colony number normalized to average control after one week of incubation. (Indicated significances: two-sided unpaired students t-test, * = $p<0.05$, n = 3).

3.5.3 Analysis of apoptotic proteins

The above described difference in the proliferative capacity between single and double mutants could be achieved by reduced levels of apoptosis in cells harboring both alterations. To investigate this in more detail, Western blot experiments were performed to analyze expression of late apoptotic proteins. Decreased levels of apoptotic proteins could be detected in single Idh1^{R132H} mutant cells, which is 45.5 ± 17.3% for the expression of clC3, 57.6 ± 20.1% for clC7 and 43.4 ± 8.9% for the expression of clPARP. Levels of apoptosis are also decreased in cells with a single knock-out of *Tp53*, which is on average a decrease to 31.3 ± 17.0% of clC3 expression, compared to controls. Expression of clC7 and clPARP is reduced

to 34.3 ± 17.4% and 39.6 ± 17.7% respectively. Interestingly, cells that harbor a combination of both alterations show increased clC3 expression levels of 158.8 ± 12.7%, compared to controls (Figure 19). clC7 and clPARP expression is also increased to 150.2 ± 36.4% and to 127.3 ± 31.5% respectively.

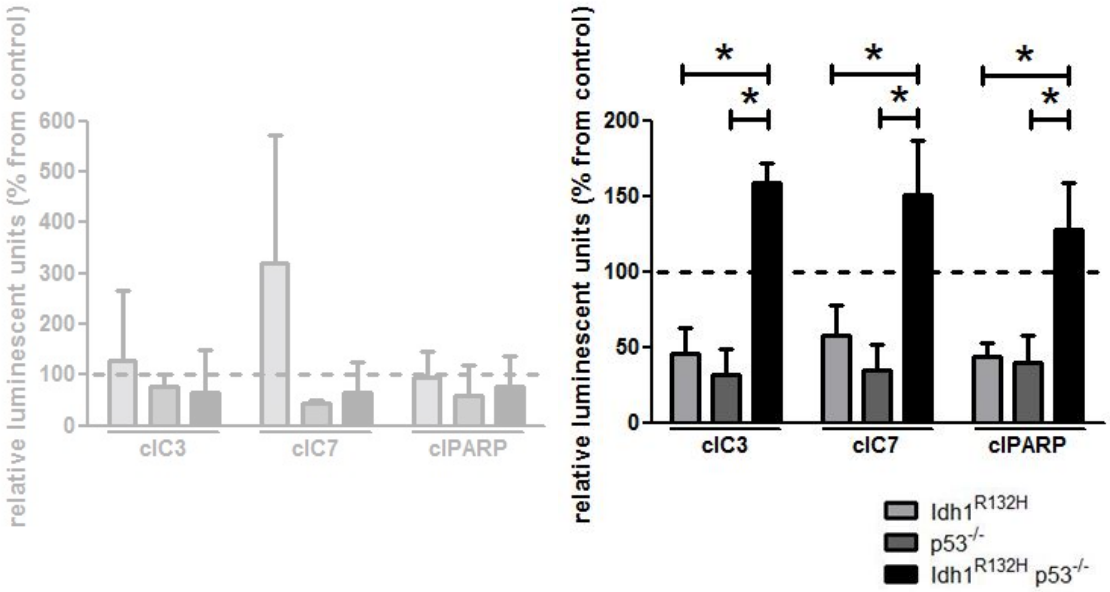

Figure 19. Apoptosis is strongly increased in long-term cells harboring both Idh1^{R132H} and p53$^{-/-}$. Whole cell lysates were prepared from 300 µl cell suspension taken from cell lines induced six months beforehand. After determining the protein concentration with BCA, lysate was subjected to western blot analysis with antibodies to the apoptotic proteins clC3, clC7 and clPARP. Expression of Idh1^{R132H} or p53$^{-/-}$ alone decreases the expression of all apoptotic proteins tested. p53$^{-/-}$ in an Idh1^{R132H} background significantly increases the level of apoptosis, reflected in an enhanced expression of clC3, clC7 and clPARP. Bar plot of the expression of apoptotic proteins, normalized to average control. (Indicated significances: two-sided unpaired students t-test, n = 4).

3.5.4 Analysis of cell cycle markers in long-term cells

Being able to investigate the increase of the proliferative capacity in more detail, long-term cells were stained with antibodies specific for cell cycle markers. After verification of the antibodies on control brain tissue, stainings of mutated cell lines were always compared to non-inducible ones (Figure 20 A). To do so, spheres were embedded in a paraffin block, histological slices prepared and stained with haematoxylin and eosin (HE). With this control staining, the presence and morphology of all embedded cell lines was verified (Figure 20 B). Subsequently, immunostainings were performed with antibodies to the antigen Ki-67 and phosphohistone H3 (pHH3). More Ki-67 positive cells can be detected in Idh1^{R132H} p53$^{-/-}$ cells compared to controls, indicating that more cells are in G_1, S, G_2, and mitosis. pHH3, a marker

for mitotic index, shows an increased number of positive cells in Idh1^{R132H} p53$^{-/-}$ cells. Taken together, both immunohistochemistry markers confirm that more cells with both genetic alterations are proliferating, which is in line with the results described before.

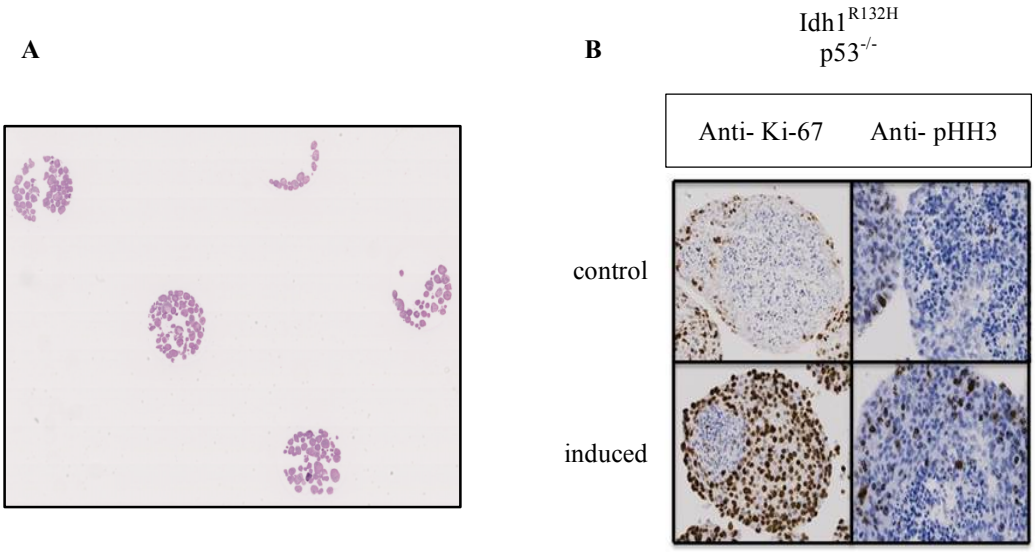

Figure 20. Immunohistochemistry of cell cycle markers. A Overview of a HE staining of all cell lines on one slide. Each circle represents the embedded spheres of one particular cell line. **B** Immunostainings of Idh1^{R132H} p53$^{-/-}$ embedded spheres reveals a strong cytoplasmic staining of Ki-67 and pHH3, pointing towards an enhanced proliferative capacity compared to controls.

3.5.5 Analysis of epigenetic effects of Idh1^{R132H}

It is known that mutant *Idh1* has various effects on epigenetics, e.g. DNA methylation. Amongst others, Idh1^{R132H} induces the inhibition of TET enzymes, regulating the conversion of DNA 5-methylcytosine (5mC) to 5-hydroxymethylcytosine (5hmC). Further, it was shown that induction of Idh1^{R132H} decreases the level of 5hmC, thereby altering gene regulation. Dotblot experiments were performed in order to investigate whether induction of the genetic alterations has an influence on DNA methylation six months after initial induction. To do so, DNA samples from different cell lines were blotted onto a nitrocellulose membrane and immunostainings against 5mC and 5hmC were carried out. Expression of mutant *Idh1* alone shows a tendency towards enhanced levels of both 5mC and 5hmC (111.7 ± 29.5% and 125.6 ± 27.0%, respectively). A knock-out of *Tp53* does not alter the abundance of 5mC (100.0 ± 22.9%), whereas levels of 5hmC are slightly decreased, with a signal of 79.1 ± 18.0%. In contrast, in Idh1^{R132H} p53$^{-/-}$ cells, there is a tendency of enhanced levels of both 5mC and 5hmC. Analysis of the dotblot membranes after staining against 5mC displayed a level of

134.6 ± 51.6% compared to the respective control cells and a 5hmC level of 120.4 ± 33.9% (Figure 21).

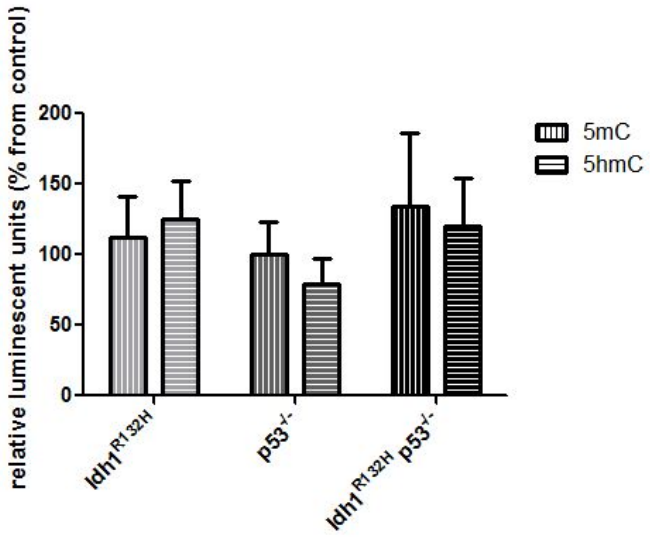

Figure 21. Induction of Idh1^{R132H} does not significantly alter DNA methylation. DNA was extracted from genetically altered cell lines induced six months beforehand. DNA concentration was determined with Qubit before it was blotted onto a nitrocellulose membrane with a dotblot device. Expression analysis of epigenetic markers was done with antibodies to 5mC and compared to 5hmC in induced cell lines and controls. Expression of Idh1^{R132H} alone shows a tendency towards an increase of both 5mC and 5hmC. A knock-out of *Tp53* does not alter the expression of 5mC, whereas 5hmC is slightly enhanced. p53$^{-/-}$ in an Idh1^{R132H} background shows a tendency of enhanced level of both epigenetic markers. Bar plot reflects the expression of 5mC and 5hmC, normalized to average control. (Indicated significances: two-sided unpaired students t-test, n = 3).

3.5.6 Production of 2-HG

The production of 2-HG was also measured in cells harboring the alterations across a period of more than six months. Surprisingly, cells harboring the Idh1^{R132H} mutation either alone, or in combination with a knock-out of *Tp53* do not produce 2-HG anymore. As depicted in figure 22, the intracellular 2-HG concentration detected is even below the quantification limit of the 2-HG enzymatic assay. Across three replicas, average 2-HG levels are 0.3 ± 0.2 mM for cells harboring the Idh1^{R132H} mutation only and 0.4 ± 0.3 mM for double mutants. 2-HG measurements of the supernatant revealed that 2-HG does not accumulate extracellularly (Supplement Figure 1). Single *Tp53* knock-out cells do not produce 2-HG, which is on average 0.5 ± 0.5 mM. These results show that the cells harboring the Idh1^{R132H} mutation lost their ability to produce 2-HG across time.

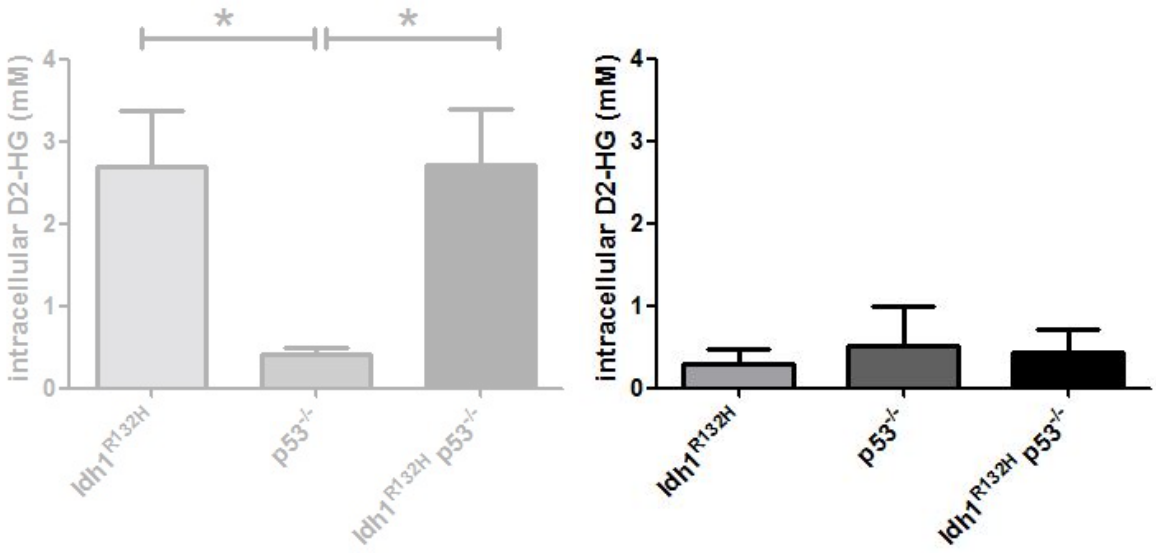

Figure 22. Long-term Idh1^{R132H} mutated cells completely lose their ability to produce 2-HG. 300 µl of cell suspension from long-term cell lines was taken for lysate production and protein concentration was determined with BCA. 2-HG concentration was determined with a 2-HG quantification assay. Production of 2-HG is absent in cells harboring the Idh1^{R132H} mutation either alone or in combination with a knock-out of *Tp53*, which is only observed in long-term cells. The appearance of p53$^{-/-}$ alone does also not result in the production of 2-HG. Bar plot of the 2-HG assay carried out in triplicates. (Indicated significances: two-sided unpaired students t-test, * = $p<0.05$, n = 3).

3.6 Loss of Idh1^{R132H} in long-term cell lines

The loss of the ability to produce 2-HG in long-term cultures pointed towards an alteration of the mutational status of the cells. To investigate this in more detail, the presence of mutant Idh1 protein was analyzed. Mutant Idh1 protein cannot be detected in long-term. In contrast, the knock-out of *Tp53* is still detectable in all cell lines, no matter if single mutant or in combination with Idh1^{R132H}. Given the fact that all cell lines were validated after initial induction, the cells must have lost the Idh1^{R132H} mutation after several weeks. In order to investigate this in more detail, cells were freshly induced and checked for the presence of the Idh1^{R132H} mutation with concomitant production of 2-HG and also the knock-out of *Tp53*. The loss of the Idh1^{R132H} mutation can be followed by measuring 2-HG levels. It starts with a tendency towards a decrease of 2-HG one month after application of 4-OHT, from 14.5 ± 2.7 mM to 12.4 ± 0.2 mM 2-HG. This drop steadily continues across a period of 10 days, where only 1.5 ± 0.1 mM of 2-HG can be detected intracellularly. In parallel to the 2-HG measurements, immunohistochemistry was performed on embedded cells with the antibody to Idh1^{R132H}. Stainings indicate that a lower number of cells is positive for Idh1^{R132H} 30 days after initial induction, matching the decreasing concentration of 2-HG. 50 days after

induction, 2-HG levels are below detection limit (0.6 ± 0.1 mM), which is accompanied by a complete loss of Idh1 mutant protein (Figure 23 A, B).

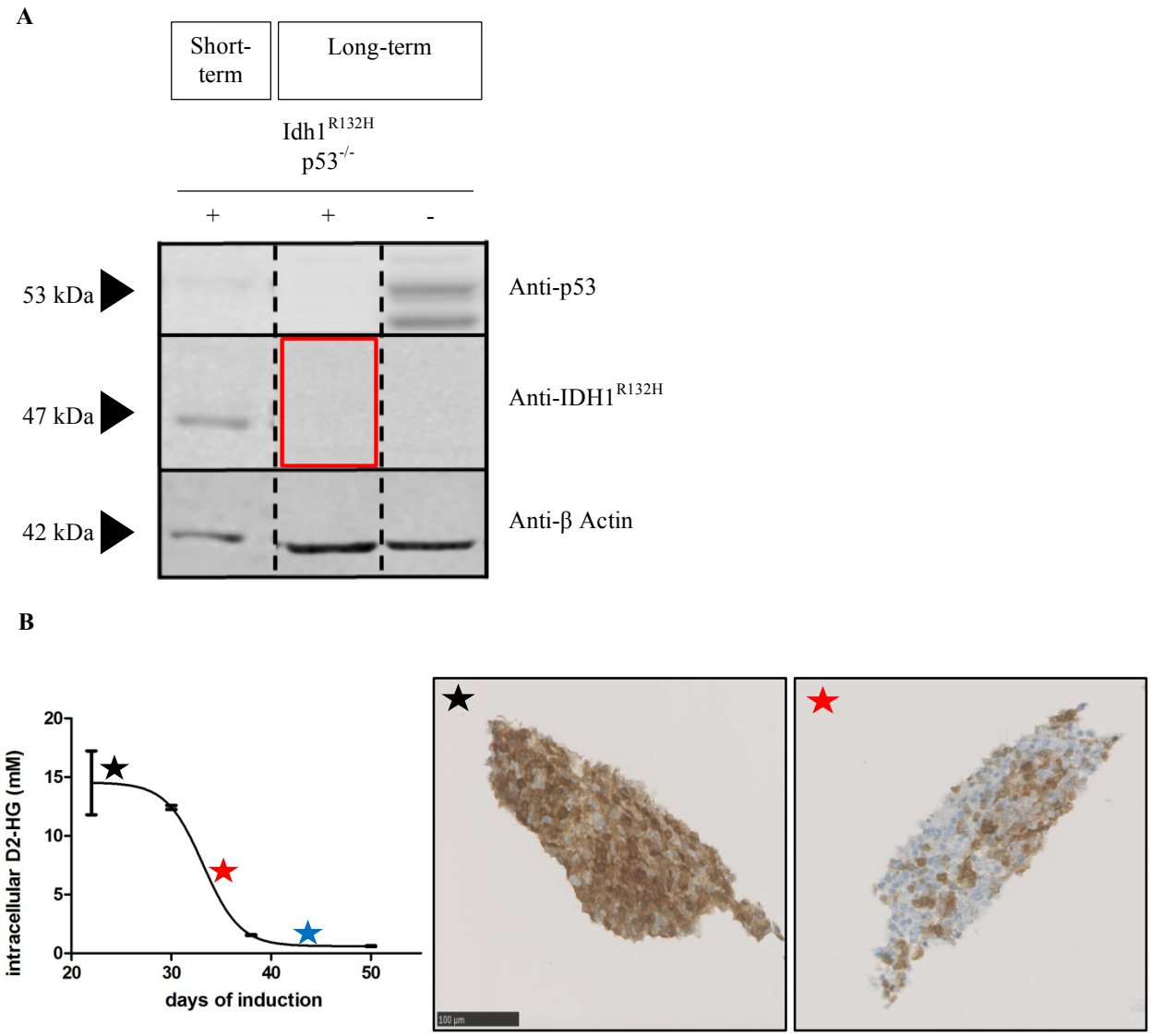

Figure 23. Loss of the Idh1^{R132H} mutation. A After protein extraction, Western blot analysis with the antibody to Idh1^{R132H} reveals a lack of mutant Idh1 protein more than 6 months after induction with 4-OHT. However, expression of mutant *Idh1* is still detectable in cells that were newly induced. The status of *Tp53* is not altered in both long- and short-term cultures. Staining against β Actin serves as a loading control. **B** Follow-up 2-HG screening of freshly induced cells starts directly after 4-OHT treatment. 2-HG level steadily decreases after 30 to 40 days, which is accompanied by a drop in the cytoplasmic expression signal of Idh1^{R132H}. (Indicated significances n = 3)

To understand the loss of Idh1^{R132H} in more detail, all cell lines were re-genotyped with primers P259/789 binding to lox P site 1 and to the exon containing the knock-in Idh1^{R132H} mutation (Supplement Table 2). Experiments confirm that the chromosomal loss is a general phenomenon in all long-term cultures that harbored the Idh1^{R132H} conditional allele, because

genotyping did not yield a PCR product in most cases, indicating that the loss encompasses a large chromosomal region. Only the PCR on DNA from cell line #13 leads to a PCR product that shifts from the normal Idh1^{R132H} knock-in at 867 bp to clearly lower product, suggesting a small chromosomal loss (Figure 24 A). In the following, this PCR product was used for sequencing analysis with primers P259 and P789. Sequencing shows a loss spanning a large region encompassing lox P site 1 up until Exon 3 (Figure 24 B). This loss leads to a frameshift mutation, finally causing the loss of mutant Idh1 protein.

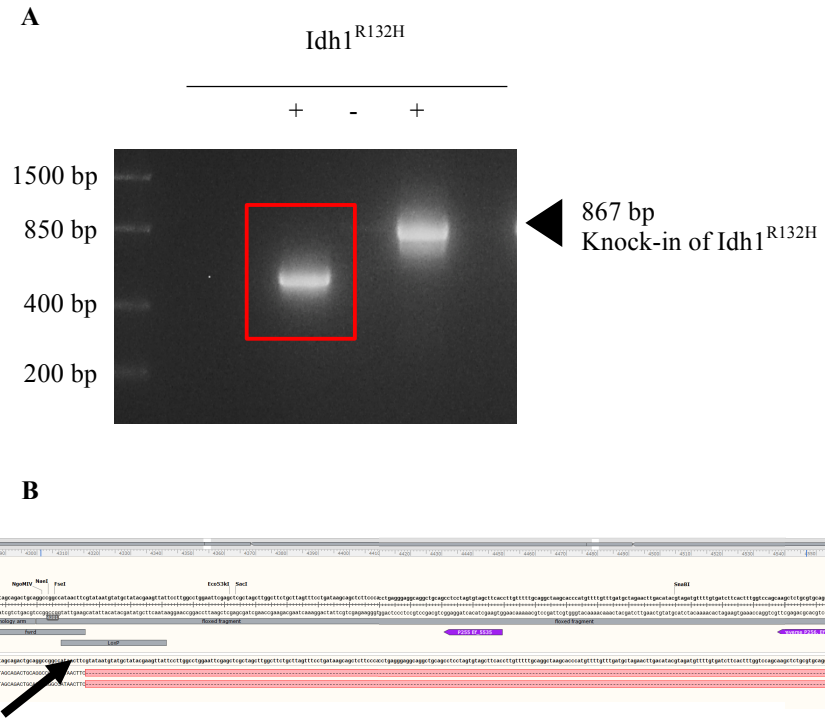

Figure 24. Analysis of the chromosomal loss of Idh1. A Re-genotyping of Idh1^{R132H} mutated cell lines reveals that the DNA of long-term cells show a shift of the PCR product towards 400 bp. Cells that previously lost the Idh1^{R132H} mutation exhibit a smaller PCR product compared to newly induced cells. **B** Sequencing alignment of the PCR product after genotyping of a cell line that lost the Idh1^{R132H} mutation. Black arrows indicate the whole region from lox P site 1 until Exon 3 that is not detectable anymore and thus cause the loss of mutant Idh1 protein.

3.6.1 Loss of Idh1^{R132H} *in vivo*?

After confirmation of the loss of the Idh1^{R132H} mutation *in vitro*, the question arose whether the same phenomenon can be observed *in vivo* as well. To answer this question, immunohistochemistry was performed. Slices were taken from a mouse that died two months after intracranial injections of Idh1^{R132H} mutated cell lines with a concomitant knock-out of *Tp53*. First, the depth of the slice was verified with a HE staining to make sure that the area of implantation was in focus. Subsequently, immunohistochemistry was performed with the

specific antibody to Idh1^{R132H}. Results clearly indicate that the implanted cells are still present, carry the Idh1^{R132H} mutation and invade the surrounding brain tissue (Figure 25). This result shows that there is a difference between the *in vivo* and the *in vitro* situation.

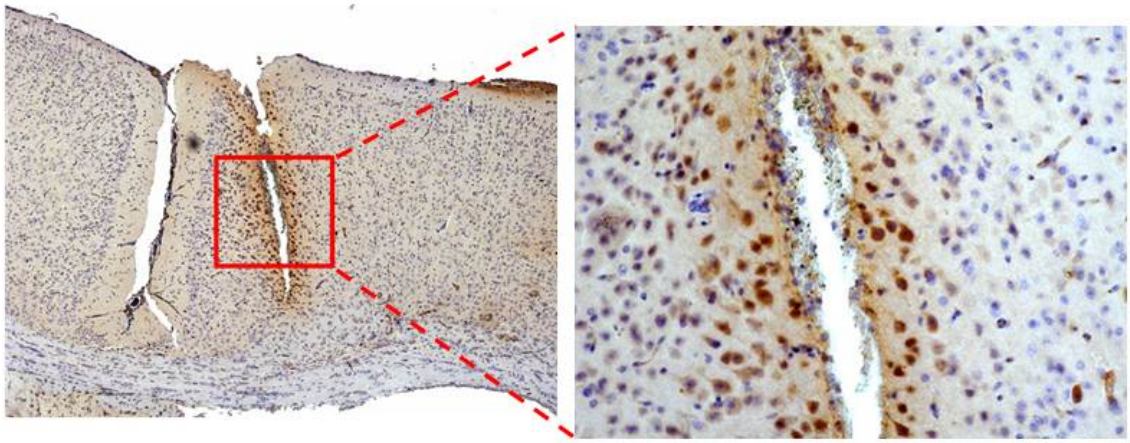

Figure 25. Positive Idh1^{R132H} staining two months after intracranial injection. Immunostainings of Idh1^{R132H} p53$^{-/-}$ implanted NSCs reveals a positive signal for Idh1^{R132H} in the surrounding brain parenchyma of the area of injection.

3.7 MRI monitoring of BALB/c nude mice after intracranial injections

Implanted mice were monthly monitored with a 1.5 T MRI scan. Usually, T2-weighted images were taken, whereas a T1-weighted recording was performed subsequently, if lesions were observed. During the first months of the *in vivo* study there was no indication of any space-consuming lesions in the area of implantation. However, 8 months post-surgery there are first indications for tumor growth in the right frontal cortex, observed in mice implanted with Idh1^{R132H} p53$^{-/-}$ cells (Figure 26 A, B). Tumor-like lesions are observed in 2/5 mice implanted with Idh1^{R132H} p53$^{-/-}$ cells, which is 2/3 mice implanted the same day from the same batch of cells. Calculated volumes of the lesions observed in T2-weighted measurements are 6 and 1.8 µl. Injection of contrast enhancing agent shows that lesions do not accumulate the substance, which is an often-observed phenomenon in murine glioma models (DKFZ, 2017). In addition, 1/3 mice intracranially injected with NSCs harboring a knock-out of *Tp53*, a control cell line, develop a lesion of 4.9 µl measured in the T2 sequence. This tumor does accumulate the contrast enhancing agent after injection and calculated volume after the T1-weighted sequence is 9.9 µl (Figure 26 C, D).

In contrast to mice injected with Idh1^{R132H} p53$^{-/-}$ NSCs, mice implanted with Idh1^{R132H} Cic$^{-/-}$ NSCs do not show any indication for tumor formation across the course of the study. This is also true for mice with Cic$^{-/-}$ cells.

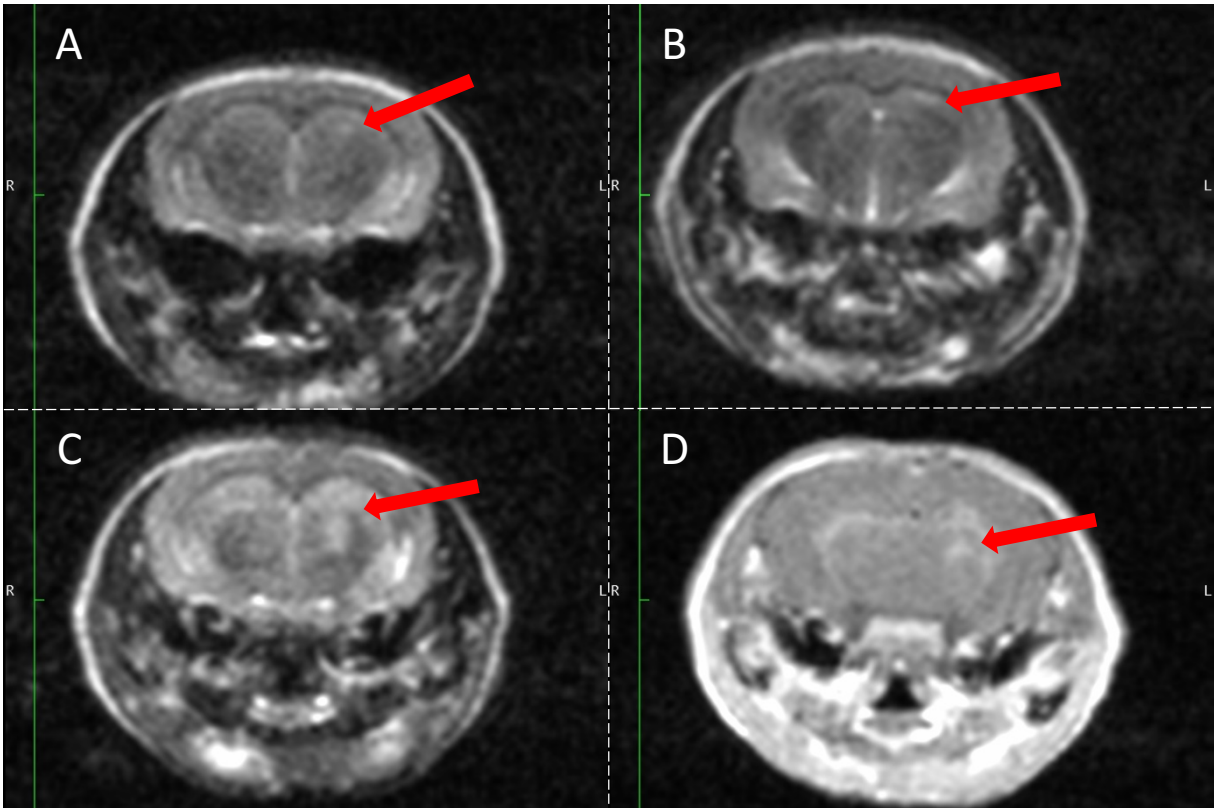

Figure 26. Murine glioma allograft generated in athymic BALB/c nude mice eight months after intracranial injections. A T2-weighted MRI of a mouse brain implanted with $Idh1^{R132H}$ $p53^{-/-}$ cells showing a lesion with a volume of 6 µl. **B** A smaller volume of 1.5 µl is measured in another mouse injected with $Idh1^{R132H}$ $p53^{-/-}$ NSCs, under comparable T2-weighted settings. **C** Picture taken from a T2-weighted sequence of a mouse that was implanted with single $p53^{-/-}$ cells eight months before. The volume of this lesion is 4.9 µl. **D** T1-weighted recording of the same mouse, indicating that the tumor accumulated the contrast enhancing agent. (Red arrows indicate the area of the lesion).

MRI signals and the calculated volumes of the lesions varied in the following months, which might be due to beginning formation of a tumor and the subsequent infiltrative growth characteristic of gliomagenesis. Thus, mice were further screened with MRI monthly. T2-weighted tumor volume of the first $Idh1^{R132H}$ $p53^{-/-}$ mouse decreases from 6 µl to 1.5 µl (Figure 27 A). The same is observed in the second mouse (Figure 27 B). Due to an already small volume of 1.8 µl, the lesion is not clearly visible anymore, one month later. In contrast, the only mouse implanted with $p53^{-/-}$, still had a detectable lesion in the next MRI. However, the volume of the lesion also dropped from 4.9 µl to 2.3 µl, calculated after T2-weighted MRI (Figure 27 C). T1-weighted images confirm the shrinkage from 9.9 µl to 2.6 µl (Figure 27 D). This lesion started to progress after ten months, which is in contrast to mice injected with $Idh1^{R132H}$ $p53^{-/-}$ NSCs (Figure 27 E).

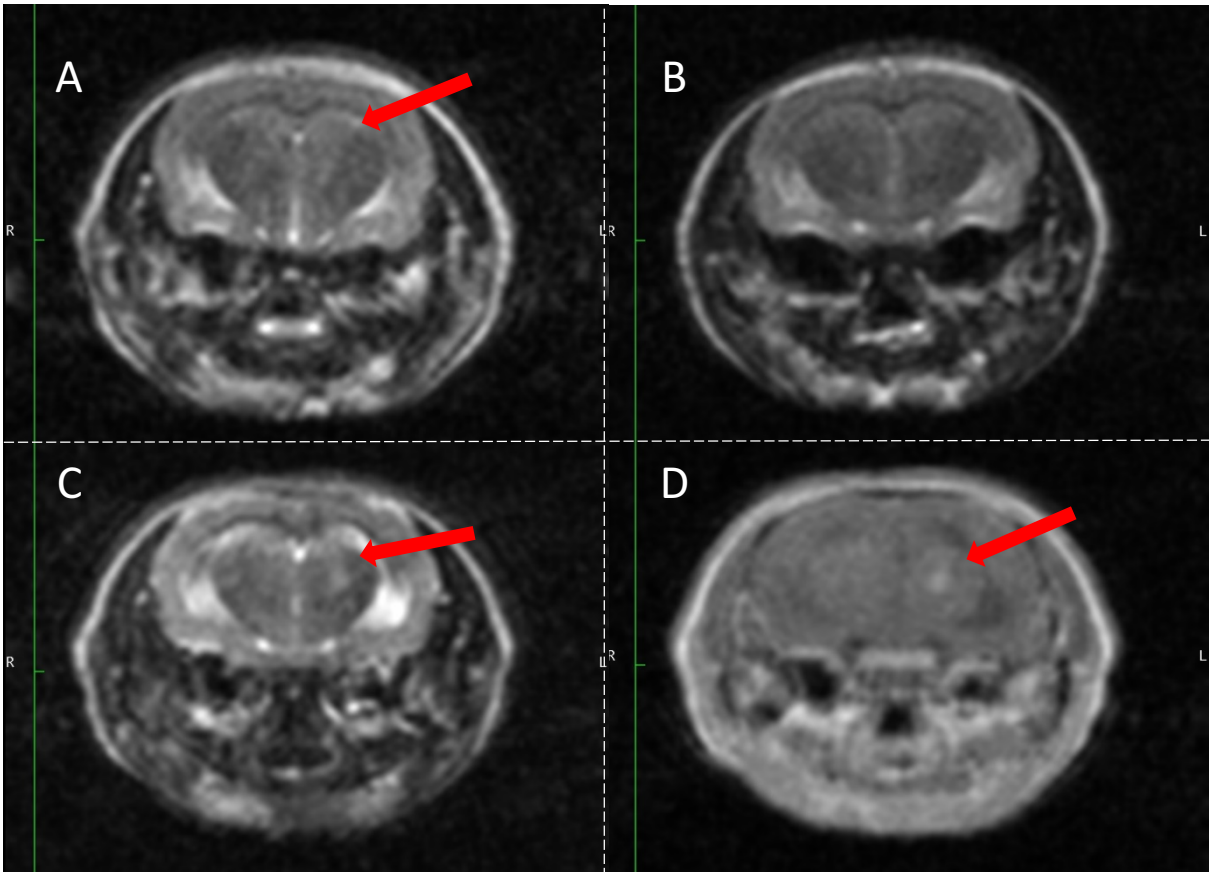

E

	June 2017	July 2017	Aug 17	Sep 17	Course
Idh1^{R132H} p53$^{-/-}$	0	6	1,5	0	
Idh1^{R132H} p53$^{-/-}$	0	1,8	0	0	
p53$^{-/-}$	0	4,9	2,3	18,7	

Figure 27. Decreasing volume of the lesions observed during MRI screen nine months after implantation. A T2-weighted MRI of a mouse brain implanted with Idh1^{R132H} p53$^{-/-}$ cells nine months previously, showing a lesion with a volume of 1.5 µl, which has a volume of 6 µl during the last scan. **B** Another mouse injected with Idh1^{R132H} p53$^{-/-}$ NSCs, has a volume of 1.8 µl eight months after implantation, whereas it is not clearly detectable anymore after nine months. **C** T2-weighted image of a mouse that was implanted with single p53$^{-/-}$ cells nine months before. The volume of this lesion is 2.3 µl, whereas it is 4.9 µl after eight months. **D** T1-weighted image of the same mouse, indicating that the tumor accumulates the contrast enhancing agent. The calculated size of the lesion after T1 recording is 2.6 µl. **E** Table depicting the course of tumor formation. Mice injected with Idh1^{R132H} p53$^{-/-}$ NSCs show a decreasing volume. Tumor growth in the p53$^{-/-}$ injected mouse also first decreases but then reaches a stable progress observable in later MRI scans (A-D, red arrows indicate the area of the lesion).

3.7.1 9.4 T scans

Due to the low resolution of the 1.5 T MRI scans, one could not exclude that there is no tumor anymore. To validate this, a 9.4 T MRI with a better spatial resolution was used for recordings before termination of the experiment. T2-weighted images were taken from each

mouse, whereas a T1-weighted recording was only performed with the animals, which showed lesions in the 1.5 T MRI. The results are not comparable to the 1.5 T MRI screens at eight months after implantation. The 9.4 T images further confirm that there are no visible lesions 12 months after surgeries. However, 9.4 T data depict the area of implantation in the frontal cortex even one year after intracranial injections. Amongst the puncture caused by the injection needle in the cortex, images show a hole further below the implantation. These holes can only be observed in 3/5 mice implanted with double mutant cells, in 2/4 mice with $Idh1^{R132H}$ cells and in 1/2 mouse with cells harboring a single knock-out of *Tp53* (Figure 28). Interestingly, the animals showing a lesion in 1.5 T MRI scans were amongst those. Comparable to 1.5 T data, mice with $Cic^{-/-}$ as well as $Idh1^{R132H}$ $Cic^{-/-}$ NSCs do not show any signs of a lesion in the area of implantation.

3.8 Immunohistochemistry

To validate the *in vivo* model immunohistochemistry was used. First a HE control staining was prepared to validate the correct position of the slice, the area of implantation. One year after surgeries, the puncture was not clearly visible in all cases. Because of this, anatomical orientation was used to find the correct depth/position. Additionally, stainings of mice implanted with induced cell lines were always compared to those with non-inducible cell lines. After the correct identification of the area of implantation by HE staining, subsequent slices were stained with antibodies to detect $Idh1^{R132H}$. To also detect non-inducible control cells, an antibody to forkhead box protein N1 (Foxn1) was used. BALB/c nude mice are deficient for this gene, which is responsible for the hairless and athymic phenotype. Implanted cells are derived from Bl6/N mice and by this, are positive for Foxn1. Although, different concentrations and pretreatments were tested, only neurons showed a reproducible positive staining. But neurons are known for false positive staining in immunohistochemistry, which could be confirmed in the parallel stained control slices.

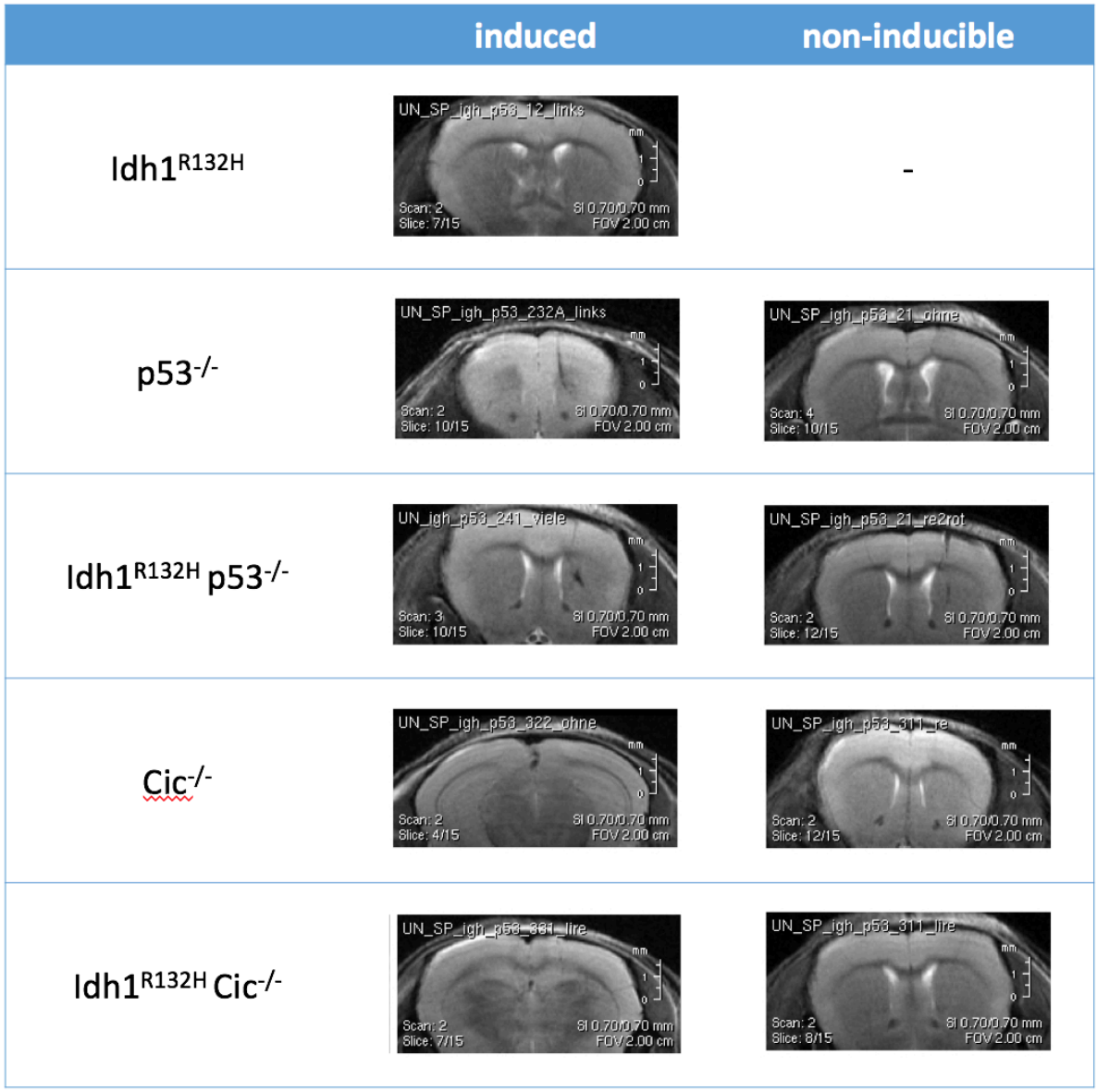

Figure 28. 9.4 T scans indicate the injection puncture 12 months after intracranial injections. T2-weighted images represent one example per group of mice with the specified NSCs injected. A lesion due to tumor formation cannot be detected in all mice imaged. (- means that no mice of the respective group were still alive during the 9.4 T MRI scan)

To be able to anyway detect the implanted cells, an antibody to Cre was used. For the validation of the antibody, slices of the mouse were taken that died two months after surgery, in which the Idh1^{R132H} staining was already positive and the injection puncture is clearly visible (Figure 29 A, B). The presence of the Idh1^{R132H} positive cells was confirmed by positive Cre recombinase staining (Figure 29 B, C). The successful application of the Cre antibody allowed using it on slices taken from mice that were alive until termination of the experiment. The challenge was to detect the implanted cells in exactly these mice as the injection point is mostly overgrown one year after surgery.

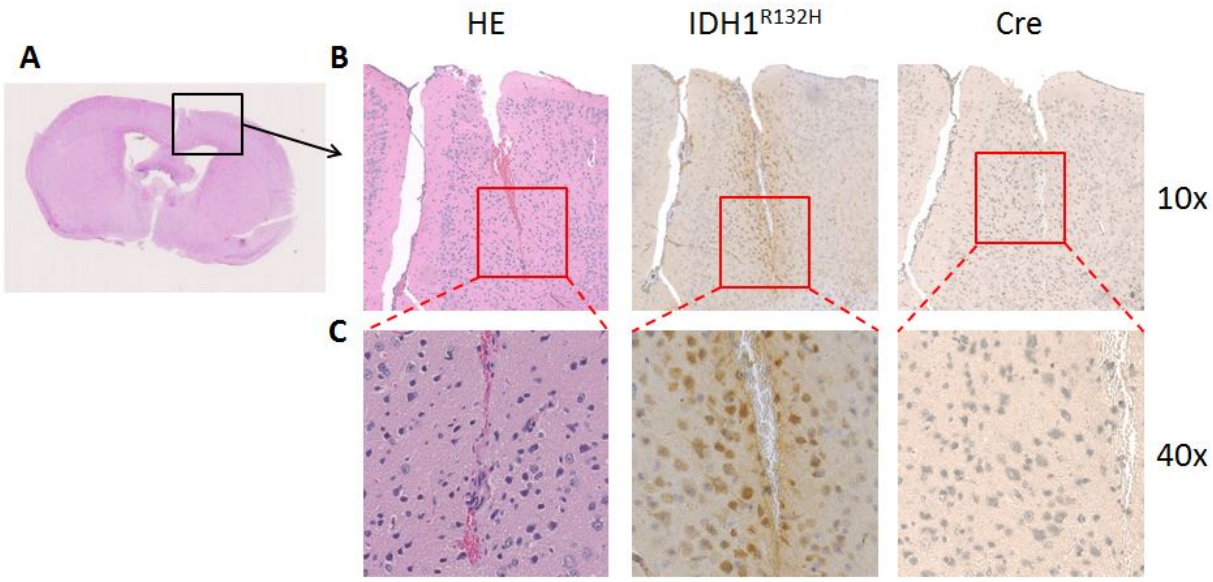

Figure 29. Two months after intracranial injections Idh1^{R132H} positive cells start to invade the brain parenchyma. A Image of a HE overview staining of a mouse brain implanted with Idh1^{R132H} p53$^{-/-}$ cells two months previously. Black box indicates the area of injection. **B** 10x magnification of this area stained with HE for morphological analysis. Application of an antibody specific to Idh1^{R132H} shows that injected cells do not lose the mutation in vivo and start to invade the brain. An antibody to Cre-recombinase additionally confirms presence of the injected cells. **C** 40x magnification of the red framed areas indicated in A.

Next, slices from a mouse that was also intracranially injected with NSCs harboring both, the Idh1^{R132H} mutation and a knock-out of *Tp53*, but lived until termination of the experiment, was analyzed. This mouse was one of the mice in which a lesion in the right frontal cortex could be observed in MRI images 8 months after implantation.

The Cre antibody was applied to detect the injected cells. No positive signal for Cre could be detected (Figure 30 B) in the area where the cells were originally implanted. After careful examination of the whole brain slice, cells with a positive cytoplasmic signal were detected in different regions. These cells are located in the corpus callosum and more lateral located brain areas of the right hemisphere (Figure 30 C, D).

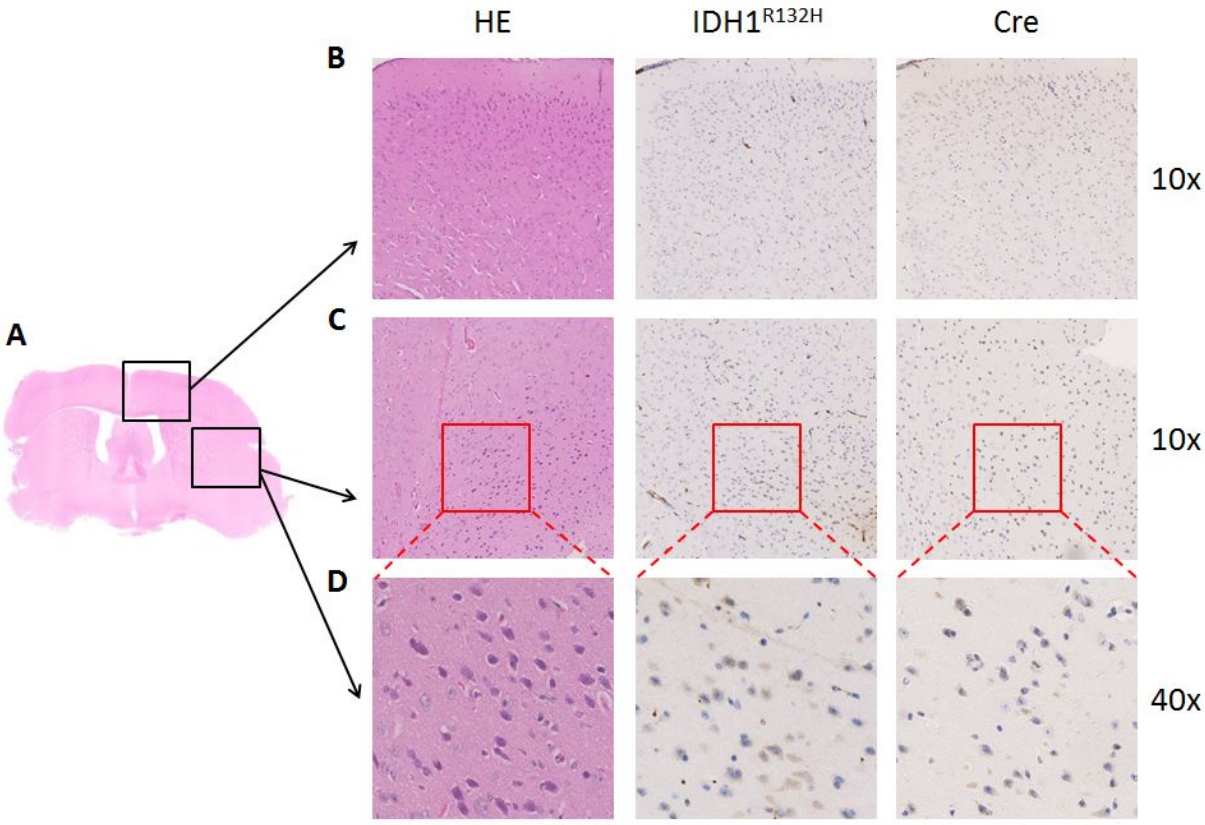

Figure 30. Two months after intracranial injections Idh1^{R132H} positive cells start to invade the brain parenchyma. A Image of a HE overview staining of a mouse brain implanted with Idh1^{R132H} p53$^{-/-}$ cells twelve months previously. Upper black box indicates the area of injection. Right black box represents the actual position of the injected cells in the right hemisphere. **B** 10x magnification of the injection area stained with HE for morphological analysis. Staining against Idh1^{R132H} and Cre-recombinase indicates that injected cells are not located in this area. **C** 10x magnification of an area in the right hemisphere with Idh1^{R132H} positive cells, showing presence of the injected cells. Cells in the same area also have an enhanced expression signal for Cre-recombinase. **D** 40x magnification of the red framed areas indicated in C.

3.9 *In vitro* analysis of a *Cic* knock-out alone and in an Idh1^{R132H} background

In the following chapter the effects of a *Cic* knock-out with or without an additional Idh1^{R132H} mutation will be described, which is a combination commonly found in oligodendroglioma. All experiments were carried out after two treatments with 4-OHT, which takes two weeks and subsequent validation of the cell lines. The effects of the Idh1^{R132H} mutation is not considered here, as the functional validation of Idh1^{R132H} alone is described in chapter 3.3.

3.9.1 Cell viability

Proliferation analysis reveals that cells harboring a single knock-out of *Cic* have a significantly increased cell viability compared to the respective controls. The cell number of Cic$^{-/-}$ cells is increased to 203.0 ± 72.9% 5 days after incubation. Interestingly, if the knock-

out of *Cic* appears in an Idh1^{R132H} background, cell viability is not altered (96.7 ± 20.7% from control; Figure 31 A). Same can be observed when measurements are performed in time series on day 0, 3 and 5. Measurements reveal that Cic$^{-/-}$ cells have a steeper growth curve compared to controls (35.9% vs. 19%, daily). In contrast, double mutant cells show a growth behavior comparable to their respective controls. The growth curve of Idh1^{R132H} Cic$^{-/-}$ cells have a slope of 14.5% daily, compared to controls (19.4%; Figure 31 B). Based on these results, the enhanced cell viability of single *Cic* knock-out cells is inhibited by a concomitant Idh1^{R132H} mutation, which is in line with the above described results on Idh1^{R132H} alone.

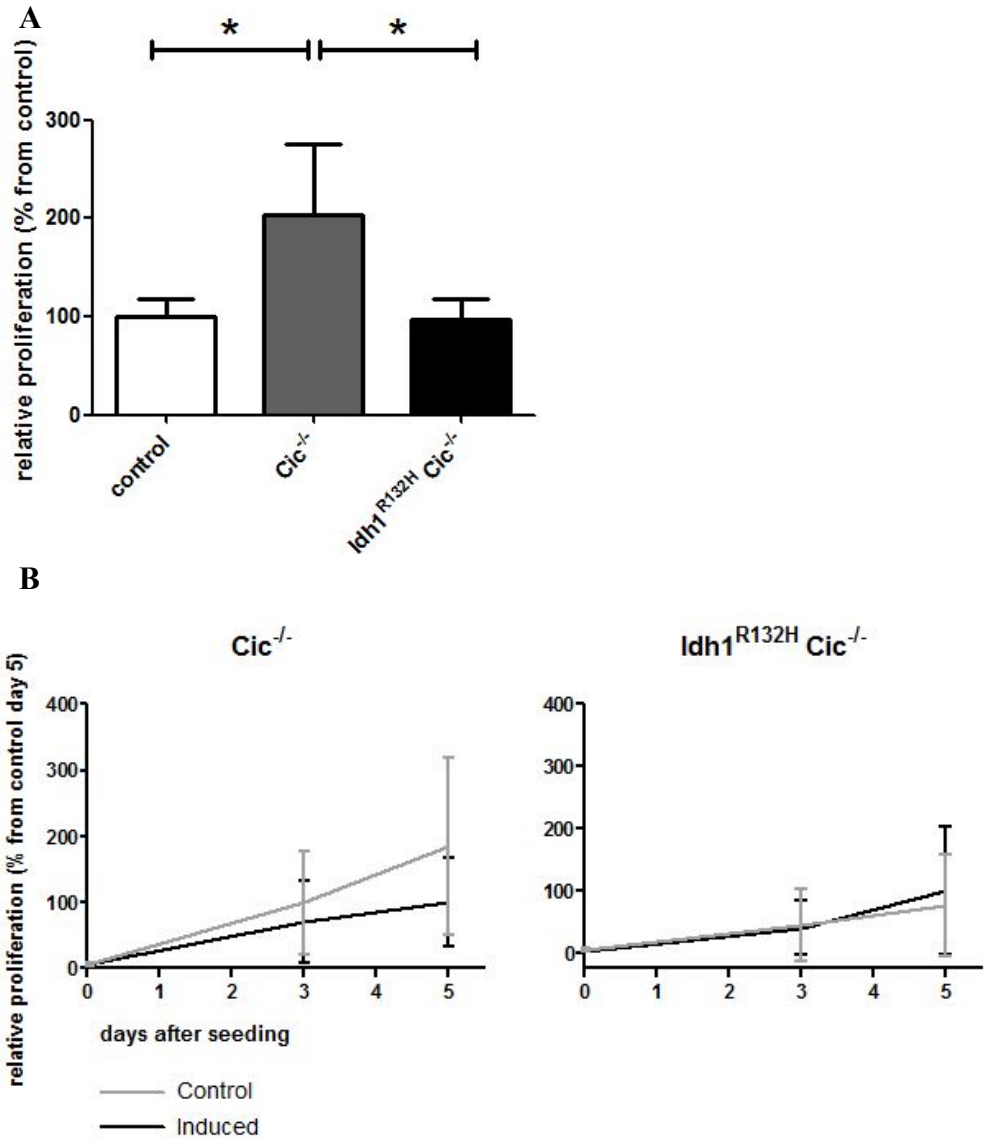

Figure 31. A knock-out of *Cic* significantly increases cell viability. A Genetically altered cells were validated prior to seeding of 5000 cells in 96-well plates and measurements using the CellTiter-Glo 3D Cell Viability Assay were performed five days after seeding. Induction of Cic$^{-/-}$ leads to a significant increase of cell viability compared to respective controls. The combination of both alterations, Cic$^{-/-}$ and Idh1^{R132H} does not alter cell viability. Bar plot of CellTiter-Glo3D assay, normalized to average control. **B** Time series of the CellTiter-Glo 3D

Cell Viability Assay reveals that cells harboring a knock-out of *Cic* have a growth advantage compared to a combination with Idh1^{R132H}. Measurements were performed after 0, 3 and 5 days of incubation. Diagram of the CellTiter-Glo 3D Cell Viability Assay measured on three time points, normalized to average control on day 5. (Indicated significances: two-sided unpaired students t-test, * = $p<0.05$, n = 3).

3.9.2 Colony formation in soft agar

Next, it was also investigated whether the knock-out of *Cic* has an effect on the cells ability to form colonies under growth aggravated circumstances. Results show that a knock-out of *Cic* does not affect colony formation, compared to the control cells (94.1 ± 8.4% from control). Further, if the knock-out of *Cic* is accompanied by the Idh1^{R132H} mutation, the cells ability to form colonies is not significantly altered as well. The average colony formation rate of double mutants compared to controls is 96.3 ± 10.3% (Figure 32). These results show that the genetically altered cells are able to grow under growth aggravated circumstances.

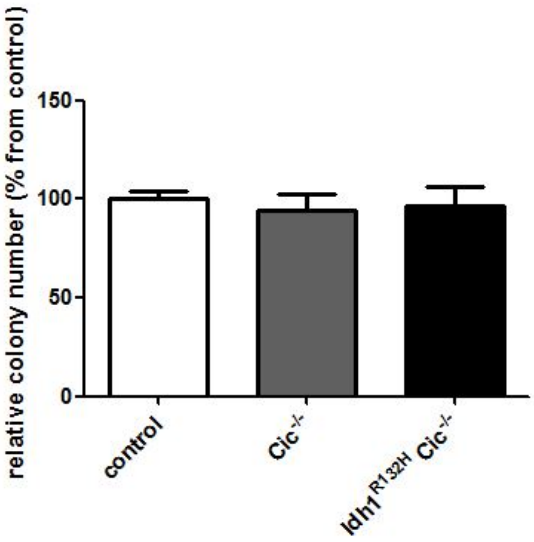

Figure 32. Induction of Cic$^{-/-}$ does not affect colony formation rate in soft agar. Previously induced and validated cell lines were seeded in a density of 2000 cells per well in a soft agar matrix. Measurements were performed using the CellTiter-Blue Assay after 7 days of incubation. Cic$^{-/-}$ alone, or in combination with Idh1^{R132H} does not alter colony formation in soft agar. Bar plot of the soft agar assay, normalized to average control after one week of incubation. (Indicated significances: two-sided unpaired students t-test, * = $p<0.05$, n = 3)

3.9.3 Effects on epigenetics

As described above, induction of Idh1^{R132H} has an effect on epigenetics, which might be affected by an additional knock-out of *Cic*. Thus, the aim was to investigate whether Idh1^{R132H} and Cic$^{-/-}$ influence abundance of 5mC and 5hmC. As effects on epigenetics might

not be detectable after initial induction, cells were cultivated for six months prior to experiments. DNA was extracted as described above and subjected to dotblot analysis on a nitrocellulose membrane with antibodies to 5mC and 5hmC. A knock-out of *Cic* alone does not influence either levels of 5mC and 5hmC. When compared to controls, the abundance of 5mC in *Cic* knock-out cells is 81.2 ± 31.7% and 5hmC 80.1 ± 20.8%. $Cic^{-/-}$ in an $Idh1^{R132H}$ background also does not alter levels of 5mC and 5hmC significantly. 5mC expression is 87.7 ± 6.9%, whereas 5hmC expression is 90.1 ± 7.9% from control (Figure 33). These results show that a knock-out of *Cic* with or without the presence of $Idh1^{R132H}$ does not alter DNA methylation by regulating the ratio of 5mC and 5hmC.

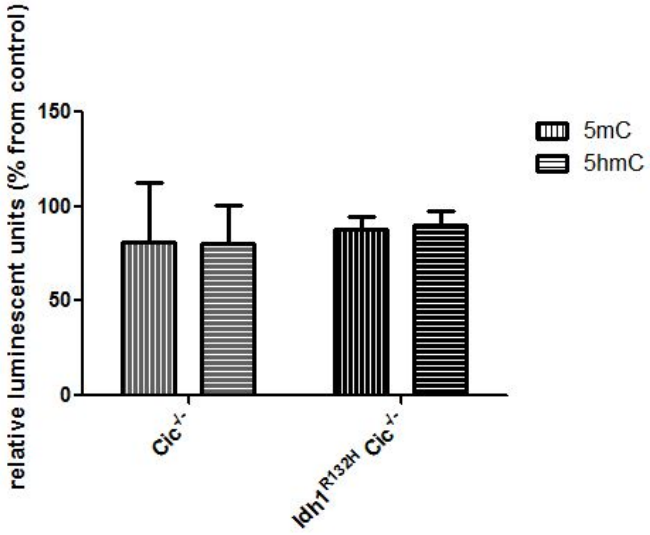

Figure 33. The presence of $Cic^{-/-}$ with or without $Idh1^{R132H}$ does not alter DNA methylation. DNA was extracted from genetically altered cell lines induced six months beforehand and concentration determined with Qubit. Samples were blotted onto a nitrocellulose membrane with a dotblot device. Expression analysis of DNA methylation markers was carried out with antibodies to 5mC and compared to 5hmC in induced cell lines and controls. Expression of $Cic^{-/-}$ alone or in an $Idh1^{R132H}$ background does not alter either 5mC or 5hmC levels. Bar plot reflects the expression of 5mC and 5hmC, normalized to average control. (Indicated significances: two-sided unpaired students t-test, * = $p<0.05$, n = 2).

3.9.4 Production of 2-HG

As cells harboring an $Idh1^{R132H}$ mutation produce remarkable amounts of 2-HG, the next aim was to investigate whether the production of 2-HG is influenced by a concomitant knock-out of *Cic*. Cells harboring the knock-out of *Cic* alone do not produce 2-HG. The values detected were below the quantification limit of the assay (0.2 ± 0.1 mM). In contrast, cells harboring an $Idh1^{R132H}$ mutation and a knock-out of *Cic* produce 2-HG concentrations, comparable to single $Idh1^{R132H}$ mutated cells (Figure 34). The intracellular concentration of 2-HG measured

in these cells is 2.4 ± 1.0 mM. The production of 2-HG in cells harboring both genetic alterations does not change across the time of cultivation of the cells, as it does for Idh1^{R132H} cells or the combination of Idh1^{R132H} and p53$^{-/-}$. Those cells show a progressing decrease of the production of 2-HG after two months latest. The decrease of 2-HG was accompanied by a loss of Idh1^{R132H}. These data show that the knock-out of *Cic* in Idh1^{R132H} cells induces different mechanisms, which distinguishes them from Idh1^{R132H} cells with or without p53$^{-/-}$.

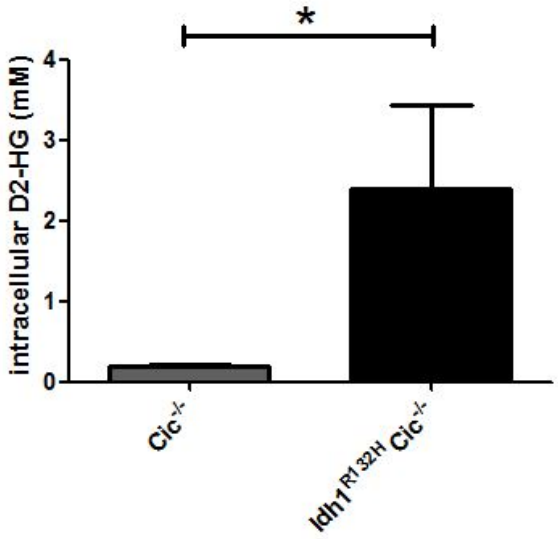

Figure 34. *Cic* knock-out cells do not produce 2-HG and it does not influence production of 2-HG in cells with an additional Idh1^{R132H} mutation. 300 µl of previously induced and validated cells was taken for lysate production and protein concentration was determined with BCA. 2-HG concentration was measured with a 2-HG quantification assay. Cic$^{-/-}$ cells do not produce 2-HG. A combination of both Idh1^{R132H} and Cic$^{-/-}$ leads to release of 2-HG. Bar plot of the 2-HG assay carried out in triplicates, normalized to average control. (Indicated significances: two-sided unpaired students t-test, * = $p<0.05$, n = 3).

3.10 PET imaging: IDH1^{R132H} and its relation to epileptogenesis

The main aim of this project was the development of an *in vivo* allograft model based on IDH1^{R132H}, but in addition this model could also be used to investigate the co-occurrence of epileptic seizures in such glioma.

To do so, it is of utmost importance to understand the relation of IDH1^{R132H} and epilepsy. First, the question is how to investigate epileptogenesis in mice, as milder types of seizures are only barely detectable by behavioral changes. To overcome this problem, the occurrence of seizures in mice harboring a glioma was investigated with imaging methods. In the long run, this method could be additionally applied to the mouse model based on the IDH1^{R132H}

mutation and show whether the induced tumor is accompanied by the development of epileptic seizures.

PET/CT scans were performed as described after accumulation of FDG used as a surrogate for potential seizure occurrence. For analysis, the mean PET/CT Standardized Uptake Value (SUV) was calculated by the animal imaging facility of the DKFZ, which serves as a marker for the distribution volume of the radiotracer. The SUV includes the concentration of the radioactivity within the region of interest, the amount of radiolabeled FDG and the weight of the animal (Kinahan and Fletcher, 2010). Uptake of FDG in the muscle was used as control tissue for analysis. Based on the findings that interictal brain activity might be accompanied by contralateral hypometabolism, region of interest was set in the left hemisphere as this is also not influenced by glucose uptake by the tumor implanted in the right hemisphere.

The experiment was successfully performed with six mice harboring a secondary GBM xenograft with $IDH1^{R132H}$ mutation (glioma xenograft w/$IDH1^{R132H}$), two mice with a primary GBM without $IDH1^{R132H}$ mutation (glioma xenograft w/o$IDH1^{R132H}$) and three mice that were implanted with control cells without mutation (control). Imaging was performed when tumor volume was about 50 µl observed in MRI images in the right hemisphere.

First PET scans reveal an average SUV_{mean} of 5.3 ± 1.5 in the glioma xenograft w/$IDH1^{R132H}$ and 4.1 ± 1.4 in the glioma xenograft w/o$IDH1^{R132H}$ group. The control group has a SUV_{mean} of 5.2 ± 0.9 (Figure 35). After initial PET measurements, mice were treated with an $IDH1^{R132H}$ specific inhibitor reducing the production of 2-HG, which is believed to be a trigger for epileptogenesis due to its structural similarity with glutamate (Kolker *et al.*, 2002; Pusch *et al.*, 2017). The idea was to investigate in a subsequent PET recording 24 h later, whether FDG uptake is altered and might thus give an indication of prior epileptogenesis. PET scans 24 h after inhibitor treatment have an average SUV_{mean} of 6.7 ± 2.4, 6.3 ± 1.9 and 3.7 ± 0.3 in the glioma xenograft w/$IDH1^{R132H}$, the glioma xenograft w/o$IDH1^{R132H}$ group and the control group respectively. Mice harboring a glioma with $IDH1^{R132H}$ mutation have a tendency towards an increase in metabolic activity after treatment with BAY1436032, but it was not significant (Figure 35).

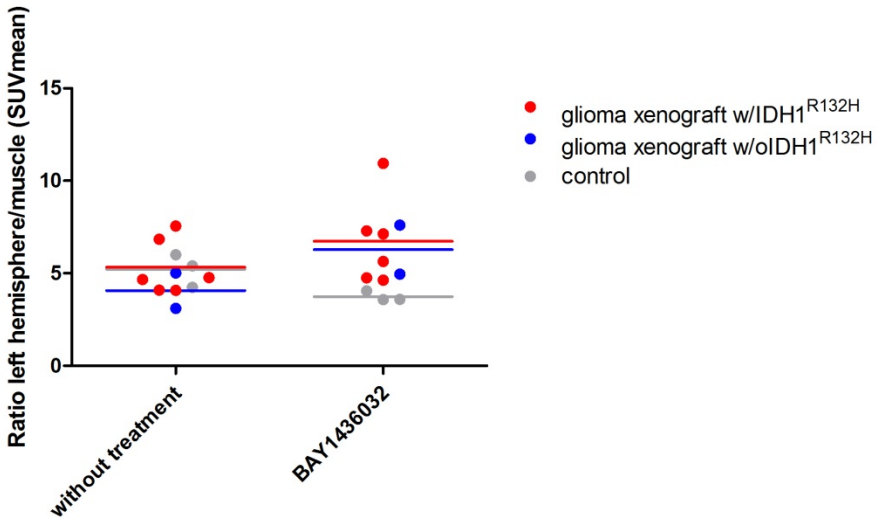

Figure 35. Suspected epileptogenesis in IDH1^{R132H} glioma mice cannot be observed with FDG kinetic analysis. SUV_{mean} of FDG accumulation does not give an indication of hypometabolism in the glioma xenograft w/IDH1^{R132H} group as values do not differ between groups. No significant effect can be observed after treatment with the IDH1^{R132H} specific inhibitor BAY1436032. (Calculated significances: two-sided unpaired students t-test, * = $p<0.05$, $n \geq 2$).

On the first day without treatment no hypometabolism can be observed in the glioma xenograft w/IDH1^{R132H} and values between groups do not significantly differ. Likewise, there is no significant effect 24 h after treatment with the IDH1^{R132H} specific inhibitor. The results indicate that there is no occurrence of epilepsy in mice with implanted glioma.

Furthermore, it can be observed that BALB/c nude mice have an atypical accumulation of FDG throughout the whole body. The radiotracer is concentrated mainly in the neck and back and only barely in the brain (Figure 36). Normally, it can be assumed that FDG should accumulate in the area of tumor growth, which is not seen at all. These results show that PET imaging in combination with BALB/c nude mice is not a suitable method to investigate the occurrence of epilepsy.

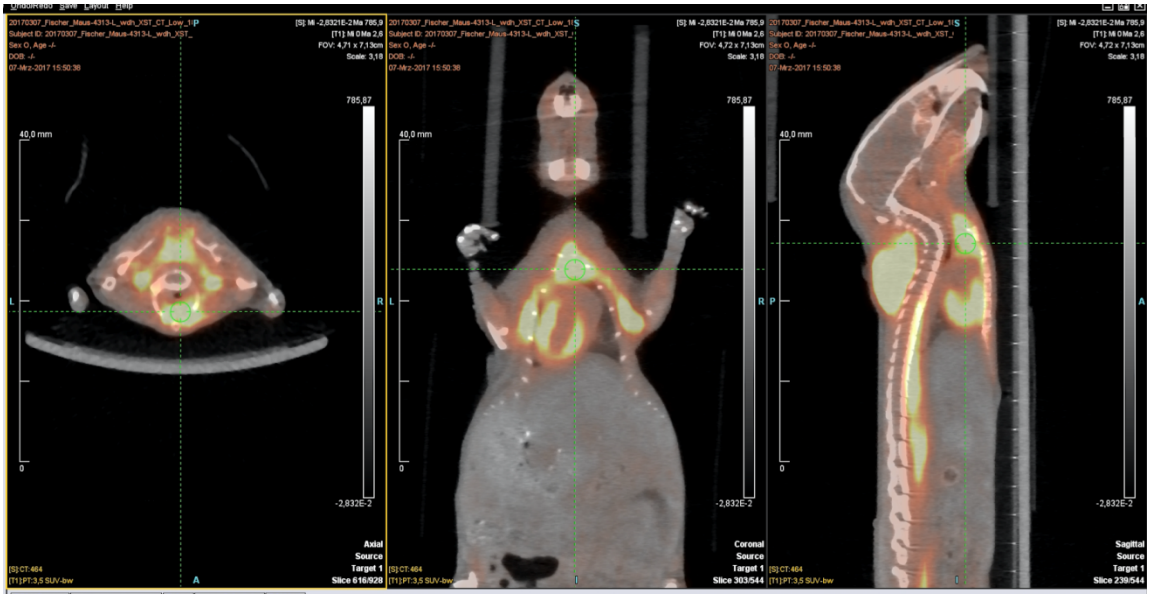

Figure 36. PET image of a BALB/c nude mouse with atypical accumulation of FDG. Scan of a mouse implanted with a glioma xenograft w/IDH1^{R132H}. Strong FDG accumulation can be observed in the thorax, especially in the neck and along the spine. Increased glucose uptake is completely missing in the area of implantation in the brain.

4 Discussion

The aim of this project was to establish an *in vivo* allograft model based on neural stem cells from mice with different genetic modifications, mimicking molecular alterations in human diffuse, *IDH*-mutant glioma. Generation and validation of these neural stem cells with different genetic modifications was successful, but these cells did not show strong tumorigenic potential compared to their unmodified counterparts. This could be due to the growth behavior of low grade gliomas that also proliferate slowly in the human situation. Nevertheless, these cells were implanted *in vivo* to analyze if the modifications have higher tumorigenic potential *in vivo*. This attempt showed more promising results, as tumor growth was visible after eight months. Unexpectedly, these tumors disappeared until the end of the observation period of twelve months. In conclusion, the project aim was only partially reached, but it delivered data and a suitable model system essential for further understanding of the function of the $Idh1^{R132H}$ mutation.

Within this project it was possible to solve the following questions:

- Is the $Idh1^{R132H}$ mutation sufficient to generate a glioma in a mouse model?
- Are the common co-occurring mutations in human glioma important for gliomagenesis in a mouse model?

Points that need further understanding and for which the established system is the best suitable model, are:

- What makes the $Idh1^{R132H}$ mutation essential in human glioma and why is it not required *in vitro*?
- Are double-strand breaks the underlying cause for genome instability? When exactly is genome instability initiated and is it probably a very early event taking place after induction?
- By which mechanism does the mutation promote its exclusion? Is this a pro-tumorigenic effect of the $Idh1^{R132H}$ mutation, causing higher mutation rates?
- What is to be learned from the behavior of these NSCs *in vivo*? Was the right cell type used?
- What is the effect of 2-HG if it is released in an environment with a normal immune system?
- Why did the tumors diminish after initial growth?

In addition to the development towards a more tumorigenic phenotype, cells harboring the Idh1^{R132H} mutation either alone, or in combination with a knock-out of *Tp53*, lost the mutation within two months. In fact, this is a very significant observation, as cultivation of cells deriving from human gliomas also show the same loss of the Idh1^{R132H} mutation. Thus, these findings display important parallels between the human system and the one described in this work.

4.1 Effects of Idh1^{R132H}

As a first attempt, cell viability was analyzed indicating that induction of the Idh1^{R132H} mutation significantly decreases the cell number (Figure 37 A). Given the fact that the CellTiter-Glo 3D Assay is based on ATP released from viable cells and 2-HG is known to inhibit ATP synthase and mTOR signaling, further experiments were performed to analyze the proliferative capacity (Fu *et al.*, 2015).

Results were further confirmed by application of the CellTiter-Blue Assay, which is independent of ATP production, but dependent on NADP. However, results confirm that Idh1^{R132H} also significantly decreases the colony formation rate (Figure 37 C). As the colony formation assay is a measure to examine the tumorigenic potential of cells, it points towards a missing capability of Idh1^{R132H} alone to induce tumor formation. Mutant IDH1 produces high concentrations of the oncometabolite 2-HG, which amongst others modifies DNA and histone methylation and induces a block in differentiation (Dang *et al.*, 2010; Ward *et al.*, 2010). Based on this, one can assume that the suppressing effect observed shortly after induction of Idh1^{R132H} is related to 2-HG.

These results are in line with other studies describing a decreased proliferation rate due to mutant IDH1. Ectopic overexpression of IDH1^{R132H} in glioblastoma cell lines leads to a reduced proliferation by downregulation of the Wnt/β-catenin signaling pathway (Cui *et al.*, 2016). Further results with comparable glioma cell line models were also reported *in vitro* and in an intracranial *in vivo* model (Bralten *et al.*, 2011). On the other hand, there is also evidence that expression of Idh1^{R132H} enhances proliferation. Expression of Idh1^{R132H} in the mouse subventricular zone stem cell niche recapitulates features known for early gliomagenesis (Bardella *et al.*, 2016). In this case it should not be disregarded that mutant cells were implanted in a neurogenic stem cell niche, which is a favorable environment and not comparable to an *in vitro* situation. Nevertheless, the present study shows that expression

of Idh1^{R132H} could potentially induce proliferation. Furthermore, it points towards the importance of the surrounding environment. Unexpected was the finding of p53$^{-/-}$ leading to a significant decrease of cell viability (Figure 37 A). These results contrast the knock-out of *Tp53* in human cancers, leading to a decrease in apoptosis and missing DNA repair, which enhances proliferation and accumulates further mutations (Brown and Wouters, 1999).

The cells used in this study were treated with 4-OHT previously, inducing Cre recombination, which might have a growth-inhibitory effect. The 4-OHT treatment might be toxic, depending on time and dosage of 4-OHT (Loonstra *et al.*, 2001). To avoid this, treatment of 4-OHT was tested in different concentrations before experiments started. It was clearly visible that a concentration of 1 µM 4-OHT did not have a growth suppressing effect, whereas cells died from tenfold higher concentrations (Supplement Figure 2). Further, control cells to p53$^{-/-}$ were also treated with 4-OHT and proliferation was not altered in these cells at all (Figure 37 A). Thus, it can be concluded that the decrease of cell viability due to induction of p53$^{-/-}$ is most probably a direct effect. As p53 is involved in several important cellular processes, such as cell cycle regulation and apoptosis, it might be that this has an impact on the cells' behavior. p53 might for example alter ATP production, as colony formation was not affected in contrast to cell viability. The colony formation assay functions independent on ATP levels, but dependent on $NADP^+$, which is also based on metabolism. Therefore, the colony formation assay should be carried out in 6-well format and colonies should be counted after staining with crystal violet.

In line with the effects of either Idh1^{R132H} or p53$^{-/-}$ alone, a combination of both did also decrease cell viability (Figure 37 A). Accordingly, the effect of mutant Idh1 with concomitant production of 2-HG cannot be rescued by an additional knock-out of *Tp53*. There is a tendency observable that double mutant cells have a growth advantage when compared to single Idh1^{R132H} cells.

In contrast to the effect of the Idh1^{R132H} mutation on cell viability and colony formation, the decreasing effect of p53$^{-/-}$ and of the combination of both alterations was not observed in the CellTiter-Blue Assay (Figure 37 C). Experiments have rather shown that cells harboring the knock-out of *Tp53* alone or in combination with mutant *Idh1* are able to grow in an extracellular matrix-like environment, which is described as a hallmark of carcinogenesis *in vitro*. This might suggest that cells might be able to develop a tumorigenic behavior *in vivo*.

An interesting question here is whether $p53^{-/-}$ is immune to the effect of $Idh1^{R132H}$ on colony formation. To unravel this, cell viability should be measured in *Tp53* knock-out cells treated with 2-HG. If 2-HG has no growth suppressing effect, this would confirm that $p53^{-/-}$ is immune to the Idh1 mutation with concomitant production of 2-HG.

To further examine whether the reduced cell viability due to $Idh1^{R132H}$ might be mimicked by an enhanced rate of apoptosis, Western blot experiments were performed. For this experiment, late apoptotic proteins were chosen for analysis, as they only affect the very downstream part of the signaling cascade. Caspase 3 and 7 are also called executioner caspases, irreversibly inducing apoptosis without another contributor (Fuchs and Steller, 2011). Results have shown that there was no significant effect of $Idh1^{R132H}$ on apoptosis, further evidencing that the proliferative capacity is decreased (Figure 37 E). This is in contrast to the enhanced levels of apoptosis associated with $IDH1^{R132H}$ (Cui *et al.*, 2016). The explanation for this opposing result might be based on a different model system. Human glioblastoma cell lines were used with an overexpression of $IDH1^{R132H}$, which is a different background. Glioblastomas are tumors that do not per se carry the $IDH1^{R132H}$ mutation, which might explain the different behavior.

A knock-out of *Tp53* either alone or in combination with $Idh1^{R132H}$ shows a tendency of decreased apoptotic levels (Figure 37 E). Protein 53 is thought to induce apoptosis by transcriptional activation of Bax, Noxa and PUMA, which subsequently stimulate the release of Diablo/Smac and also cytochrome c from mitochondria. These meanwhile inhibit specific inhibitors of apoptosis proteins and finally activate caspases (Schuler and Green, 2001). Thus, the tendency towards decreased levels of clC 3, clC 7 and clPARP could be explained by a reduced p53 induced apoptotic signaling due to the knock-out. As it can also be inferred from the figure, small effects can only hardly be observed due to a high variance between replicas. This variance might be due to detection of very small proteins with Western blot, but also because of cellular changes influencing apoptosis. Although experiments were performed consecutively, it took three weeks to collect lysate from three biological replicas. If the induction of genetic alterations might have impacted apoptosis in this period, this could lead to a higher variance seen in Western blot results. To exclude technical problems, experiments should be carried out examining rates of apoptosis, which are not based on protein. As a first attempt, a new assay was applied allowing real-time monitoring of apoptosis with a luminescent readout, which did not work reliably.

The experiments carried out after induction of Idh1^{R132H} with or without a knock-out of *Tp53* have shown that induction of Idh1^{R132H} has a growth suppressing function (Figure 37). The effects are most probably due to the high amounts of 2-HG produced and indicate that these cells are not able to induce tumorigenesis.

4.2 The difference between short- and long-term inductions

Long term cultivation of the cells leads to a different phenotype compared to short-term cultures. The proliferative capacity of cells harboring both Idh1^{R132H} mutation and a knock-out of *Tp53* is significantly enhanced compared to single mutants (Figure 37 B). Immunohistochemistry with antibodies to cell cycle markers additionally revealed that more cells with both alterations are proliferating. This growth advantage observed in double mutants compared to single mutants points towards a cooperative effect of p53$^{-/-}$ in an Idh1^{R132H} background. This was further confirmed with the soft agar assay, showing that double mutants formed about three times more colonies compared to single mutants (Figure 37 D). The data indicate that a development towards a more tumorigenic phenotype took place across time, as the potential to grow in an extracellular matrix-like environment is described as a hallmark of carcinogenesis *in vitro*. Proliferative behavior did only change in cells with a combination of the genetic alterations and not in single mutants, which proposes the question about the difference between the occurrence of the mutations alone and in combination. The increase of the colony formation rate in double mutants was not significant, but there was a strong tendency towards enhanced formation. This could be explained by a large variance between biological and technical replicates, which might be due to for example different charges of the soft agar prepared. As already explained one should consider conducting the assay in a greater format and count the colonies after crystal violet staining.

DNA methylation was analyzed with Dotblot experiments, showing that the presence of mutant *Idh1* did not significantly alter 5mC and 5hmC levels. However, Idh1^{R132H} expressed alone, revealed a tendency towards increased levels of both markers. This tendency was not observable in cell lines harboring the knock-out of *Tp53* only. These experiments indicate that DNA methylation was not altered after presence of the genetic alterations for several months.
Given the fact that mutant IDH1 has effects on epigenetics through the inhibition of α-KG dependent enzymes, it should be taken into account to perform further experiments to analyze hydroxymethylation. Although the dotblot method could be used to analyze the samples, the variance was high between technical replicates, which might be due to sample normalization.

Normalization was performed on the methylene blue control staining on each spotted DNA dot, which strongly depends on the brightness of the picture. As a different method to quantify abundance of 5mC and 5hmC one might perform mass spectrometry, which is a very sensitive method. With this approach, the different intermediate stages (such as 5-formylcytosine) between 5mC and 5hmC can also be quantified.

As for short-term cells, apoptosis was also examined in more detail in cells with alterations present for a period of more than six months. $Idh1^{R132H}$ $p53^{-/-}$ cells showed an enhanced expression signal for all apoptotic proteins tested (Figure 37 F). This result was in strong contrast to the decreased level of apoptosis measured in cells with one alteration only. On the one hand, this result is in line with previous experiments indicating that double mutants behave in an opposite way compared to single mutants, which was not seen shortly after induction. This increase might suggest that cell numbers measured in the cell viability assay should be even higher, which is hidden by enhanced apoptosis. On the other hand, an enhanced rate of apoptosis is to be against the observation that cells have an increased proliferative capacity. A knock-out of *Tp53* should lead to decreased levels of apoptosis because of the missing p53-induced signal initiating apoptotic pathways. A possible explanation for this might be that other members of the p53-family might have induced apoptotic pathways. In a drosophila model cells do have caspase-dependent but p53-independent pathways of apoptosis induced via other proteins of the p53 family, such as p73 (Wichmann *et al.*, 2006). It was described that the transcription factor E2F-1, inducing the transcription of p73, induces apoptosis in p53-defective tumor cells and $p53^{-/-}$ mouse embryo fibroblasts (Irwin *et al.*, 2000). In line with the results about enhanced apoptosis but also proliferation, expression of p73 is increased in some human cancers, as for example in glioma (Pietsch *et al.*, 2008). Thus, the results on apoptosis might be explained by other proteins involved in signaling cascades of cell death.

Another different approach to explain enhanced levels of apoptosis would be the model itself, in other words the formation of spheres. As sphere formation and proliferation takes place faster in these cultures, the core of spheres gets apoptotic faster as well. The core of the spheres gets hypoxic as nutrients cannot reach all cells, which leads to apoptosis (Edmondson *et al.*, 2014). Additionally, larger spheres also have more apoptotic cells, which are still present in the lysate used for Western blot analysis. From a technical point of view, this might

also explain an increase of apoptosis in double mutant cells with an enhanced proliferative capacity.

The results further challenge why the double mutants behave in a different way compared to single mutants. It is known that loss of p53 induces chromosomal instability, which might point towards the occurrence of unknown other mutations. The accumulation of additional mutations could further support cell viability and proliferation, which was also observed. Interestingly, one mutation alone was not sufficient to induce this phenotype, suggesting that the possible chromosomal instability induced by $Idh1^{R132H}$ and $p53^{-/-}$ led to the accumulation of additional mutations. To further investigate this, sequencing analysis of exactly these long-term cultures should be performed in order to check for possible other mutations. Recent evidence suggests that mutant IDH1 affects DNA repair enzymes thereby favoring induction of genome instability and accumulation of additional mutations (Chen *et al.*, 2017a). In line with this, $Idh1^{R132H}$ alone induces genome instability in cells as well, but it remains to be investigated, why p53 is needed to induce enhanced cell viability and proliferation.

Another interesting aspect is that cells harboring one mutation only do not have normal levels of apoptosis but rather decreased levels (Figure 37 F). In case of the knock-out of *Tp53* alone, this could be explained by a reduction of apoptosis initiated by the knock-out. However, $Idh1^{R132H}$ cells obviously also have a reduction accompanied by a decrease of proliferation. This observation might be explained by the slowly growing behavior of the cells, which means that there is only a small number of apoptotic cells present per sphere.

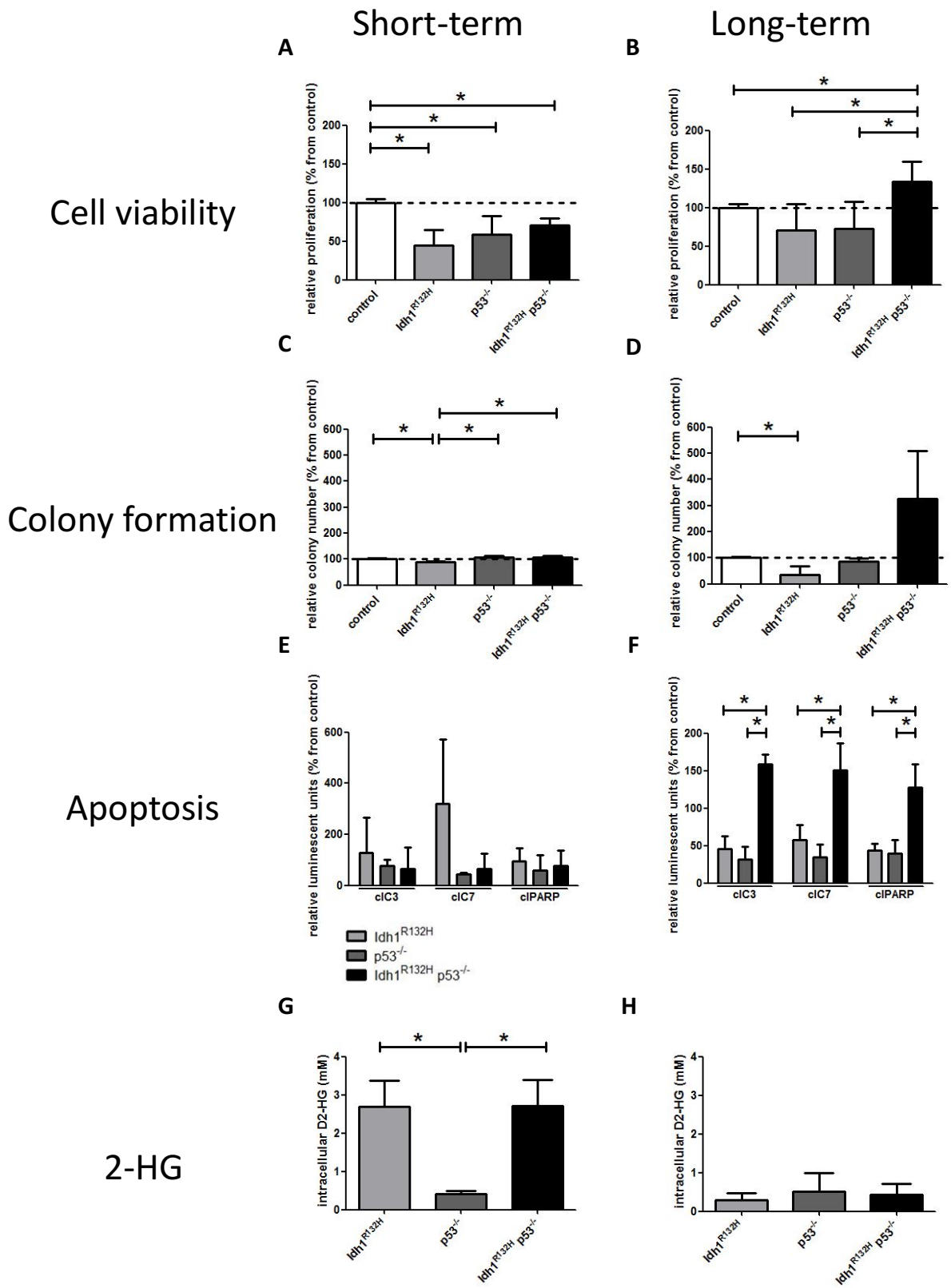

Figure 37. Summary of the functional analysis of the established cell lines at different time points. A Cell viability is significantly decreased in Idh1^{R132H} mutated cells as well as p53$^{-/-}$ cells and double mutants. **B** The growth disadvantage of single mutant cells in short-term cultures cannot be observed in long-term cultures. A combination of Idh1^{R132H} and p53$^{-/-}$ significantly increases cell viability six months after initial induction. **C** Idh1^{R132H} significantly decreases colony formation rate, whereas no effect can be observed in p53$^{-/-}$ cells and double mutants. **D** The reducing effect of Idh1^{R132H} on colony formation can still be

observed after long-term cultivation. Idh1^{R132H} in combination with p53$^{-/-}$ shows a tendency to build more colonies in soft agar. **E** Abundance of late apoptotic proteins is not significantly altered after induction of the genetic alterations. **F** Cultivation across six months leads to a significant increase of apoptotic rates in double mutant cells, but not in single mutants. **G** Induction of Idh1^{R132H} leads to a high production of 2-HG, also in combination with p53$^{-/-}$. **H** Production of 2-HG cannot be measured in all long-term cultures, independent of the initial induction of Idh1^{R132H}.

4.3 Loss of Idh1^{R132H} *in vitro*

Genotyping revealed that Idh1^{R132H} was lost in all long-term cultures, but it appeared always in a different manner. As a next step, it would be crucial to investigate this loss in more detail and compare the result of different cultures. Whole-genome bisulfite sequencing of the different cell lines could unravel whether the breaking points at the borders of the loss have different features in addition to methylation patterns. One of the challenges in this regard is the missing specificity of mouse libraries, strongly depending on the genetic background. The differences of the libraries make it difficult to discriminate between genome and mutations. In other words, it is difficult to detect the true mutations. To avoid these problems, it would be crucial to prepare an own reference genome dependent on the mice strain worked with.

In this context first attempts were undertaken to investigate what actually initiated the genetic aberration. Genome instability is defined as an increase of genome required mutations. The mechanisms leading to genome instability include defects in the DNA damage response or more often in DNA double-strand breaks repair (Georgoulis *et al.*, 2017). To investigate whether double-strand breaks might be the reason for genome instability and the concomitant loss of the Idh1^{R132H} mutation, Western blot experiments should be performed to check for the level of γH2AX. When double-strand breaks are generated into DNA, γ-phosphorylation takes place at serine 139 of the histone H2AX, which can be visualized with specific antibodies (Kuo and Yang, 2008). A first experiment has indicated that newly induced cells might have enhanced expression levels of γH2AX protein (Supplement Figure 3). Experiments need to be repeated with lysates prepared in SDS buffer to improve blot results. Due to the difficulties with Western blot experiments, one might also conduct cytospins of the cells to perform immunofluorescent stainings on these slices to detect γH2AX expression. As another approach, it might also be possible to carry out a Comet assay, which has not been established so far.

A further interesting question is the time of initiation of these events. To answer this question, cell lines induced from different time points should be checked for genome instability and compared. Based on the results that mutant Idh1 is completely lost in a whole culture after one to two months suggests that it might be an event that takes place early after induction.

If the initiation of the $IDH1^{R132H}$ mutation is associated with the induction of genome instability, it might be conceivable that the production of 2-HG is responsible for this. Experiments should be conducted with newly induced cells and the respective controls and treated with an inhibitor against $IDH1^{R132H}$, diminishing the production of 2-HG. If there would be no evidence for genome instability in the induced cell lines after inhibitor treatment, the effect could most probably be ascribed to 2-HG.

Murine NSCs harboring an $Idh1^{R132H}$ mutation lose the mutation *in vitro*, which could also be observed when cultivating human glioma derived cells (Pusch, 2017). It would be very interesting to compare the loss of mutant *IDH1* between the different human cultures and the properties of the original tumor. The question should be answered whether there is a correlation between human and murine derived cultures.

Regarding the comparison between human and murine system, it should be investigated why cells obviously do not lose the $Idh1^{R132H}$ mutation *in vivo*.

4.4 Migration of induced NSCs *in vivo*

Intracranial injection of the induced NSCs was successful and cells started to invade the brain, which was observed two months after implantations. Monthly MRI screens showed a lesion in the area of implantation eight months after injection. A lesion could be observed in one mouse implanted with $p53^{-/-}$ cells and in two mice with $Idh1^{R132H}$ $p53^{-/-}$ cells. A progression of tumor growth could not be achieved in $Idh1^{R132H}$ $p53^{-/-}$ mice and a lesion could only barely be detected two months later. It could be questioned whether the length of the experiment was chosen correctly (Figure 38). The decrease of the lesion volume during the course of the experiment suggests that it should be terminated at eight months for detailed analysis of the observed lesions. However, the experiment was carried out twelve months as planned and histological analysis was performed afterwards. These stainings indicate that a solid tumor was not observable twelve months after surgery and that the implanted cells started to migrate across the corpus callosum to different lateral brain areas.

Another interesting observation is that the mouse implanted with $p53^{-/-}$ cells first showed a decrease of the tumor volume at the ninths months, but than a progression from months ten onwards. This finding is in contrast to mice injected with double mutant NSCs. A possible explanation might be that the $p53^{-/-}$ cells accumulated further mutations promoting tumorigenesis, which did not happen in double mutants.

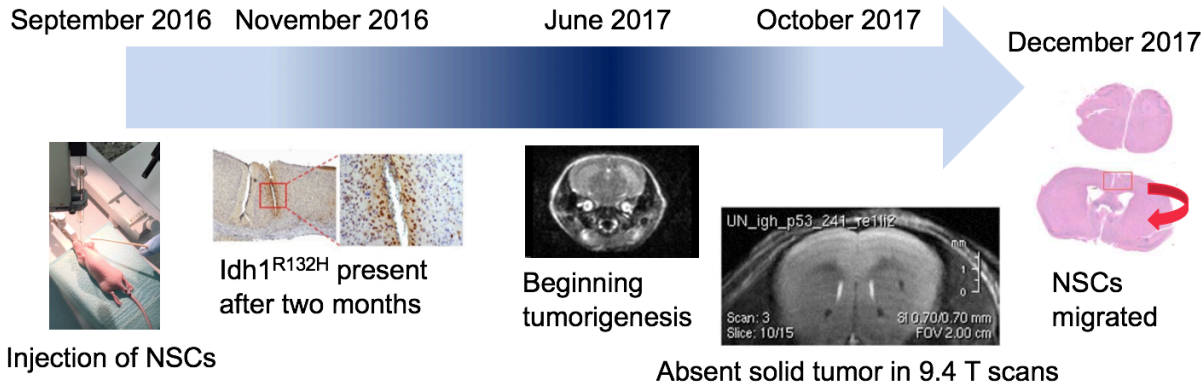

Figure 38. Timeline of the *in vivo* study. Implanted NSCs started to invade the brain tissue after intracranial injection. Tumor outgrowth was observed in mice implanted with $IDH1^{R132H}$ $p53^{-/-}$ cells after eight months. After eight months, tumors disappeared in MRI images due to migration of the implanted NSCs observed after termination of the experiment.

4.5 Cell type

Studies have identified tumorigenic, stem-cell like precursor cells in advanced stage gliomas, suggesting a neural stem cell origin (Noushmehr *et al.*, 2010; Turcan *et al.*, 2012). These findings are not in line with the results described here, indicating that it might be another cell type involved in the initiation of gliomagenesis. The injected NSCs migrated to different brain areas and did not form a solid tumor. It might be a further differentiated cell type such as astrocytes for example that is able to induce tumor formation if genetically altered. In this context, the mutated NSCs should be further differentiated in culture before intracranial injection.

It was observable that the presence of the genetic alterations across a period of more than six months altered the behavior towards a more tumorigenic phenotype. Thus, it would be interesting to know whether these cells behave differently in an *in vivo* environment, compared to the newly induced cells that were actually implanted. However, disregarding the proliferative advantage of these cells *in vitro*, it was shown that the $Idh1^{R132H}$ mutation was

not present anymore. This is definitely an issue that would discriminate this system from the human one. Independent on the hypothesis that IDH1^{R132H} is believed to be a driver mutation, human gliomas do only very rarely lose the mutation. Given that the aim was to build an *in vivo* allograft model that mimics the features of human gliomagenesis, it would be reasonable to next implant the genetically altered NSCs in another differentiation stage.

4.6 Additional mutation

In addition to the cell of origin that is able to induce tumorigenesis, another important aspect is certainly the combination of mutations. In the present study, Idh1^{R132H} was tested as a possible initiating mutation and combined with a knock-out of *Tp53* to mimic the genetic features of astrocytoma, or with a knock-out of *Cic* trying to mimic oligodendroglioma. Other alterations are known to occur mutually exclusive from others and are specific for tumor entities. Conceivably, further or at least a third alteration might be needed to induce gliomagenesis. As a third alteration specific for astrocytoma, the knock-down of *Atrx* should be implemented. In the long run, triple mutant cells harboring the Idh1^{R132H} mutation, a knock-out of *Tp53* and a knock-down of *Atrx* cells should be analyzed *in vitro* and later be injected intracranially.

4.7 Genetic background of mice

To further improve the model system, the mouse strain worked with is an important issue to discuss. Working with immunodeficient BALB/c nude mice on a long term was very difficult with respect to unexpected diseases, such as infections. These incidences as well as major problems experienced with injection anesthesia during surgeries reduced the mouse number per group during the course of the study for reasons not related to the initial question. Additionally, the study was aimed at observing possible tumor outgrowth on a long run, which needs stable conditions. It was reported that the adaptive immune response, normally absent in BALB/c mice, tends to return. This important change might have influenced the beginning tumor formation observed in MRI recordings after eight months. If the immune response started to increase during this time, it might have altered tumor growth and thus, did finally lead to a reduction of tumor volume. This observation was made in the upcoming months until lesions could not be detected anymore. These results suggest that re-implantation should be performed in a different immunodeficient mouse strain, as for example Rag2.

Concerning the presence of the immune system, it would be of high importance to also investigate the effects of implantations of NSCs with production of 2-HG in an immune background. In this context, different scenarios are imaginable. Studies have shown that 2-HG causes down-regulation of leukocyte chemotaxis, which leads to suppression of the tumor-associated immune system by decreasing tumor cell infiltration (Amankulor *et al.*, 2017). 2-HG decreases the production of the T cell-attracting chemokines CXCL 9 and 10 as well as its regulator STAT1, which in turn inhibits migration of T cells towards the tumor (Kohanbash *et al.*, 2017). This might explain why *IDH1* mutated tumors behave less aggressive and infiltration of immune cells is linked to a poor prognosis in patients. Thus, it might be possible that the effect of $Idh1^{R132H}$ is suppressive in immunocompetent mice and tumorigenesis is inhibited irrespective of the initial presence of the immune system. In contrast, as *Idh* mutations influence genome instability and most probably induce the accumulation of additional mutations, it might be feasible that selection of a more aggressive phenotype takes place. This in turn might be enough to initiate tumorigenesis even in an immunocompetent background.

4.8 Detection of implanted cells

Two months after implantation, $Idh1^{R132H}$ positive cells surrounding the injection puncture invaded the brain parenchyma. This is in contrast to mice that lived until termination of the experiment, where no $Idh1^{R132H}$ positive cells could be detected in the initial area of implantation but in different lateral brain areas. Application of the mouse $Idh1^{R132H}$ antibody on murine tissue has some disadvantages, such as the high background signal due to the mouse secondary antibody used. However, careful analysis of the slices indicates that $Idh1^{R132H}$ $p53^{-/-}$ cells in the lateral brain areas showed a light brownish cytoplasmic granular staining whereas the nucleus was clearly omitted. Staining against $Idh1^{R132H}$ gives only information about the induced cells and does not prove existence of non-inducible control cells. But application of different antibodies, such as Foxn1, did not deliver reliable results. Taken together, detection of the injected cells after termination of the experiment seems to be challenging, making it inevitable to think about different detection methods for future experiments.

First, it could be an option to label cells prior to injection, with a fluorescent protein such as GFP. However, the insertion of GFP is questionable due to its immunogenicity when used in an immunocompetent background (Ansari *et al.*, 2016). Another option would be to

implement dyes, which are not immunogenic. It should be taken into account that the establishment of an *in vivo* glioma model is always accompanied by a long observation period and dyes might not be kept in the cells on a long run. One possible scenario would be to implement a fluorescent protein in mice prior to final matings for stem cell preparation. The already existing mice harboring the conditional alleles might be crossed with e.g. a mCherry mouse, also with a Bl6N background. After preparation of NSCs from these mice, injections could be performed into Bl6N tomato mice, making it finally possible to discriminate between the differentially labeled cells.

Second, a completely different approach would be to make use of the production of 2-HG from injected cells harboring the Idh1^{R132H} cells. Preliminary experiments have already been performed at the University Clinics Heidelberg, trying to map the release of 2-HG from glioma cells with 9.4 T MRI scans (Neuberger, 2017). However, it is questionable, whether the given resolution is sufficient to clearly detect the cells by using this approach. This option would not solve the problem of detecting any type of injected cell, independent of the mutational status.

Third, one method to validate protein expression with immunohistochemistry is the analysis of RNA levels with RNAscope *in situ* hybridization. RNAscope provides a higher resolution signal at cellular level and probes are available to detect Cre recombinase as the protein of interest. Some additional devices are needed for these experiments, which are not yet established in the lab.

Fourth, yet another possibility is the detection of 2-HG with Matrix Assisted Laser Desorption Ionization - Time of Flight (MALDI-TOF). This method was recently published to be suitable for the detection of 2-HG in brain tumor slices with a resolution of 50 µm (Giampa *et al.*, 2016; Longuespee *et al.*, 2018). This resolution might be too weak for the detection of single cells, making it inevitable to use another device with a better resolution.

4.9 Implementation of Cic$^{-/-}$ in an Idh1^{R132H} background

Cells harboring a knock-out of *Cic* in an Idh1^{R132H} background were generated and analyzed *in vitro* but also *in vivo* by intracranial injection into immunodeficient mice. CIC was described to have a key role in regulating growth by the RTK/Ras pathway and cell fate determination, which does vary between tissues (Tseng *et al.*, 2007). The result that Cic$^{-/-}$ cells

show enhanced cell viability is in line with studies describing that CIC acts as a tumor suppressor gene by repressing downstream targets of RAS/MAPK signals. In brain tumors, *CIC* mutations are specific to oligodendroglioma and are frequently associated with *IDH1* and *FUBP1* mutations, questioning its cooperativity (Jiao *et al.*, 2012). Implementing the $Idh1^{R132H}$ mutation and $Cic^{-/-}$ showed that cell viability as well as colony formation in soft agar was not altered. Cultivation of these double mutant cells across a long term has shown that overall proliferation was much slower compared to other NSCs with different genetic alterations. This observation is also in line with another study reporting that mutations in *CIC* and *IDH1* negatively affect cell clonogenicity by affecting the cytosolic citrate metabolism (Chittaranjan *et al.*, 2014). Combination of the *IDH1* and *CIC* mutation increased levels of 2-HG compared to wild-type *CIC* in an $IDH1^{R132H}$ background. In the present study, there was only a tendency of enhanced levels of 2-HG, but the calculated mean did not significantly differ between single $Idh1^{R132H}$ cells and double mutants. This difference between experiments might be based on differences in the model systems. Another significant observation was that double mutant cells did not lose the $Idh1^{R132H}$ mutation if it was accompanied by $Cic^{-/-}$. This result is in contrast to cells harboring the $Idh1^{R132H}$ mutation either alone, or together with a knock-out of *Tp53*. Mutant Idh1 is accompanied by a significant growth disadvantage, as long as the mutation is present in the cells, which might explain why $Idh1^{R132H}$ $Cic^{-/-}$ cells tend to grow slower. The repressing effect of $Idh1^{R132H}$ $Cic^{-/-}$ on proliferation also fits the common growth behavior of oligodendroglioma, which does proliferate slower compared to astrocytoma for example. The slowly growing phenotype observed *in vitro* might also explain why no lesion could be detected in MRI screens. Missing formation of a solid tumor might also be due to recurring of the immune system in BALB/c nude mice inhibiting beginning tumorigenesis.

The *Cic* knock-out does not alter the phenotype of $Idh1^{R132H}$ regarding cell viability and proliferation, DNA methylation and production of 2-HG. These results allow the hypothesis that the *Cic* knock-out alone does not mimic the complete 1p/19q loss of heterozygosity, which might require additional genetic alterations. An additional genetic alteration is the mutation of the telomerase reverse transcriptase promoter (*pTERT*). These mutations occur in about 90% of gliomas with 1p/19q co-deletions. *CIC* mutations are associated with *pTERT* mutations in 85% of oligodendrogliomas with 1p/19q LOH (Labussiere *et al.*, 2014). Telomere maintenance mechanisms, such as *pTERT* mutations in oligodendroglioma, or *ATRX* mutations in astrocytoma, is described in more than 80% of gliomas and thus seems to

be a unique feature of these tumor entities. The close correlation of IDH1^{R132H}, with *CIC* and *pTERT* alterations known as the molecular signature of oligodendroglioma, would definitely improve the model system described here. It remains to be seen whether an additional *pTERT* mutation affects the Idh1^{R132H} phenotype described here.

4.10 Functional neuroimaging of glioma xenografts with IDH1^{R132H} mutation

To investigate the association between IDH1^{R132H} and epileptogenesis, functional neuroimaging was performed with FDG PET. PET results showed that there is no indication of hypometabolism in the left hemisphere of mice harboring a glioma with IDH1^{R132H} mutation in the right hemisphere. There is no difference in glucose metabolism between all experimental groups (Figure 35). Furthermore, BALB/c nude mice behave in a different way as expected, as accumulation of FDG was only barely observed in the brain. This points towards a general problem of the mouse strain used for PET recordings. For future experiments, it should be taken into account to use immunodeficient mice with fur. The strongly enhanced regions of glucose metabolism in regions of the thorax in BALB/c nudes might be associated with prevention to lose warmth during PET recordings and anesthesia. This problem is not known for fur mice and might thus help to perform PET imaging with normal uptake of FDG.

Pretreatment with an IDH1^{R132H} specific inhibitor before PET recordings does not significantly alter FDG distribution between groups. No clear evidence of seizure activity can be detected. These data suggest that the given parameters are most probably not sufficient to clearly detect seizures in mice. However, there was a tendency of an increase in activity after treatment with BAY1436032 in the group harboring a glioma with IDH1^{R132H} mutation. This might point towards a state of hypometabolism prior to inhibitor treatment, possibly because of epileptogenesis in these mice. Here, it would be an advantage to also image a mouse from an epileptic animal model to finally investigate whether seizure activity can be observed with the given methods and compare it to the data obtained.

It is still a matter of debate whether FDG can be used as a reliable radiotracer for the detection of seizures. It was reported that glucose hypometabolism monitored with FDG PET does not precisely correlate with, for example, the alteration within hippocampal sclerosis responsible for epileptogenesis observed by MRI. It was suggested that for example Benzodiazepine-receptor imaging might be a promising alternative to image the epileptogenic zone.

Concerning different radiotracers, ^{18}F-flumazenil (FMZ) was described to be a tracer of choice in patients suffering from refractory epilepsy, because of a better sensitivity and anatomical resolution (Hodolic *et al.*, 2016). Independent of the precision of different tracers, it seems to be a general problem that different tracers are more or less suitable for different types of seizures, which should be taken into account in further studies.

Due to this issue, for further *in vivo* studies targeting the question of the concomitant occurrence of IDH1^{R132H} mutated glioma and epileptogenesis, more invasive approaches might be used. Intracranial EEG with electrodes located in the area surrounding the tumor would reveal whether ictal high frequency oscillations can be observed as an indication for seizures. But also in this case it would be very interesting to examine whether IDH1^{R132H} and the treatment with BAY1436032 affect seizure occurrence. As this inhibitor is also being used in patients, it would be important to investigate this aspect.

In vitro, it would additionally be interesting to investigate the direct effect of 2-HG on intrinsic brain activity. With slice cultures and electrophysiological methods, such as field recordings, it could be observed whether treatment with exogenous 2-HG does affect levels of excitation and inhibition. The experimental settings are however not that trivial as 2-HG only barely enters cells. Another aspect to analyze *in vitro* would be to look in slice cultures from glioma bearing mice whether activity in the area surrounding the tumor differs between mice with an IDH1^{R132H} mutated glioma and those that lack this mutation. This would not only give an indication for an alteration of normal brain activity, but application of epileptic drugs might directly confirm whether this activity can be blocked.

In addition to *in vivo* and *in vitro* analysis, it might also be investigated with immunohistochemistry and the application of different antibodies, whether there are differences between different groups of mice. A recent publication has shown that high expression of cysteine-glutamate antiporter xCT (SLC7A11) serves as a biomarker for initial occurrence of seizures in patients with glioma (Sorensen *et al.*, 2018). However, this finding was not associated with the presence of IDH1^{R132H}. Nevertheless, it shows that biomarkers investigated with immunohistochemistry might help to detect epilepsy in brain slices as well.

5 Summary

The aim of this project was to develop a mouse allograft model based on neural stem cells displaying the key properties of human glioma on the molecular level. Therefore, neural stem cells were prepared from mice harboring different genetic features of astrocytoma or oligodendroglioma. Common to both are mutations of isocitrate dehydrogenase. A specific type of mutation leads to production of D-2-hydroxyglutarate, a known oncometabolite, which is thought to be essential for tumor initiation. The accumulation of D-2-hydroxyglutarate leads to epigenetic reprogramming and thereby to tumor formation.

Neural stem cells with inducible isocitrate dehydrogenase R132H knock-in and inducible *Tp53* knock-out were analyzed for their tumorigenic potential with different assays. None of the manipulations or combinations thereof showed an enhanced tumorigenic potential. While in cells with isocitrate dehydrogenase mutation R132H cell growth was compromised by D-2-hydroxyglutarate production, this was not observed in combination with the loss of p53. To analyze if these cells show a different tumorigenic potential *in vivo*, they were injected intracranially into immunodeficient mice. Potential tumor outgrowth was monitored with regular MRI screens and was evident after eight months. It was reasonable to keep the cells in culture for a longer time, because epigenetic reprogramming can take several passages to manifest. Those “long-term” cultures grew more aggressively compared to their recently induced (“short-term”) counterparts. This could mainly be explained by the loss of the isocitrate dehydrogenase mutation, which is a negative selection marker under *in vitro* conditions. Such a phenomenon is already described in human cell lines. In contrast to the *in vitro* situation, the isocitrate dehydrogenase mutation was kept *in vivo*, although the tumors disappeared within twelve months.

In conclusion, the project could show that the combination of isocitrate dehydrogenase mutation R132H together with the loss of p53 is beneficial for the cells and sufficient to initiate tumor formation. The model nicely pictures the human system, in which cells in culture lose the mutation, but tumors only rarely do. It is perfectly suited for the investigation of the essential function of isocitrate dehydrogenase mutation in glioma. By this it will help to understand this function, uncover weaknesses of these tumors and help to predict resistance mechanisms against isocitrate dehydrogenase mutation inhibitors. Further development of the system by addition of other genetic alterations will potentially lead to more durable tumors *in vivo*.

6 Zusammenfassung

Ziel des Projekts war die Entwicklung eines murinen Gliom Modells. Dieses auf neuralen Stammzellen basierende Modell, sollte die molekularen Veränderungen von humanen Gliomen aufweisen und in der Maus zu einem Tumor führen. Um dieses Ziel zu erreichen wurden neurale Stammzellen aus Mäusen gewonnen, welche die genetischen Eigenschaften von Astrozytomen und Oligodendrogliomen haben. Eine Gemeinsamkeit von beiden Entitäten ist die Mutation des Enzyms Isocitrat-Dehydrogenase. Eine bestimmte Mutation dieses Enzyms führt zu der Produktion des Onkometaboliten D-2-Hydroxyglutarat. Man vermutet, dass dies ein essentieller Schritt in der Tumorentstehung ist, weil die Anreicherung von D-2-Hydroxyglutarat zur epigenetischen Umprogrammierung führt und damit die Tumorentstehung fördert.

Das tumorigene Potential von neuralen Stammzellen mit einer induzierbaren Isocitrat-Dehydrogenase R132H Knock-in Mutation und einem induzierbaren *Tp53* Knock-out wurde mit verschiedenen Methoden untersucht. Keine Kombination der genetischen Veränderungen zeigte ein erhöhtes tumorigenes Potential. Die spezifische Isocitrat-Dehydrogenase R132H Mutation zusammen mit einem Verlust von p53weist nicht die reduzierte Zellvitalität auf, wie sie in Zellen mit nur der Isocitrat-Dehydrogenase Mutation beobachtet wurde. Um zu analysieren, ob die Zellen *in vivo* ein anderes tumorigenes Verhalten zeigen, wurden die Zellen intrakranial implantiert. Tumorwachstum wurde mit regelmäßigen MRT Untersuchungen kontrolliert und konnte nach acht Monaten beobachtet werden. Da epigenetische Veränderungen erst nach mehreren Passagen sichtbar werden, wurden die Zellen für eine längere Zeit kultiviert. Diese Langzeitkulturen zeigten wesentliche Unterschiede zu ihren genetisch vergleichbaren frisch induzierten Zellen. Dieses Verhalten kann durch den Verlust der Isocitrat-Dehydrogenase Mutation erklärt werden, die ein negativer Selektionsmarker unter *in vitro*-Bedingungen ist. Ein solches Phänomen wurde schon für humane Zelllinien beschrieben. Im Gegensatz zu der *in vitro*-Situation blieb die Isocitrat-Dehydrogenase Mutation *in vivo* erhalten, auch wenn die Tumore innerhalb von zwölf Monaten wieder verschwunden waren.

Zusammenfassend konnte dieses Projekt zeigen, dass die Kombination aus der Isocitrat-Dehydrogenase R132H Mutation gemeinsam mit dem Verlust von p53 vorteilhaft für Zellen ist und ausreicht, um Tumorwachstum zu initiieren. Dieses Modell spiegelt sehr gut das humane System wieder, bei dem auch Zellen in Kultur die Mutation verlieren, was hingegen

nicht in Tumoren zu beobachten ist. Des Weiteren ist es sehr gut geeignet, um die essentiellen Funktionen der Isocitrat-Dehydrogenase Mutation in Gliomen zu untersuchen. Dies würde helfen, die Funktion zu verstehen, die Schwachstellen dieser Tumore aufzudecken und dazu beitragen, Resistenzmechanismen gegen spezifische Inhibitoren der Isocitrat-Dehydrogenase Mutation zu finden. Die Weiterentwicklung dieses Systems, zum Beispiel durch das Einbinden weiterer genetischer Veränderungen, hat das Potential, zu stabilerem Tumorwachstum *in vivo* zu führen.

7 References

Abbas, S., Lugthart, S., Kavelaars, F. G., Schelen, A., Koenders, J. E., Zeilemaker, A., van Putten, W. J., Rijneveld, A. W., Lowenberg, B. and Valk, P. J. (2010). **Acquired mutations in the genes encoding IDH1 and IDH2 both are recurrent aberrations in acute myeloid leukemia: prevalence and prognostic value**. Blood *116*, 2122-2126, doi: 10.1182/blood-2009-11-250878.

Amankulor, N. M., Kim, Y., Arora, S., Kargl, J., Szulzewsky, F., Hanke, M., Margineantu, D. H., Rao, A., Bolouri, H., Delrow, J., Hockenbery, D., Houghton, A. M. and Holland, E. C. (2017). **Mutant IDH1 regulates the tumor-associated immune system in gliomas**. Genes Dev *31*, 774-786, doi: 10.1101/gad.294991.116.

Amary, M. F., Bacsi, K., Maggiani, F., Damato, S., Halai, D., Berisha, F., Pollock, R., O'Donnell, P., Grigoriadis, A., Diss, T., Eskandarpour, M., Presneau, N., Hogendoorn, P. C., Futreal, A., Tirabosco, R. and Flanagan, A. M. (2011a). **IDH1 and IDH2 mutations are frequent events in central chondrosarcoma and central and periosteal chondromas but not in other mesenchymal tumours**. J Pathol *224*, 334-343, doi: 10.1002/path.2913.

Amary, M. F., Damato, S., Halai, D., Eskandarpour, M., Berisha, F., Bonar, F., McCarthy, S., Fantin, V. R., Straley, K. S., Lobo, S., Aston, W., Green, C. L., Gale, R. E., Tirabosco, R., Futreal, A., Campbell, P., Presneau, N. and Flanagan, A. M. (2011b). **Ollier disease and Maffucci syndrome are caused by somatic mosaic mutations of IDH1 and IDH2**. Nat Genet *43*, 1262-1265, doi: 10.1038/ng.994.

Ansari, A. M., Ahmed, A. K., Matsangos, A. E., Lay, F., Born, L. J., Marti, G., Harmon, J. W. and Sun, Z. (2016). **Cellular GFP Toxicity and Immunogenicity: Potential Confounders in in Vivo Cell Tracking Experiments**. Stem Cell Rev *12*, 553-559, doi: 10.1007/s12015-016-9670-8.

Appin, C. L. and Brat, D. J. (2015). **Molecular pathways in gliomagenesis and their relevance to neuropathologic diagnosis**. Adv Anat Pathol *22*, 50-58, doi: 10.1097/PAP.0000000000000048.

Arita, H., Narita, Y., Fukushima, S., Tateishi, K., Matsushita, Y., Yoshida, A., Miyakita, Y., Ohno, M., Collins, V. P., Kawahara, N., Shibui, S. and Ichimura, K. (2013). **Upregulating mutations in the TERT promoter commonly occur in adult malignant gliomas and are strongly associated with total 1p19q loss**. Acta Neuropathol *126*, 267-276, doi: 10.1007/s00401-013-1141-6.

Bailey, P. and Cushing, H. (1926). **A classification of tumors of the glioma group on a histogenetic basis with a correlation study of prognosis**.

Balss, J., Meyer, J., Mueller, W., Korshunov, A., Hartmann, C. and von Deimling, A. (2008). **Analysis of the IDH1 codon 132 mutation in brain tumors**. Acta Neuropathol *116*, 597-602, doi: 10.1007/s00401-008-0455-2.

Balss, J., Pusch, S., Beck, A. C., Herold-Mende, C., Kramer, A., Thiede, C., Buckel, W., Langhans, C. D., Okun, J. G. and von Deimling, A. (2012). **Enzymatic assay for**

quantitative analysis of (D)-2-hydroxyglutarate. Acta Neuropathol *124*, 883-891, doi: 10.1007/s00401-012-1060-y.

Bardella, C., Al-Dalahmah, O., Krell, D., Brazauskas, P., Al-Qahtani, K., Tomkova, M., Adam, J., Serres, S., Lockstone, H., Freeman-Mills, L., Pfeffer, I., Sibson, N., Goldin, R., Schuster-Boeckler, B., Pollard, P. J., Soga, T., McCullagh, J. S., Schofield, C. J., Mulholland, P., Ansorge, O., Kriaucionis, S., Ratcliffe, P. J., Szele, F. G. and Tomlinson, I. (2016). **Expression of Idh1(R132H) in the Murine Subventricular Zone Stem Cell Niche Recapitulates Features of Early Gliomagenesis**. Cancer Cell *30*, 578-594, doi: 10.1016/j.ccell.2016.08.017.

Beiko, J., Suki, D., Hess, K. R., Fox, B. D., Cheung, V., Cabral, M., Shonka, N., Gilbert, M. R., Sawaya, R., Prabhu, S. S., Weinberg, J., Lang, F. F., Aldape, K. D., Sulman, E. P., Rao, G., McCutcheon, I. E. and Cahill, D. P. (2014). **IDH1 mutant malignant astrocytomas are more amenable to surgical resection and have a survival benefit associated with maximal surgical resection**. Neuro Oncol *16*, 81-91, doi: 10.1093/neuonc/not159.

Bettegowda, C., Agrawal, N., Jiao, Y., Sausen, M., Wood, L. D., Hruban, R. H., Rodriguez, F. J., Cahill, D. P., McLendon, R., Riggins, G., Velculescu, V. E., Oba-Shinjo, S. M., Marie, S. K., Vogelstein, B., Bigner, D., Yan, H., Papadopoulos, N. and Kinzler, K. W. (2011). **Mutations in CIC and FUBP1 contribute to human oligodendroglioma**. Science *333*, 1453-1455, doi: 10.1126/science.1210557.

Bleeker, F. E., Lamba, S., Leenstra, S., Troost, D., Hulsebos, T., Vandertop, W. P., Frattini, M., Molinari, F., Knowles, M., Cerrato, A., Rodolfo, M., Scarpa, A., Felicioni, L., Buttitta, F., Malatesta, S., Marchetti, A. and Bardelli, A. (2009). **IDH1 mutations at residue p.R132 (IDH1(R132)) occur frequently in high-grade gliomas but not in other solid tumors**. Hum Mutat *30*, 7-11, doi: 10.1002/humu.20937.

Borger, D. R., Tanabe, K. K., Fan, K. C., Lopez, H. U., Fantin, V. R., Straley, K. S., Schenkein, D. P., Hezel, A. F., Ancukiewicz, M., Liebman, H. M., Kwak, E. L., Clark, J. W., Ryan, D. P., Deshpande, V., Dias-Santagata, D., Ellisen, L. W., Zhu, A. X. and Iafrate, A. J. (2012). **Frequent mutation of isocitrate dehydrogenase (IDH)1 and IDH2 in cholangiocarcinoma identified through broad-based tumor genotyping**. Oncologist *17*, 72-79, doi: 10.1634/theoncologist.2011-0386.

Borowicz, S., Van Scoyk, M., Avasarala, S., Karuppusamy Rathinam, M. K., Tauler, J., Bikkavilli, R. K. and Winn, R. A. (2014). **The soft agar colony formation assay**. J Vis Exp, e51998, doi: 10.3791/51998.

Bralten, L. B., Kloosterhof, N. K., Balvers, R., Sacchetti, A., Lapre, L., Lamfers, M., Leenstra, S., de Jonge, H., Kros, J. M., Jansen, E. E., Struys, E. A., Jakobs, C., Salomons, G. S., Diks, S. H., Peppelenbosch, M., Kremer, A., Hoogenraad, C. C., Smitt, P. A. and French, P. J. (2011). **IDH1 R132H decreases proliferation of glioma cell lines in vitro and in vivo**. Ann Neurol *69*, 455-463, doi: 10.1002/ana.22390.

Brehmer, S., Pusch, S., Schmieder, K., von Deimling, A. and Hartmann, C. (2011). **Mutational analysis of D2HGDH and L2HGDH in brain tumours without IDH1**

or IDH2 mutations. Neuropathol Appl Neurobiol *37*, 330-332, doi: 10.1111/j.1365-2990.2010.01114.x.

Brown, J. M. and Wouters, B. G. (1999). **Apoptosis, p53, and tumor cell sensitivity to anticancer agents**. Cancer Res *59*, 1391-1399.

Cairncross, G., Wang, M., Shaw, E., Jenkins, R., Brachman, D., Buckner, J., Fink, K., Souhami, L., Laperriere, N., Curran, W. and Mehta, M. (2013). **Phase III trial of chemoradiotherapy for anaplastic oligodendroglioma: long-term results of RTOG 9402**. J Clin Oncol *31*, 337-343, doi: 10.1200/JCO.2012.43.2674.

Capper, D., Reuss, D., Schittenhelm, J., Hartmann, C., Bremer, J., Sahm, F., Harter, P. N., Jeibmann, A. and von Deimling, A. (2011). **Mutation-specific IDH1 antibody differentiates oligodendrogliomas and oligoastrocytomas from other brain tumors with oligodendroglioma-like morphology**. Acta Neuropathol *121*, 241-252, doi: 10.1007/s00401-010-0770-2.

Capper, D., Weissert, S., Balss, J., Habel, A., Meyer, J., Jager, D., Ackermann, U., Tessmer, C., Korshunov, A., Zentgraf, H., Hartmann, C. and von Deimling, A. (2010). **Characterization of R132H mutation-specific IDH1 antibody binding in brain tumors**. Brain Pathol *20*, 245-254, doi: 10.1111/j.1750-3639.2009.00352.x.

Capper, D., Zentgraf, H., Balss, J., Hartmann, C. and von Deimling, A. (2009). **Monoclonal antibody specific for IDH1 R132H mutation**. Acta Neuropathol *118*, 599-601, doi: 10.1007/s00401-009-0595-z.

Chang, E. F., Potts, M. B., Keles, G. E., Lamborn, K. R., Chang, S. M., Barbaro, N. M. and Berger, M. S. (2008). **Seizure characteristics and control following resection in 332 patients with low-grade gliomas**. J Neurosurg *108*, 227-235, doi: 10.3171/JNS/2008/108/2/0227.

Chen, F., Bian, K., Tang, Q., Fedeles, B. I., Singh, V., Humulock, Z. T., Essigmann, J. M. and Li, D. (2017a). **Oncometabolites d- and l-2-Hydroxyglutarate Inhibit the AlkB Family DNA Repair Enzymes under Physiological Conditions**. Chem Res Toxicol *30*, 1102-1110, doi: 10.1021/acs.chemrestox.7b00009.

Chen, H., Judkins, J., Thomas, C., Wu, M., Khoury, L., Benjamin, C. G., Pacione, D., Golfinos, J. G., Kumthekar, P., Ghamsari, F., Chen, L., Lein, P., Chetkovich, D. M., Snuderl, M. and Horbinski, C. (2017b). **Mutant IDH1 and seizures in patients with glioma**. Neurology *88*, 1805-1813, doi: 10.1212/WNL.0000000000003911.

Chittaranjan, S., Chan, S., Yang, C., Yang, K. C., Chen, V., Moradian, A., Firme, M., Song, J., Go, N. E., Blough, M. D., Chan, J. A., Cairncross, J. G., Gorski, S. M., Morin, G. B., Yip, S. and Marra, M. A. (2014). **Mutations in CIC and IDH1 cooperatively regulate 2-hydroxyglutarate levels and cell clonogenicity**. Oncotarget *5*, 7960-7979, doi: 10.18632/oncotarget.2401.

Choi, C., Ganji, S. K., DeBerardinis, R. J., Hatanpaa, K. J., Rakheja, D., Kovacs, Z., Yang, X. L., Mashimo, T., Raisanen, J. M., Marin-Valencia, I., Pascual, J. M., Madden, C. J., Mickey, B. E., Malloy, C. R., Bachoo, R. M. and Maher, E. A. (2012). **2-**

hydroxyglutarate detection by magnetic resonance spectroscopy in IDH-mutated patients with gliomas. Nat Med *18*, 624-629, doi: 10.1038/nm.2682.

Chowdhury, R., Yeoh, K. K., Tian, Y. M., Hillringhaus, L., Bagg, E. A., Rose, N. R., Leung, I. K., Li, X. S., Woon, E. C., Yang, M., McDonough, M. A., King, O. N., Clifton, I. J., Klose, R. J., Claridge, T. D., Ratcliffe, P. J., Schofield, C. J. and Kawamura, A. (2011). **The oncometabolite 2-hydroxyglutarate inhibits histone lysine demethylases**. EMBO Rep *12*, 463-469, doi: 10.1038/embor.2011.43.

Cui, D., Ren, J., Shi, J., Feng, L., Wang, K., Zeng, T., Jin, Y. and Gao, L. (2016). **R132H mutation in IDH1 gene reduces proliferation, cell survival and invasion of human glioma by downregulating Wnt/beta-catenin signaling**. Int J Biochem Cell Biol *73*, 72-81, doi: 10.1016/j.biocel.2016.02.007.

Dang, L., White, D. W., Gross, S., Bennett, B. D., Bittinger, M. A., Driggers, E. M., Fantin, V. R., Jang, H. G., Jin, S., Keenan, M. C., Marks, K. M., Prins, R. M., Ward, P. S., Yen, K. E., Liau, L. M., Rabinowitz, J. D., Cantley, L. C., Thompson, C. B., Vander Heiden, M. G. and Su, S. M. (2010). **Cancer-associated IDH1 mutations produce 2-hydroxyglutarate**. Nature *465*, 966, doi: 10.1038/nature09132.

DKFZ, Animal imaging facility (2017). Personal communication.

Edmondson, R., Broglie, J. J., Adcock, A. F. and Yang, L. (2014). **Three-dimensional cell culture systems and their applications in drug discovery and cell-based biosensors**. Assay Drug Dev Technol *12*, 207-218, doi: 10.1089/adt.2014.573.

Fathi, A. T., Sadrzadeh, H., Borger, D. R., Ballen, K. K., Amrein, P. C., Attar, E. C., Foster, J., Burke, M., Lopez, H. U., Matulis, C. R., Edmonds, K. M., Iafrate, A. J., Straley, K. S., Yen, K. E., Agresta, S., Schenkein, D. P., Hill, C., Emadi, A., Neuberg, D. S., Stone, R. M. and Chen, Y. B. (2012). **Prospective serial evaluation of 2-hydroxyglutarate, during treatment of newly diagnosed acute myeloid leukemia, to assess disease activity and therapeutic response**. Blood *120*, 4649-4652, doi: 10.1182/blood-2012-06-438267.

Feyissa, A. M., Worrell, G. A., Tatum, W. O., Mahato, D., Brinkmann, B. H., Rosenfeld, S. S., ReFaey, K., Bechtle, P. S. and Quinones-Hinojosa, A. (2018). **High-frequency oscillations in awake patients undergoing brain tumor-related epilepsy surgery**. Neurology, doi: 10.1212/WNL.0000000000005216.

Figueroa, M. E., Abdel-Wahab, O., Lu, C., Ward, P. S., Patel, J., Shih, A., Li, Y., Bhagwat, N., Vasanthakumar, A., Fernandez, H. F., Tallman, M. S., Sun, Z., Wolniak, K., Peeters, J. K., Liu, W., Choe, S. E., Fantin, V. R., Paietta, E., Lowenberg, B., Licht, J. D., Godley, L. A., Delwel, R., Valk, P. J., Thompson, C. B., Levine, R. L. and Melnick, A. (2010). **Leukemic IDH1 and IDH2 mutations result in a hypermethylation phenotype, disrupt TET2 function, and impair hematopoietic differentiation**. Cancer Cell *18*, 553-567, doi: 10.1016/j.ccr.2010.11.015.

Fu, X., Chin, R. M., Vergnes, L., Hwang, H., Deng, G., Xing, Y., Pai, M. Y., Li, S., Ta, L., Fazlollahi, F., Chen, C., Prins, R. M., Teitell, M. A., Nathanson, D. A., Lai, A., Faull, K. F., Jiang, M., Clarke, S. G., Cloughesy, T. F., Graeber, T. G., Braas, D., Christofk, H. R., Jung, M. E., Reue, K. and Huang, J. (2015). **2-Hydroxyglutarate Inhibits**

ATP Synthase and mTOR Signaling. Cell Metab *22*, 508-515, doi: 10.1016/j.cmet.2015.06.009.

Fuchs, Y. and Steller, H. (2011). **Programmed cell death in animal development and disease**. Cell *147*, 742-758, doi: 10.1016/j.cell.2011.10.033.

Georgoulis, A., Vorgias, C. E., Chrousos, G. P. and Rogakou, E. P. (2017). **Genome Instability and gammaH2AX**. Int J Mol Sci *18*, doi: 10.3390/ijms18091979.

Giampa, M., Lissel, M. B., Patschkowski, T., Fuchser, J., Hans, V. H., Gembruch, O., Bednarz, H. and Niehaus, K. (2016). **Maleic anhydride proton sponge as a novel MALDI matrix for the visualization of small molecules (<250 m/z) in brain tumors by routine MALDI ToF imaging mass spectrometry**. Chem Commun (Camb) *52*, 9801-9804, doi: 10.1039/c6cc02387h.

Gross, S., Cairns, R. A., Minden, M. D., Driggers, E. M., Bittinger, M. A., Jang, H. G., Sasaki, M., Jin, S., Schenkein, D. P., Su, S. M., Dang, L., Fantin, V. R. and Mak, T. W. (2010). **Cancer-associated metabolite 2-hydroxyglutarate accumulates in acute myelogenous leukemia with isocitrate dehydrogenase 1 and 2 mutations**. J Exp Med *207*, 339-344, doi: 10.1084/jem.20092506.

Hartmann, C., Hentschel, B., Wick, W., Capper, D., Felsberg, J., Simon, M., Westphal, M., Schackert, G., Meyermann, R., Pietsch, T., Reifenberger, G., Weller, M., Loeffler, M. and von Deimling, A. (2010). **Patients with IDH1 wild type anaplastic astrocytomas exhibit worse prognosis than IDH1-mutated glioblastomas, and IDH1 mutation status accounts for the unfavorable prognostic effect of higher age: implications for classification of gliomas**. Acta Neuropathol *120*, 707-718, doi: 10.1007/s00401-010-0781-z.

Hartmann, C., Meyer, J., Balss, J., Capper, D., Mueller, W., Christians, A., Felsberg, J., Wolter, M., Mawrin, C., Wick, W., Weller, M., Herold-Mende, C., Unterberg, A., Jeuken, J. W., Wesseling, P., Reifenberger, G. and von Deimling, A. (2009). **Type and frequency of IDH1 and IDH2 mutations are related to astrocytic and oligodendroglial differentiation and age: a study of 1,010 diffuse gliomas**. Acta Neuropathol *118*, 469-474, doi: 10.1007/s00401-009-0561-9.

Hashiguchi, K., Morioka, T., Yoshida, F., Kawamura, T., Miyagi, Y., Kuwabara, Y., Sasaki, M., Koga, H., Nagata, S. and Sasaki, T. (2007). **Thalamic hypometabolism on 18FDG-positron emission tomography in medial temporal lobe epilepsy**. Neurol Res *29*, 215-222, doi: 10.1179/174313206X153851.

Hasselblatt, M., Jaber, M., Reuss, D., Grauer, O., Bibo, A., Terwey, S., Schick, U., Ebel, H., Niederstadt, T., Stummer, W., von Deimling, A. and Paulus, W. (2018). **Diffuse Astrocytoma, IDH-Wildtype: A Dissolving Diagnosis**. J Neuropathol Exp Neurol, doi: 10.1093/jnen/nly012.

Hausinger, R. P. (2004). **FeII/alpha-ketoglutarate-dependent hydroxylases and related enzymes**. Crit Rev Biochem Mol Biol *39*, 21-68, doi: 10.1080/10409230490440541.

Hodolic, M., Topakian, R. and Pichler, R. (2016). **(18)F-fluorodeoxyglucose and (18)F-flumazenil positron emission tomography in patients with refractory epilepsy**. Radiol Oncol *50*, 247-253, doi: 10.1515/raon-2016-0032.

Horbinski, C. (2013). **What do we know about IDH1/2 mutations so far, and how do we use it?** Acta Neuropathol *125*, 621-636, doi: 10.1007/s00401-013-1106-9.

Horn, S., Figl, A., Rachakonda, P. S., Fischer, C., Sucker, A., Gast, A., Kadel, S., Moll, I., Nagore, E., Hemminki, K., Schadendorf, D. and Kumar, R. (2013). **TERT promoter mutations in familial and sporadic melanoma**. Science *339*, 959-961, doi: 10.1126/science.1230062.

Houillier, C., Wang, X., Kaloshi, G., Mokhtari, K., Guillevin, R., Laffaire, J., Paris, S., Boisselier, B., Idbaih, A., Laigle-Donadey, F., Hoang-Xuan, K., Sanson, M. and Delattre, J. Y. (2010). **IDH1 or IDH2 mutations predict longer survival and response to temozolomide in low-grade gliomas**. Neurology *75*, 1560-1566, doi: 10.1212/WNL.0b013e3181f96282.

Irwin, M., Marin, M. C., Phillips, A. C., Seelan, R. S., Smith, D. I., Liu, W., Flores, E. R., Tsai, K. Y., Jacks, T., Vousden, K. H. and Kaelin, W. G., Jr. (2000). **Role for the p53 homologue p73 in E2F-1-induced apoptosis**. Nature *407*, 645-648, doi: 10.1038/35036614.

Jiao, Y., Killela, P. J., Reitman, Z. J., Rasheed, A. B., Heaphy, C. M., de Wilde, R. F., Rodriguez, F. J., Rosemberg, S., Oba-Shinjo, S. M., Nagahashi Marie, S. K., Bettegowda, C., Agrawal, N., Lipp, E., Pirozzi, C., Lopez, G., He, Y., Friedman, H., Friedman, A. H., Riggins, G. J., Holdhoff, M., Burger, P., McLendon, R., Bigner, D. D., Vogelstein, B., Meeker, A. K., Kinzler, K. W., Papadopoulos, N., Diaz, L. A. and Yan, H. (2012). **Frequent ATRX, CIC, FUBP1 and IDH1 mutations refine the classification of malignant gliomas**. Oncotarget *3*, 709-722, doi: 10.18632/oncotarget.588.

Jin, G., Pirozzi, C. J., Chen, L. H., Lopez, G. Y., Duncan, C. G., Feng, J., Spasojevic, I., Bigner, D. D., He, Y. and Yan, H. (2012). **Mutant IDH1 is required for IDH1 mutated tumor cell growth**. Oncotarget *3*, 774-782, doi: 10.18632/oncotarget.577.

Jin, G., Reitman, Z. J., Spasojevic, I., Batinic-Haberle, I., Yang, J., Schmidt-Kittler, O., Bigner, D. D. and Yan, H. (2011). **2-hydroxyglutarate production, but not dominant negative function, is conferred by glioma-derived NADP-dependent isocitrate dehydrogenase mutations**. PLoS One *6*, e16812, doi: 10.1371/journal.pone.0016812.

Jo, S. H., Lee, S. H., Chun, H. S., Lee, S. M., Koh, H. J., Lee, S. E., Chun, J. S., Park, J. W. and Huh, T. L. (2002). **Cellular defense against UVB-induced phototoxicity by cytosolic NADP(+)-dependent isocitrate dehydrogenase**. Biochem Biophys Res Commun *292*, 542-549, doi: 10.1006/bbrc.2002.6667.

Kerkhof, M., Benit, C., Duran-Pena, A. and Vecht, C. J. (2015). **Seizures in oligodendroglial tumors**. CNS Oncol *4*, 347-356, doi: 10.2217/cns.15.29.

Killela, P. J., Pirozzi, C. J., Reitman, Z. J., Jones, S., Rasheed, B. A., Lipp, E., Friedman, H., Friedman, A. H., He, Y., McLendon, R. E., Bigner, D. D. and Yan, H. (2014). **The genetic landscape of anaplastic astrocytoma**. Oncotarget *5*, 1452-1457, doi: 10.18632/oncotarget.1505.

Kinahan, P. E. and Fletcher, J. W. (2010). **Positron emission tomography-computed tomography standardized uptake values in clinical practice and assessing response to therapy**. Semin Ultrasound CT MR *31*, 496-505, doi: 10.1053/j.sult.2010.10.001.

Klein, M., Engelberts, N. H., van der Ploeg, H. M., Kasteleijn-Nolst Trenite, D. G., Aaronson, N. K., Taphoorn, M. J., Baaijen, H., Vandertop, W. P., Muller, M., Postma, T. J. and Heimans, J. J. (2003). **Epilepsy in low-grade gliomas: the impact on cognitive function and quality of life**. Ann Neurol *54*, 514-520, doi: 10.1002/ana.10712.

Kohanbash, G., Carrera, D. A., Shrivastav, S., Ahn, B. J., Jahan, N., Mazor, T., Chheda, Z. S., Downey, K. M., Watchmaker, P. B., Beppler, C., Warta, R., Amankulor, N. A., Herold-Mende, C., Costello, J. F. and Okada, H. (2017). **Isocitrate dehydrogenase mutations suppress STAT1 and CD8+ T cell accumulation in gliomas**. J Clin Invest *127*, 1425-1437, doi: 10.1172/JCI90644.

Kohling, R., Senner, V., Paulus, W. and Speckmann, E. J. (2006). **Epileptiform activity preferentially arises outside tumor invasion zone in glioma xenotransplants**. Neurobiol Dis *22*, 64-75, doi: 10.1016/j.nbd.2005.10.001.

Kolker, S., Pawlak, V., Ahlemeyer, B., Okun, J. G., Horster, F., Mayatepek, E., Krieglstein, J., Hoffmann, G. F. and Kohr, G. (2002). **NMDA receptor activation and respiratory chain complex V inhibition contribute to neurodegeneration in d-2-hydroxyglutaric aciduria**. Eur J Neurosci *16*, 21-28.

Kranendijk, M., Struys, E. A., Salomons, G. S., Van der Knaap, M. S. and Jakobs, C. (2012). **Progress in understanding 2-hydroxyglutaric acidurias**. J Inherit Metab Dis *35*, 571-587, doi: 10.1007/s10545-012-9462-5.

Krell, D., Assoku, M., Galloway, M., Mulholland, P., Tomlinson, I. and Bardella, C. (2011). **Screen for IDH1, IDH2, IDH3, D2HGDH and L2HGDH mutations in glioblastoma**. PLoS One *6*, e19868, doi: 10.1371/journal.pone.0019868.

Kuo, L. J. and Yang, L. X. (2008). **Gamma-H2AX - a novel biomarker for DNA double-strand breaks**. In Vivo *22*, 305-309.

Labussiere, M., Di Stefano, A. L., Gleize, V., Boisselier, B., Giry, M., Mangesius, S., Bruno, A., Paterra, R., Marie, Y., Rahimian, A., Finocchiaro, G., Houlston, R. S., Hoang-Xuan, K., Idbaih, A., Delattre, J. Y., Mokhtari, K. and Sanson, M. (2014). **TERT promoter mutations in gliomas, genetic associations and clinico-pathological correlations**. Br J Cancer *111*, 2024-2032, doi: 10.1038/bjc.2014.538.

Labussiere, M., Idbaih, A., Wang, X. W., Marie, Y., Boisselier, B., Falet, C., Paris, S., Laffaire, J., Carpentier, C., Criniere, E., Ducray, F., El Hallani, S., Mokhtari, K., Hoang-Xuan, K., Delattre, J. Y. and Sanson, M. (2010). **All the 1p19q codeleted**

gliomas are mutated on IDH1 or IDH2. Neurology *74*, 1886-1890, doi: 10.1212/WNL.0b013e3181e1cf3a.

Latini, A., da Silva, C. G., Ferreira, G. C., Schuck, P. F., Scussiato, K., Sarkis, J. J., Dutra Filho, C. S., Wyse, A. T., Wannmacher, C. M. and Wajner, M. (2005). **Mitochondrial energy metabolism is markedly impaired by D-2-hydroxyglutaric acid in rat tissues**. Mol Genet Metab *86*, 188-199, doi: 10.1016/j.ymgme.2005.05.002.

Latini, A., Scussiato, K., Rosa, R. B., Llesuy, S., Bello-Klein, A., Dutra-Filho, C. S. and Wajner, M. (2003). **D-2-hydroxyglutaric acid induces oxidative stress in cerebral cortex of young rats**. Eur J Neurosci *17*, 2017-2022.

Lee, S. H., Jo, S. H., Lee, S. M., Koh, H. J., Song, H., Park, J. W., Lee, W. H. and Huh, T. L. (2004). **Role of NADP+-dependent isocitrate dehydrogenase (NADP+-ICDH) on cellular defence against oxidative injury by gamma-rays**. Int J Radiat Biol *80*, 635-642.

Lee, S. M., Koh, H. J., Park, D. C., Song, B. J., Huh, T. L. and Park, J. W. (2002). **Cytosolic NADP(+)-dependent isocitrate dehydrogenase status modulates oxidative damage to cells**. Free Radic Biol Med *32*, 1185-1196.

Li, Y., Shan, X., Wu, Z., Wang, Y., Ling, M. and Fan, X. (2018). **IDH1 mutation is associated with a higher preoperative seizure incidence in low-grade glioma: A systematic review and meta-analysis**. Seizure *55*, 76-82, doi: 10.1016/j.seizure.2018.01.011.

Liu, X. Y., Gerges, N., Korshunov, A., Sabha, N., Khuong-Quang, D. A., Fontebasso, A. M., Fleming, A., Hadjadj, D., Schwartzentruber, J., Majewski, J., Dong, Z., Siegel, P., Albrecht, S., Croul, S., Jones, D. T., Kool, M., Tonjes, M., Reifenberger, G., Faury, D., Zadeh, G., Pfister, S. and Jabado, N. (2012). **Frequent ATRX mutations and loss of expression in adult diffuse astrocytic tumors carrying IDH1/IDH2 and TP53 mutations**. Acta Neuropathol *124*, 615-625, doi: 10.1007/s00401-012-1031-3.

Longuespee, R., Wefers, A. K., De Vita, E., Miller, A. K., Reuss, D. E., Wick, W., Herold-Mende, C., Kriegsmann, M., Schirmacher, P., von Deimling, A. and Pusch, S. (2018). **Rapid detection of 2-hydroxyglutarate in frozen sections of IDH mutant tumors by MALDI-TOF mass spectrometry**. Acta Neuropathol Commun *6*, 21, doi: 10.1186/s40478-018-0523-3.

Loonstra, A., Vooijs, M., Beverloo, H. B., Allak, B. A., van Drunen, E., Kanaar, R., Berns, A. and Jonkers, J. (2001). **Growth inhibition and DNA damage induced by Cre recombinase in mammalian cells**. Proc Natl Acad Sci U S A *98*, 9209-9214, doi: 10.1073/pnas.161269798.

Louis, D. N., Ohgaki, H., Wiestler, O. D., Cavenee, W. K., Ellison, D. W., Figarella-Branger, D., Perry, A., Reifenberger, G. and von Deimling, A. (2016a). **WHO Classification of Tumours of the Central Nervous System**.

Louis, D. N., Perry, A., Reifenberger, G., von Deimling, A., Figarella-Branger, D., Cavenee, W. K., Ohgaki, H., Wiestler, O. D., Kleihues, P. and Ellison, D. W. (2016b). **The 2016 World Health Organization Classification of Tumors of the Central**

Nervous System: a summary. Acta Neuropathol *131*, 803-820, doi: 10.1007/s00401-016-1545-1.

Lu, C., Ward, P. S., Kapoor, G. S., Rohle, D., Turcan, S., Abdel-Wahab, O., Edwards, C. R., Khanin, R., Figueroa, M. E., Melnick, A., Wellen, K. E., O'Rourke, D. M., Berger, S. L., Chan, T. A., Levine, R. L., Mellinghoff, I. K. and Thompson, C. B. (2012). **IDH mutation impairs histone demethylation and results in a block to cell differentiation**. Nature *483*, 474-478, doi: 10.1038/nature10860.

Mardis, E. R., Ding, L., Dooling, D. J., Larson, D. E., McLellan, M. D., Chen, K., Koboldt, D. C., Fulton, R. S., Delehaunty, K. D., McGrath, S. D., Fulton, L. A., Locke, D. P., Magrini, V. J., Abbott, R. M., Vickery, T. L., Reed, J. S., Robinson, J. S., Wylie, T., Smith, S. M., Carmichael, L., Eldred, J. M., Harris, C. C., Walker, J., Peck, J. B., Du, F., Dukes, A. F., Sanderson, G. E., Brummett, A. M., Clark, E., McMichael, J. F., Meyer, R. J., Schindler, J. K., Pohl, C. S., Wallis, J. W., Shi, X., Lin, L., Schmidt, H., Tang, Y., Haipek, C., Wiechert, M. E., Ivy, J. V., Kalicki, J., Elliott, G., Ries, R. E., Payton, J. E., Westervelt, P., Tomasson, M. H., Watson, M. A., Baty, J., Heath, S., Shannon, W. D., Nagarajan, R., Link, D. C., Walter, M. J., Graubert, T. A., DiPersio, J. F., Wilson, R. K. and Ley, T. J. (2009). **Recurring mutations found by sequencing an acute myeloid leukemia genome**. N Engl J Med *361*, 1058-1066, doi: 10.1056/NEJMoa0903840.

Neal, A., Kwan, P., O'Brien, T. J., Buckland, M. E., Gonzales, M. and Morokoff, A. (2018). **IDH1 and IDH2 mutations in postoperative diffuse glioma-associated epilepsy**. Epilepsy Behav *78*, 30-36, doi: 10.1016/j.yebeh.2017.10.027.

Neuberger, U. (2017). Personal communication.

Nobusawa, S., Watanabe, T., Kleihues, P. and Ohgaki, H. (2009). **IDH1 mutations as molecular signature and predictive factor of secondary glioblastomas**. Clin Cancer Res *15*, 6002-6007, doi: 10.1158/1078-0432.CCR-09-0715.

Noushmehr, H., Weisenberger, D. J., Diefes, K., Phillips, H. S., Pujara, K., Berman, B. P., Pan, F., Pelloski, C. E., Sulman, E. P., Bhat, K. P., Verhaak, R. G., Hoadley, K. A., Hayes, D. N., Perou, C. M., Schmidt, H. K., Ding, L., Wilson, R. K., Van Den Berg, D., Shen, H., Bengtsson, H., Neuvial, P., Cope, L. M., Buckley, J., Herman, J. G., Baylin, S. B., Laird, P. W., Aldape, K. and Cancer Genome Atlas Research, N. (2010). **Identification of a CpG island methylator phenotype that defines a distinct subgroup of glioma**. Cancer Cell *17*, 510-522, doi: 10.1016/j.ccr.2010.03.017.

Ohgaki, H. and Kleihues, P. (2011). **Genetic profile of astrocytic and oligodendroglial gliomas**. Brain Tumor Pathol *28*, 177-183, doi: 10.1007/s10014-011-0029-1.

Olar, A., Wani, K. M., Alfaro-Munoz, K. D., Heathcock, L. E., van Thuijl, H. F., Gilbert, M. R., Armstrong, T. S., Sulman, E. P., Cahill, D. P., Vera-Bolanos, E., Yuan, Y., Reijneveld, J. C., Ylstra, B., Wesseling, P. and Aldape, K. D. (2015). **IDH mutation status and role of WHO grade and mitotic index in overall survival in grade II-III diffuse gliomas**. Acta Neuropathol *129*, 585-596, doi: 10.1007/s00401-015-1398-z.

Otani, R., Uzuka, T. and Ueki, K. (2017). **Classification of adult diffuse gliomas by molecular markers-a short review with historical footnote**. Jpn J Clin Oncol *47*, 2-6, doi: 10.1093/jjco/hyw142.

Parsons, D. W., Jones, S., Zhang, X., Lin, J. C., Leary, R. J., Angenendt, P., Mankoo, P., Carter, H., Siu, I. M., Gallia, G. L., Olivi, A., McLendon, R., Rasheed, B. A., Keir, S., Nikolskaya, T., Nikolsky, Y., Busam, D. A., Tekleab, H., Diaz, L. A., Jr., Hartigan, J., Smith, D. R., Strausberg, R. L., Marie, S. K., Shinjo, S. M., Yan, H., Riggins, G. J., Bigner, D. D., Karchin, R., Papadopoulos, N., Parmigiani, G., Vogelstein, B., Velculescu, V. E. and Kinzler, K. W. (2008). **An integrated genomic analysis of human glioblastoma multiforme**. Science *321*, 1807-1812, doi: 10.1126/science.1164382.

Pietsch, E. C., Sykes, S. M., McMahon, S. B. and Murphy, M. E. (2008). **The p53 family and programmed cell death**. Oncogene *27*, 6507-6521, doi: 10.1038/onc.2008.315.

Pusch, S. (2016). Personal communication.

Pusch, S., Krausert, S., Fischer, V., Balss, J., Ott, M., Schrimpf, D., Capper, D., Sahm, F., Eisel, J., Beck, A. C., Jugold, M., Eichwald, V., Kaulfuss, S., Panknin, O., Rehwinkel, H., Zimmermann, K., Hillig, R. C., Guenther, J., Toschi, L., Neuhaus, R., Haegebart, A., Hess-Stumpp, H., Bauser, M., Wick, W., Unterberg, A., Herold-Mende, C., Platten, M. and von Deimling, A. (2017). **Pan-mutant IDH1 inhibitor BAY 1436032 for effective treatment of IDH1 mutant astrocytoma in vivo**. Acta Neuropathol *133*, 629-644, doi: 10.1007/s00401-017-1677-y.

Pusch, S., Schweizer, L., Beck, A. C., Lehmler, J. M., Weissert, S., Balss, J., Miller, A. K. and von Deimling, A. (2014). **D-2-Hydroxyglutarate producing neo-enzymatic activity inversely correlates with frequency of the type of isocitrate dehydrogenase 1 mutations found in glioma**. Acta Neuropathol Commun *2*, 19, doi: 10.1186/2051-5960-2-19.

Pusch, S. and other scientists (2017). Personal communication.

Ramachandran, N. and Colman, R. F. (1980). **Chemical characterization of distinct subunits of pig heart DPN-specific isocitrate dehydrogenase**. J Biol Chem *255*, 8859-8864.

Reuss, D. E., Sahm, F., Schrimpf, D., Wiestler, B., Capper, D., Koelsche, C., Schweizer, L., Korshunov, A., Jones, D. T., Hovestadt, V., Mittelbronn, M., Schittenhelm, J., Herold-Mende, C., Unterberg, A., Platten, M., Weller, M., Wick, W., Pfister, S. M. and von Deimling, A. (2015). **ATRX and IDH1-R132H immunohistochemistry with subsequent copy number analysis and IDH sequencing as a basis for an "integrated" diagnostic approach for adult astrocytoma, oligodendroglioma and glioblastoma**. Acta Neuropathol *129*, 133-146, doi: 10.1007/s00401-014-1370-3.

Sahm, F., Capper, D., Jeibmann, A., Habel, A., Paulus, W., Troost, D. and von Deimling, A. (2012a). **Addressing diffuse glioma as a systemic brain disease with single-cell analysis**. Arch Neurol *69*, 523-526, doi: 10.1001/archneurol.2011.2910.

Sahm, F., Capper, D., Pusch, S., Balss, J., Koch, A., Langhans, C. D., Okun, J. G. and von Deimling, A. (2012b). **Detection of 2-hydroxyglutarate in formalin-fixed paraffin-embedded glioma specimens by gas chromatography/mass spectrometry**. Brain Pathol *22*, 26-31, doi: 10.1111/j.1750-3639.2011.00506.x.

Sahm, F., Koelsche, C., Meyer, J., Pusch, S., Lindenberg, K., Mueller, W., Herold-Mende, C., von Deimling, A. and Hartmann, C. (2012c). **CIC and FUBP1 mutations in oligodendrogliomas, oligoastrocytomas and astrocytomas**. Acta Neuropathol *123*, 853-860, doi: 10.1007/s00401-012-0993-5.

Sanson, M., Marie, Y., Paris, S., Idbaih, A., Laffaire, J., Ducray, F., El Hallani, S., Boisselier, B., Mokhtari, K., Hoang-Xuan, K. and Delattre, J. Y. (2009). **Isocitrate dehydrogenase 1 codon 132 mutation is an important prognostic biomarker in gliomas**. J Clin Oncol *27*, 4150-4154, doi: 10.1200/JCO.2009.21.9832.

Sasaki, M., Knobbe, C. B., Itsumi, M., Elia, A. J., Harris, I. S., Chio, II, Cairns, R. A., McCracken, S., Wakeham, A., Haight, J., Ten, A. Y., Snow, B., Ueda, T., Inoue, S., Yamamoto, K., Ko, M., Rao, A., Yen, K. E., Su, S. M. and Mak, T. W. (2012). **D-2-hydroxyglutarate produced by mutant IDH1 perturbs collagen maturation and basement membrane function**. Genes Dev *26*, 2038-2049, doi: 10.1101/gad.198200.112.

Schuler, M. and Green, D. R. (2001). **Mechanisms of p53-dependent apoptosis**. Biochem Soc Trans *29*, 684-688.

Schumacher, T., Bunse, L., Pusch, S., Sahm, F., Wiestler, B., Quandt, J., Menn, O., Osswald, M., Oezen, I., Ott, M., Keil, M., Balss, J., Rauschenbach, K., Grabowska, A. K., Vogler, I., Diekmann, J., Trautwein, N., Eichmuller, S. B., Okun, J., Stevanovic, S., Riemer, A. B., Sahin, U., Friese, M. A., Beckhove, P., von Deimling, A., Wick, W. and Platten, M. (2014). **A vaccine targeting mutant IDH1 induces antitumour immunity**. Nature *512*, 324-327, doi: 10.1038/nature13387.

Sellner, L., Capper, D., Meyer, J., Langhans, C. D., Hartog, C. M., Pfeifer, H., Serve, H., Ho, A. D., Okun, J. G., Kramer, A. and Von Deimling, A. (2010). **Increased levels of 2-hydroxyglutarate in AML patients with IDH1-R132H and IDH2-R140Q mutations**. Eur J Haematol *85*, 457-459, doi: 10.1111/j.1600-0609.2010.01505.x.

Shamji, M. F., Fric-Shamji, E. C. and Benoit, B. G. (2009). **Brain tumors and epilepsy: pathophysiology of peritumoral changes**. Neurosurg Rev *32*, 275-284; discussion 284-276, doi: 10.1007/s10143-009-0191-7.

Shibata, S., Matsuhashi, M., Kunieda, T., Yamao, Y., Inano, R., Kikuchi, T., Imamura, H., Takaya, S., Matsumoto, R., Ikeda, A., Takahashi, R., Mima, T., Fukuyama, H., Mikuni, N. and Miyamoto, S. (2017). **Magnetoencephalography with temporal spread imaging to visualize propagation of epileptic activity**. Clin Neurophysiol *128*, 734-743, doi: 10.1016/j.clinph.2017.01.010.

Sjoblom, T., Jones, S., Wood, L. D., Parsons, D. W., Lin, J., Barber, T. D., Mandelker, D., Leary, R. J., Ptak, J., Silliman, N., Szabo, S., Buckhaults, P., Farrell, C., Meeh, P., Markowitz, S. D., Willis, J., Dawson, D., Willson, J. K., Gazdar, A. F., Hartigan, J., Wu, L., Liu, C., Parmigiani, G., Park, B. H., Bachman, K. E., Papadopoulos, N.,

Vogelstein, B., Kinzler, K. W. and Velculescu, V. E. (2006). **The consensus coding sequences of human breast and colorectal cancers**. Science *314*, 268-274, doi: 10.1126/science.1133427.

Sorensen, M. F., Heimisdottir, S. B., Sorensen, M. D., Mellegaard, C. S., Wohlleben, H., Kristensen, B. W. and Beier, C. P. (2018). **High expression of cystine-glutamate antiporter xCT (SLC7A11) is an independent biomarker for epileptic seizures at diagnosis in glioma**. J Neurooncol, doi: 10.1007/s11060-018-2785-9.

Steenweg, M. E., Jakobs, C., Errami, A., van Dooren, S. J., Adeva Bartolome, M. T., Aerssens, P., Augoustides-Savvapoulou, P., Baric, I., Baumann, M., Bonafe, L., Chabrol, B., Clarke, J. T., Clayton, P., Coker, M., Cooper, S., Falik-Zaccai, T., Gorman, M., Hahn, A., Hasanoglu, A., King, M. D., de Klerk, H. B., Korman, S. H., Lee, C., Meldgaard Lund, A., Mejaski-Bosnjak, V., Pascual-Castroviejo, I., Raadhyaksha, A., Rootwelt, T., Roubertie, A., Ruiz-Falco, M. L., Scalais, E., Schimmel, U., Seijo-Martinez, M., Suri, M., Sykut-Cegielska, J., Trefz, F. K., Uziel, G., Valayannopoulos, V., Vianey-Saban, C., Vlaho, S., Vodopiutz, J., Wajner, M., Walter, J., Walter-Derbort, C., Yapici, Z., Zafeiriou, D. I., Spreeuwenberg, M. D., Celli, J., den Dunnen, J. T., van der Knaap, M. S. and Salomons, G. S. (2010). **An overview of L-2-hydroxyglutarate dehydrogenase gene (L2HGDH) variants: a genotype-phenotype study**. Hum Mutat *31*, 380-390, doi: 10.1002/humu.21197.

Stockhammer, F., Misch, M., Helms, H. J., Lengler, U., Prall, F., von Deimling, A. and Hartmann, C. (2012). **IDH1/2 mutations in WHO grade II astrocytomas associated with localization and seizure as the initial symptom**. Seizure *21*, 194-197, doi: 10.1016/j.seizure.2011.12.007.

Stoddard, B. L., Dean, A. and Koshland, D. E., Jr. (1993). **Structure of isocitrate dehydrogenase with isocitrate, nicotinamide adenine dinucleotide phosphate, and calcium at 2.5-A resolution: a pseudo-Michaelis ternary complex**. Biochemistry *32*, 9310-9316.

Struys, E. A. (2006). **D-2-Hydroxyglutaric aciduria: unravelling the biochemical pathway and the genetic defect**. J Inherit Metab Dis *29*, 21-29, doi: 10.1007/s10545-006-0317-9.

Takami, H., Yoshida, A., Fukushima, S., Arita, H., Matsushita, Y., Nakamura, T., Ohno, M., Miyakita, Y., Shibui, S., Narita, Y. and Ichimura, K. (2015). **Revisiting TP53 Mutations and Immunohistochemistry--A Comparative Study in 157 Diffuse Gliomas**. Brain Pathol *25*, 256-265, doi: 10.1111/bpa.12173.

Tian, X. and Fang, J. (2007). **Current perspectives on histone demethylases**. Acta Biochim Biophys Sin (Shanghai) *39*, 81-88.

Toedt, G., Barbus, S., Wolter, M., Felsberg, J., Tews, B., Blond, F., Sabel, M. C., Hofmann, S., Becker, N., Hartmann, C., Ohgaki, H., von Deimling, A., Wiestler, O. D., Hahn, M., Lichter, P., Reifenberger, G. and Radlwimmer, B. (2011). **Molecular signatures classify astrocytic gliomas by IDH1 mutation status**. Int J Cancer *128*, 1095-1103, doi: 10.1002/ijc.25448.

Toledo, M., Sarria-Estrada, S., Quintana, M., Maldonado, X., Martinez-Ricarte, F., Rodon, J., Auger, C., Aizpurua, M., Salas-Puig, J., Santamarina, E. and Martinez-Saez, E. (2017). **Epileptic features and survival in glioblastomas presenting with seizures**. Epilepsy Res *130*, 1-6, doi: 10.1016/j.eplepsyres.2016.12.013.

Tseng, A. S., Tapon, N., Kanda, H., Cigizoglu, S., Edelmann, L., Pellock, B., White, K. and Hariharan, I. K. (2007). **Capicua regulates cell proliferation downstream of the receptor tyrosine kinase/ras signaling pathway**. Curr Biol *17*, 728-733, doi: 10.1016/j.cub.2007.03.023.

Turcan, S., Rohle, D., Goenka, A., Walsh, L. A., Fang, F., Yilmaz, E., Campos, C., Fabius, A. W., Lu, C., Ward, P. S., Thompson, C. B., Kaufman, A., Guryanova, O., Levine, R., Heguy, A., Viale, A., Morris, L. G., Huse, J. T., Mellinghoff, I. K. and Chan, T. A. (2012). **IDH1 mutation is sufficient to establish the glioma hypermethylator phenotype**. Nature *483*, 479-483, doi: 10.1038/nature10866.

van Breemen, M. S., Wilms, E. B. and Vecht, C. J. (2007). **Epilepsy in patients with brain tumours: epidemiology, mechanisms, and management**. Lancet Neurol *6*, 421-430, doi: 10.1016/S1474-4422(07)70103-5.

Vinton, A. B., Carne, R., Hicks, R. J., Desmond, P. M., Kilpatrick, C., Kaye, A. H. and O'Brien, T. J. (2007). **The extent of resection of FDG-PET hypometabolism relates to outcome of temporal lobectomy**. Brain *130*, 548-560, doi: 10.1093/brain/awl232.

von Oertzen, T. J. (2017). **PET and ictal SPECT can be helpful for localizing epileptic foci**. Curr Opin Neurol *30*.

Wang, P., Dong, Q., Zhang, C., Kuan, P. F., Liu, Y., Jeck, W. R., Andersen, J. B., Jiang, W., Savich, G. L., Tan, T. X., Auman, J. T., Hoskins, J. M., Misher, A. D., Moser, C. D., Yourstone, S. M., Kim, J. W., Cibulskis, K., Getz, G., Hunt, H. V., Thorgeirsson, S. S., Roberts, L. R., Ye, D., Guan, K. L., Xiong, Y., Qin, L. X. and Chiang, D. Y. (2013). **Mutations in isocitrate dehydrogenase 1 and 2 occur frequently in intrahepatic cholangiocarcinomas and share hypermethylation targets with glioblastomas**. Oncogene *32*, 3091-3100, doi: 10.1038/onc.2012.315.

Ward, P. S., Cross, J. R., Lu, C., Weigert, O., Abel-Wahab, O., Levine, R. L., Weinstock, D. M., Sharp, K. A. and Thompson, C. B. (2012). **Identification of additional IDH mutations associated with oncometabolite R(-)-2-hydroxyglutarate production**. Oncogene *31*, 2491-2498, doi: 10.1038/onc.2011.416.

Ward, P. S., Patel, J., Wise, D. R., Abdel-Wahab, O., Bennett, B. D., Coller, H. A., Cross, J. R., Fantin, V. R., Hedvat, C. V., Perl, A. E., Rabinowitz, J. D., Carroll, M., Su, S. M., Sharp, K. A., Levine, R. L. and Thompson, C. B. (2010). **The common feature of leukemia-associated IDH1 and IDH2 mutations is a neomorphic enzyme activity converting alpha-ketoglutarate to 2-hydroxyglutarate**. Cancer Cell *17*, 225-234, doi: 10.1016/j.ccr.2010.01.020.

Watanabe, T., Nobusawa, S., Kleihues, P. and Ohgaki, H. (2009). **IDH1 mutations are early events in the development of astrocytomas and oligodendrogliomas**. Am J Pathol *174*, 1149-1153, doi: 10.2353/ajpath.2009.080958.

Wesseling, P. and Capper, D. (2017). **WHO 2016 Classification of Gliomas**. Neuropathol Appl Neurobiol, doi: 10.1111/nan.12432.

Wichmann, A., Jaklevic, B. and Su, T. T. (2006). **Ionizing radiation induces caspase-dependent but Chk2- and p53-independent cell death in Drosophila melanogaster**. Proc Natl Acad Sci U S A *103*, 9952-9957, doi: 10.1073/pnas.0510528103.

Wong, C. H., Bleasel, A., Wen, L., Eberl, S., Byth, K., Fulham, M., Somerville, E. and Mohamed, A. (2010). **The topography and significance of extratemporal hypometabolism in refractory mesial temporal lobe epilepsy examined by FDG-PET**. Epilepsia *51*, 1365-1373, doi: 10.1111/j.1528-1167.2010.02552.x.

Xu, W., Yang, H., Liu, Y., Yang, Y., Wang, P., Kim, S. H., Ito, S., Yang, C., Wang, P., Xiao, M. T., Liu, L. X., Jiang, W. Q., Liu, J., Zhang, J. Y., Wang, B., Frye, S., Zhang, Y., Xu, Y. H., Lei, Q. Y., Guan, K. L., Zhao, S. M. and Xiong, Y. (2011). **Oncometabolite 2-hydroxyglutarate is a competitive inhibitor of alpha-ketoglutarate-dependent dioxygenases**. Cancer Cell *19*, 17-30, doi: 10.1016/j.ccr.2010.12.014.

Yan, H., Parsons, D. W., Jin, G., McLendon, R., Rasheed, B. A., Yuan, W., Kos, I., Batinic-Haberle, I., Jones, S., Riggins, G. J., Friedman, H., Friedman, A., Reardon, D., Herndon, J., Kinzler, K. W., Velculescu, V. E., Vogelstein, B. and Bigner, D. D. (2009). **IDH1 and IDH2 mutations in gliomas**. N Engl J Med *360*, 765-773, doi: 10.1056/NEJMoa0808710.

Yip, S., Butterfield, Y. S., Morozova, O., Chittaranjan, S., Blough, M. D., An, J., Birol, I., Chesnelong, C., Chiu, R., Chuah, E., Corbett, R., Docking, R., Firme, M., Hirst, M., Jackman, S., Karsan, A., Li, H., Louis, D. N., Maslova, A., Moore, R., Moradian, A., Mungall, K. L., Perizzolo, M., Qian, J., Roldan, G., Smith, E. E., Tamura-Wells, J., Thiessen, N., Varhol, R., Weiss, S., Wu, W., Young, S., Zhao, Y., Mungall, A. J., Jones, S. J., Morin, G. B., Chan, J. A., Cairncross, J. G. and Marra, M. A. (2012). **Concurrent CIC mutations, IDH mutations, and 1p/19q loss distinguish oligodendrogliomas from other cancers**. J Pathol *226*, 7-16, doi: 10.1002/path.2995.

8 Supplement

Supplement Table 1. All established neural stem cell cultures with the dates of preparation and respective genotypes. C, conditional allele; T, transgenic allele.

Date of preparation	Cell culture number	$Idh1^{R132H}$ genotype	ROSA-CreERT2 genotype	p53 genotype	Cic genotype
12.01.2015	#1	C/+	T/+	-	-
12.01.2015	#2	C/+	+/+	-	-
12.01.2015	#3	C/+	T/+	-	-
12.01.2015	#4	C/+	T/+	-	-
12.01.2015	#5	C/+	T/+	-	-
12.01.2015	#6	C/+	T/+	-	-
12.01.2015	#7	C/+	T/+	-	-
12.01.2015	#8	C/+	T/+	-	-
12.01.2015	#9	C/+	+/+	-	-
12.01.2015	#10	C/+	T/+	-	-
15.01.2015	#11	C/+	T/+	-	-
15.01.2015	#12	C/+	+/+	-	-
15.01.2015	#13	C/+	T/+	-	-
15.01.2015	#14	C/+	T/+	-	-
15.01.2015	#15	C/+	+/+	-	-
15.01.2015	#16	C/+	+/+	-	-
15.01.2015	#17	C/+	T/+	-	-
18.08.2015	#18	C/+	T/+	C/C	-
18.08.2015	#19	+/+	T/+	C/C	-
18.08.2015	#20	+/+	T/+	C/C	-
18.08.2015	#21	C/+	T/+	C/C	-
18.08.2015	#22	+/+	T/+	C/C	-
18.08.2015	#23	C/+	T/+	C/C	-
18.08.2015	#24	+/+	T/+	C/C	-
18.08.2015	#25	C/+	T/+	C/C	-
14.10.2015	#26	C/+	+/+	C/C	-
14.10.2015	#27	+/+	+/+	C/C	-
14.10.2015	#28	C/+	+/+	C/C	-
14.10.2015	#29	+/+	T/+	C/C	-
14.10.2015	#30	C/+	+/+	C/C	-
14.10.2015	#31	C/C	T/+	C/C	-
14.10.2015	#32	+/+	+/+	-	+/+
14.10.2015	#33	+/+	+/+	-	C/+
14.10.2015	#34	+/+	T/+	-	+/+
14.10.2015	#35	+/+	+/+	-	C/+
14.10.2015	#36	+/+	T/T	-	C/+
14.10.2015	#37	+/+	+/+	-	C/+
14.10.2015	#38	+/+	T/T	-	C/+
14.10.2015	#39	+/+	+/+	-	C/+
14.10.2015	#40	+/+	T/+	-	C/+
08.12.2015	#41	+/+	T/+	-	C/C
08.12.2015	#42	+/+	T/+	-	C/C
08.12.2015	#43	+/+	T/+	-	C/+
08.12.2015	#44	+/+	+/+	-	C/C
08.12.2015	#45	+/+	T/+	-	C/C
08.12.2015	#46	+/+	+/+	-	C/+
08.12.2015	#47	+/+	+/+	-	C/+
10.12.2015	#48	+/+	+/+	-	C/+
10.12.2015	#49	+/+	T/+	-	C/C
10.12.2015	#50	+/+	+/+	-	C/+
10.12.2015	#51	+/+	+/+	-	C/C
10.12.2015	#52	+/+	T/+	-	C/C
10.12.2015	#53	+/+	+/+	-	C/C

10.12.2015	#54	+/+	+/+	-	C/+
20.05.2016	#55	+/+	T/+	-	C/+
20.05.2016	#56	+/+	T/+	-	C/C
20.05.2016	#57	C/+	T/+	-	C/C
20.05.2016	#58	+/+	T/+	-	C/C
20.05.2016	#59	C/+	+/+	-	C/C
20.05.2016	#60	+/+	T/+	-	C/C
24.05.2016	#61	C/+	T/+	-	C/+
24.05.2016	#62	+/+	+/+	-	C/C
24.05.2016	#63	+/+	T/+	-	C/+
24.05.2016	#64	C/+	+/+	-	C/C
24.05.2016	#65	+/+	T/+	-	C/+
24.05.2016	#66	C/+	+/+	-	C/+
24.05.2016	#67	+/+	T/+	-	C/C
31.05.2016	#68	C/+	+/+	-	C/+
31.05.2016	#69	+/+	T/+	-	C/+
31.05.2016	#70	+/+	+/+	-	C/C
31.05.2016	#71	C/+	T/+	-	C/C
31.05.2016	#72	+/+	T/T	-	C/C
31.05.2016	#73	+/+	T/T	-	C/C
31.05.2016	#74	+/+	T/+	-	C/C
31.05.2016	#75	C/+	T/+	-	C/C

Supplement Table 2. List of primers with respective sequences and annealing temperatures for PCR analysis.

	No.	Name	Sequence	Length	Annealing Temperature
$Idh1^{R132H}$	P259	Lf_5534	AAGAGTTCTCAGCTCTTTTGGCACGG	26	62
	P262	Mr_5541	GCATCACGATTCTCTATGC	19	45,1
Rosa	P268	Rosa-Cre1	AAAGTCGCTCTGAGTTGTTAT	21	64
	P269	Rosa-Cre2	GGAGCGGGAGAAATGGATATG	21	64
	P270	Rosa-Cre3	CCTGATCCTGGCAATTTCG	19	64
p53	P307	OIMR 8543	GGTTAAACCCAGCTTGACCA	20	66
	P308	OIMR 8544	GGAGGCAGAGACAGTTGGAG	20	66
Cic	P636	E8_f	AAGAAGGGGATGATGATGTCATTG	24	55,8
	P637	LoxP2_r	GAGCTTCCGTGGCTGAAGC	19	54,8
	P638	E9_r	CTTGTTACCCTCTGGGTCCTCC	22	55,5
	P404	LoxP3 rv	AAACAGTGTCTTCCCTGGTGGAC	23	55,9
Flp	P643	FLP-1	CACTGATATTGTAAGTAGTTTGC	23	43,7
	P644	FLP-2	CTAGTGCGAAGTAGTGATCAGG	22	48,7
	P645	FLP-3	CTAGGCCACAGAATTGAAAGATCT	24	52,9
	P646	FLP-4	GTAGGTGGAAATTCTAGCATCATCC	25	54,3
Cic RT	P714	Cic_RT_E9_10_f	GATGACAGCTTTGGCACCAC	20	52,8
	P715	Cic_RT_E9_10_r	AGGTGAAGAGGAGGATGATGG	21	52
	P716	Cic_RT_E10_11_f	CAGCTTCAAGTGGCACCTGC	20	55,7
	P717	Cic_RT_E10_11_r	GAGAAAGGCGAGCTAACCAGG	21	54,8
$Idh1^{R132H}$ KI	P789	Idh1R132H_KI_rev	CTTACTTGGTCCCCATATGCATGAT	25	57,3
$Idh1^{R132H}$ KI WT	P790	Idh1wt_cond_rev	CTTACTTGGTCCCCATATGCATGTC	25	57,6

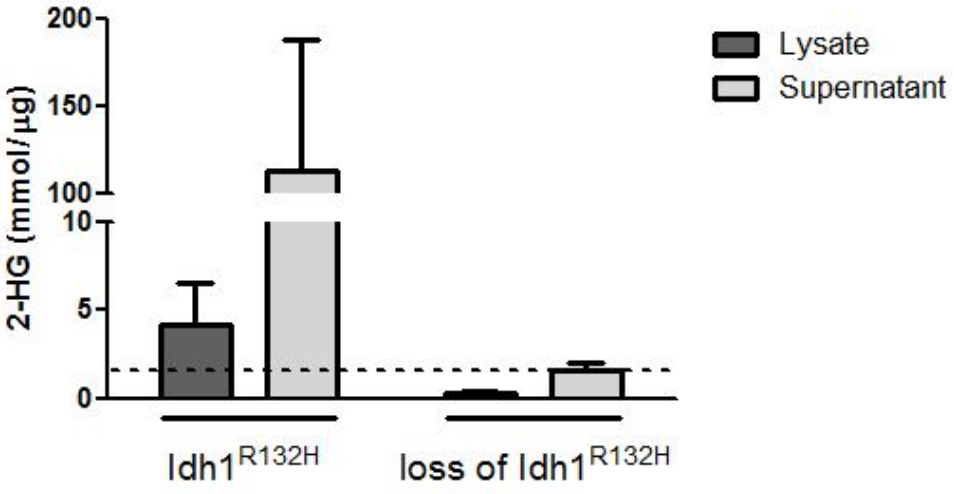

Supplement Figure 1. Long-term cultures lose the ability to produce 2-HG. Idh1^{R132H} mutated cells produce 2-HG. After long term cultivation and concomitant loss of Idh1^{R132H}, cells lose the ability to produce 2-HG, represented in 2-HG levels below detection limit in both supernatant and whole cell lysate. Dashed line indicates detection limit of the assay. (n = 3)

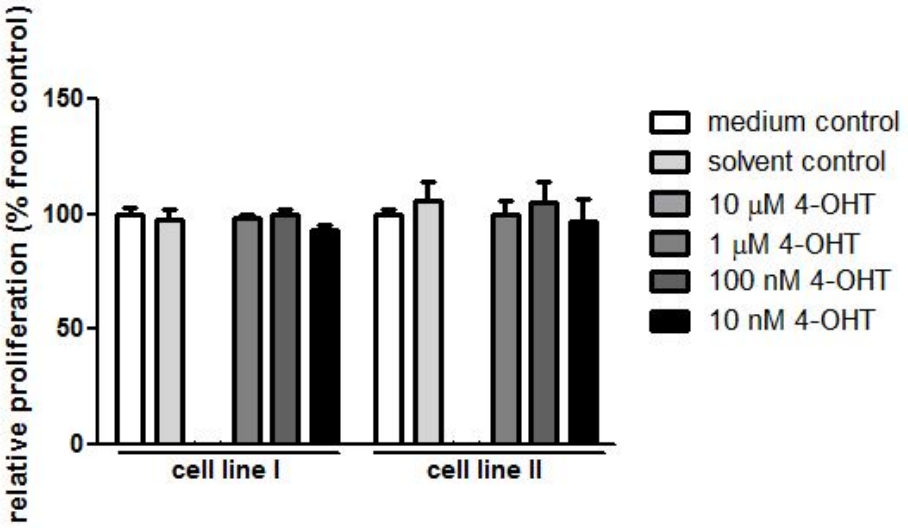

Supplement Figure 2. Impact of 4-OHT treatment on cell viability. The standard concentration of 1µM is not toxic to the cells. Treatment with 10-fold higher 4-OHT concentration reduces cell viability to zero.

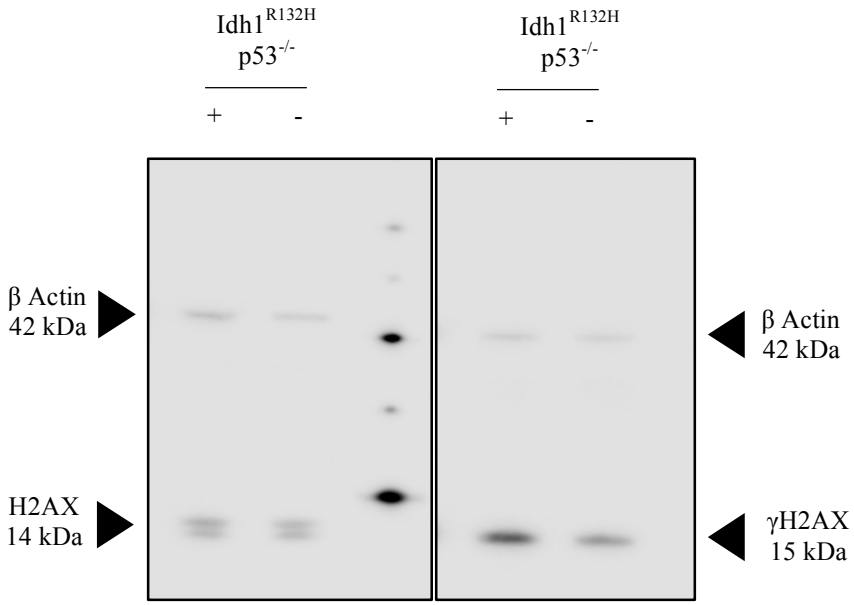

Supplement Figure 3. Genome instability might be caused by upregulated levels of γ-H2AX in Idh1^{R132H} p53$^{-/-}$ cells. Western blot with antibodies to H2AX and γ-H2AX shows an increased expression of γ-H2AX, after induction of the genetic alterations. Data are preliminary, as blot reproducibility is very difficult. (n = 1)

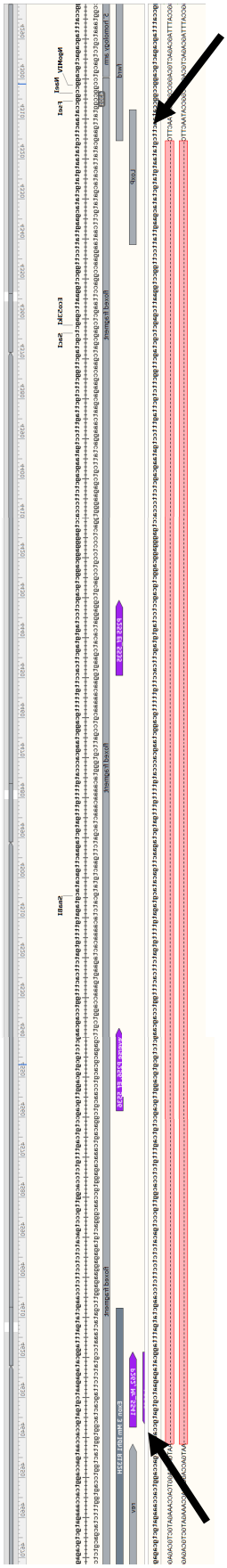

Supplement Figure 4. Sequencing alignment of the PCR product of a cell line that lost the Idh1^{R132H} mutation. Black arrows indicate the undetectable region from lox P site 1 until Exon 3, which caused the loss of mutant Idh1 protein.

9 Acknowledgements

First and foremost, I would like to express my gratitude to my supervisor **Prof. Andreas von Deimling**. He has supported me academically and emotionally through the rough road to finish this thesis. Having started as an electrophysiologist he provided me with the knowledge and advice I needed as a newcomer in the new field of glioma research. His trust in my abilities and capacities had been a strong encouragement. It had been a pleasure to work with him, implement his suggestions and to learn from his research. He arranged excellent working conditions for my experiments and was available whenever I needed his advice. The different social activities, such as the pool party or Christmas dinner, to get the research group into a different mode of thinking, will be remembered.

I would like to thank all members of **Prof. Andreas von Deimling`s Clinical Cooperation Unit Neuropathology** with whom I spent a fantastic, unforgettable and instructive time during the last three years.

I would like to thank wholeheartedly my mentor **Dr. Stefan Pusch** for supporting me during the whole period of my project. I will never forget his support when we first talked in 2014 and I tried to express my interest in glioma research and would like to learn everything but from the beginning. I appreciate his broad experimental knowledge, skills and ideas that helped me a lot during the last three years. It was not only the knowledge on molecular biology, but also about things that certainly not a lot of people know, for example why a fig is not suitable for vegetarians. We were an invincible team also when we had to face difficult problems, such as eight hours surgeries without a single break. I would like to thank him for his encouragement and support. Further, I would also like to thank him for the many times he invited us as a team for a BBQ or to prepare sushi together. Everything I learned from him will certainly help me during the next steps of my career.

I would also like to underline the assistance I received by **Prof. Michael Platten**. His advice has been a great help in all TAC meetings. Him being a member of my TAC group and one of my examiners was crucial in steadily and firmly pursuing my goals. I will also remember the nice supportive atmosphere of the TAC meetings and his unexpected questions that convinced me to strengthen more the immunological perspective in my research.

I wish to thank wholeheartedly **Prof. Andreas Draguhn**. He was one of the key persons to achieve student and academic progress. He strongly influenced my perspectives as a researcher, guided me in all phases of my studies and PhD. My continuing interest in electrophysiology, which is also reflected in this thesis, is based on his work. A special gratitude for his contributions, his stimulating suggestions and him being an engaged member of my TAC group and examiner.

I would like to emphasize the help of the following members of the department of neuropathology. **David** and **Jana Reuss** helped me in discussions about cell culture, antibodies and gliomas in general. I really appreciated their effort to establish the Cre antibody. I would also like to thank **Antje Habel** for providing me with various antibodies and teaching me how to perform immunohistochemistry. I definitely learned a lot from it.

I would like to mention the people without whom the animal experiments would not have been possible - amongst others, **Anja Rathgeb, Kerstin Musielak** and **Alexander Voise**. I want to mention their enormous support, their reliability and trust, but also the nice conversations we had especially during the weekends and holidays. For the advice during all of the surgeries I would also like to thank the members of the **groups of Prof. Platten and Prof. Winkler**.

Lotta without doubt, had been the best roommate during the time of my thesis. She always cheered me up at any time, especially on those days I had to face difficult problems with animals that really challenged me.

I would also like to thank **Markus Lechner** who did his best to teach me how to perform cell culture experiments and with whom I spend the first coffee breaks within the time of my PhD.

I also wish to thank **Sebastian Kruse** for the nice time after work, whether it was a beer to talk about not-working experiments, the fun evenings when we planned the next PhD party with the party committee or when he organized one of the legendary flat parties. These memories will last.

Certainly, I would like to name the central person of our lab, **Jessica Eisel**. I would like to thank her for her understanding when I started to work in the lab and her support. I felt uncomfortable because of my lack of knowledge about molecular biology techniques, but she patiently explained everything to me. Establishing a new lab in DKFZ made us become more than lab mates sharing one office. I always admired her planned way of working and it was always exciting to unravel certain mysteries of genotyping with her – tough, but always with success! I thank her for these efforts regarding the genotyping, as in the end it was not only about mice… Thanks to her I never felt that I was the only PhD student in the lab and I always had the impression that I might ask her whenever I needed to. Importantly, she was also with me in difficult situations and her advice was invaluable and honest. I will truly miss our profound conversations in the late afternoon in front of the bakery.

Talking about support from the lab, I would also like to thank **Gordon Haldenhof**. It was always nice to work with him in the lab and I am very grateful for his ideas about different experiments, especially the soft agar assay. Remembering difficult times, I will never forget the way we talked and the number of lab gloves with funny faces he had been creating for me.

I would also like to mention my former Master students I worked with during the first and second year of my project. I am grateful for the help of **Monika Bäumler**, **Christina Kellerer** and **Frederik Cichon** during very challenging times of my PhD – I definitely learned a lot from them as well. It was not only fun to work with them but they were very helpful to discuss the actual difficulties, such as new assays or surgeries, and plan the next experiments. Retrospectively, I know that they did not only support me, but I gained much more self-confidence in this field of research, which was totally new to me.

Special thanks go to my favorite Master student **Julia Zaman**. With the decision to supervise her I did not only get a Master student but also a wonderful friend. I would like to thank her for the enormous support and for all of the fruitful discussions we had. I immediately sensed that we have the same opinion about research and I knew that I could trust her when I saw her to be in control of the "Zelli" (cell culture room). The more closely we were working together, the more interesting the project became and it was a pleasure to work with her on new experiments and discuss upcoming problems. I wholeheartedly would like to thank her for the time after work as well. I will not forget the PhD parties or when we had wine with baguette and goat cheese at my place. Although we will work on different projects in the

future, I am convinced that our friendship will last – and as you know "we have to stay friends…".

I would like to thank **Matthias Brendel** for the time outside the lab – and definitely also for the nice company in DKFZ. I met him during the time of my PhD and this made the time even more special and unforgettable, especially when we started to talk about glioma. I would like to express my gratitude for the wonderful moments we shared during the last year, which helped me to get my mind off lab problems, for the understanding and encouragement. I really cherish his continuous invaluable support, because he already knew how it feels to work on a thesis to become a "Dr.". I would also like to thank **Ingrid and Joachim Brendel** for their very kind support at a special time.

I would like to express my deep gratitude to my wonderful family back home in Bochum and in other parts of the world. I would like to thank my sister **Sophie** for believing in me at any time of my work. She always cared whenever, independent of the of the time zones during day and night, there had been – apparently unresolvable – problems that needed a sophisticated plan. Further, I would like to thank my **grandparents**, my aunt **Bärbel** and cousin **Julian** for their invaluable support in all the years since I started to work on the thesis. Their interest in my work and various means of encouragement including letters, phone calls and visits were always a great assistance.

I would like to express my deep thanks and gratitude to my **parents** who have been a source of encouragement and support during my whole studies. Without their love and faith, I would not have been where I am today. They were always supporting me when I had to take difficult decisions, including the one deciding to finally work in my present field of research. I really cherish that they were always honest with me. Our discussions helped me to manage challenging situations and made me feel stronger. Although they do not live close to me, I always felt that they were with me all along. I know they understood the importance of what I was doing and why it was often difficult to travel back home, even if it was only because of one sick mouse. The motivation parcels of my mom and little black or pink gifts of my dad were the highlights in my daily routine and their regular visits to Heidelberg and Ludwigshafen provided the impetus needed to sustain especially my PhD period.

Publications

1. Pusch, S., Krausert, S., Fischer, V., Balss, J., Ott, M., Schrimpf, D., Capper, D., Sahm, F., Eisel, J., Beck A.C., Jugold, M., Eichwald, V., Kaulfuss, S., Panknin O., Rehwinkel H., Zimmermann, K., Hillig, R.C., Guenther, J., Toschi, L., Neuhaus, R., Haegebart, A., Hess-Stumpp, H., Bauser, M., Wick, W., Unterberg, A., Herold-Mende, C., Platten, M., von Deimling, A. (2017). **Pan-mutant IDH1 inhibitor BAY 1436032 for effective treatment of IDH1 mutant astrocytoma in vivo.** Acta Neuropathol. *133(4)*: 629-644.

Publication 1 is not content of the present project and is used as a reference only.

Further publications:

2. Fischer, V., Both, M., Draguhn, A., Egorov, A.V. (2014). **Choline-mediated modulation of hippocampal sharp wave-ripple complexes in vitro.** J Neurochem. *129(5)*: 792-805.

Eidesstattliche Versicherung

EIDESSTATTLICHE ERKLÄRUNG

zum Antrag auf Zulassung zur Promotion gemäß PromO „Dr.sc.hum."

AFFIDAVIT

1. Ich habe an keiner anderen Stelle einen Antrag auf Zulassung zur Promotion gestellt oder bereits einen Doktortitel auf der Grundlage des vorgelegten Studienabschlusses erworben und mich auch nicht einer Doktorprüfung erfolglos unterzogen (dies schließt äquivalente Verfahren bzw. Titel ausserhalb Deutschlands ein). *I have not applied anywhere else for a doctoral degree nor have I obtained a doctoral title on the basis of my presented studies or failed a doctoral examination (this includes similar procedures and titles in countries other than Germany).*

2. Die an der Medizinischen Fakultät der Universität Heidelberg zur Promotion eingereichte Arbeit mit dem Titel: *This thesis, submitted to the Medical Faculty of the University of Heidelberg is entitled:*

in der Klinik/am Institut für .....
in the clinic/at the insitute of

unter Anleitung von (Doktorvater/ -mutter) .....
under the supervision of (name of offical supervisor)

habe ich selbst verfasst und bei der Abfassung der Arbeit keine anderen als die in der Abhandlung aufgeführten Hilfsmittel benutzt. *I have written this thesis independently and I have not used any sources other than indicated in the thesis.*

3. Die Arbeit oder Teile davon habe ich bislang an keiner Hochschule des In- oder Auslands als Bestandteil einer Prüfungs- oder Qualifikationsleistung vorgelegt. *I have not yet presented this thesis or parts thereof to a university as part of an examination or degree.*

4. Die Dissertation wurde ohne Hinzuziehung einer kommerziellen Promotionsberatung erstellt. *This thesis was written without the assistance of any kind of commercial doctoral consulting agency.*

5. Mit der Veröffentlichung meines Lebenslaufes im Rahmen des Promotionsverfahrens (Dissertation) bin ich einverstanden. *I agree to the publication of my CV as part of my thesis.*

6. Ich komme der Veröffentlichungspflicht gemäß § 13 PromO nach und stimme der Veröffentlichung der Zusammenfassung meiner Dissertation im Internet unter Angabe meines Namens und des Studienabschlusses zu. *I will fulfill the publication requirement according to § 13 of the doctoral regulations and respectively agree to the publication of the summary of my thesis on the internet, quoting my name and the type of degree conferred.*

7. Die Bedeutung der eidesstattlichen Erklärung und die strafrechtlichen Folgen einer unrichtigen oder unvollständigen eidesstattlichen Erklärung sind mir bekannt. *I am aware of the importance of a sworn affidavit and the prosecution in case of a false or incomplete affidavit.*

Ich versichere an Eides statt, dass ich nach bestem Wissen die reine Wahrheit erklärt und nichts verschwiegen habe.
I declare in lieu of oath that to the best of my knowledge, all the declarations are true and that I have not concealed anything.

....

Ort und Datum / *place and date* Unterschrift / *signature*

The German text is legally binding.